1989

Diffusion Independent, Bimolecular, Photoinduced Electron Transfer Reactions

Joyce Elizabeth Stilborn

NOTICE

The quality of this microform is heavily dependent upon the quality of the original thesis submitted for microfilming. Every effort has been made to ensure the highest quality of reproduction possible.

If pages are missing, contact the university which granted the degree.

Some pages may have indistinct print especially if the original pages were typed with a poor typewriter ribbon or if the university sent us an inferior photocopy.

Reproduction in full or in part of this microform is governed by the Canadian Copyright Act, R.S.C. 1970, c. C-30, and subsequent amendments.

AVIS

La qualité de cette microforme dépend grandement de la qualité de la thèse soumise au microfilmage. Nous avons tout fait pour assurer une qualité supérieure de reproduction.

S'il manque des pages, veuillez communiquer avec l'université qui a conféré le grade.

La qualité d'impression de certaines pages peut laisser à désirer, surtout si les pages originales ont été dactylographiées à l'aide d'un ruban usé ou si l'université nous a fait parvenir une photocopie de qualité inférieure.

La reproduction, même partielle, de cette microforme est soumise à la Loi canadienne sur le droit d'auteur, SRC 1970, c. C-30, et ses amendements subséquents.

DIFFUSION INDEPENDENT, BIMOLECULAR, PHOTOINDUCED ELECTRON TRANSFER REACTIONS

by

Joyce Elizabeth Stilborn

Department of Chemistry

Submitted in partial fulfillment
of the requirements for the degree of
Doctor of Philosophy

Faculty of Graduate Studies
The University of Western Ontario
London, Ontario
December, 1988

ISBN 0-315-49340-2

ABSTRACT

A variety of expressions have been developed which relate the Gibbs energy of activation to the net Gibbs energy change of a reaction. One of these, the Marcus relation, was developed specifically for outer-sphere electron transfer reactions. It predicted that as the reaction exergonicity increased, the activation energy would decrease to zero and then increase. Consequently, the reaction rate constant should increase to a maximum and then decrease in the so-called inverted region.

Extensive investigation over many years failed to find evidence for the inverted region. Recently, five types of experiments have yielded clear evidence of inverted behavior. In all five cases the reactions were unimolecular or pseudo-unimolecular.

This thesis describes the investigation of a series of photo-induced electron transfer reactions. The bimolecular quenching constants k_q and the static quenching critical distances R_c were found from transient and steady-state emission spectroscopies, using emission from the reactant electron donors. R_c was also determined by EPR measurements on the product acceptor radicals.

The chemical systems comprised an electron acceptor, methyl viologen, a sacrificial electron donor for EPR experiments, EDTA, and a homologous series of photosensitive ruthenium electron donors. All ruthenium compounds except $Ru[bpy]_3Cl_2$ were synthesized by literature methods and identified by optical absorption and fast atom bombardment mass spectroscopies. The reactants were dispersed in glycerol at room temperature.

The results show that k_q remains at a diffusion controlled maximum as the reactions become more exergonic. R_c increases to a maximum when

$\Delta G \simeq -0.6$ eV and then decreases. A similar curve is found for R_c calculated from EPR data, proving that the reaction under investigation is indeed electron transfer, and that the parameter R_c is real and independent of the species (reactant or product) used to identify it.

It is concluded that the Marcus relation applies to bimolecular charge-separation outer-sphere electron-transfer reactions and is observed in the absence of diffusion.

An initial project which examined electron transfer in the same systems at low temperature and was not completed is described briefly.

ACKNOWLEDGEMENTS

I am indebted beyond words to the people I have known in this Chemistry Department who have been helpful, encouraging, and supportive.

I particularly thank Dr. Aleksander Siemiarczuk for technical assistance and very helpful discussions. I am also very grateful to Dr. Douglas James and Dr. Alan McIntosh for assistance and discussions.

I thank Dr. W. Ware for the use of his transient and steady state emission apparatus. I also thank all the other faculty members whose equipment I borrowed.

I am grateful to all the Chemistry Department support staff for help and advice, and I particularly thank Mr. J. Vanstone, Mr. W. Lindsay, Ms. L. Harnick, and Mr. B. Harwood for building equipment and making emergency repairs. I also thank Mr. D. Hairsine for performing the FAB mass spectrometry.

Finally, I am extremely grateful to my supervisor, Dr. J. R. Bolton, for making this work possible.

TABLE OF CONTENTS

LIST OF TABLES

LIST OF FIGURES

CHAPTER 1 INTRODUCTION

1.1 Synopsis

Outer-sphere electron transfer (ET) reactions in solution have been the subject of extensive experimental and theoretical investigation for the past three decades. A number of quantitative predictions have been made, many of which have been confirmed experimentally. One prediction which has found little support until recently is that, as reactions become highly exergonic, rates will decrease in the so-called "inverted region". One of the many explanations which have been suggested to account for the failure to find inverted behavior in bimolecular ET is that, for very fast reactions, the observed rate is limited by diffusion. The top of the rate-energy curve is masked by diffusion control and observable decreases are expected at large exergonicities which have not been attained. Support for this explanation has been obtained by several experiments which have examined unimolecular or pseudo-unimolecular ET reactions and found clear evidence of inverted behavior.

This thesis describes an experiment designed to examine bimolecular ET in the absence of diffusion. Under the condition of high quencher concentration, some of the reactants in an emission quenching experiment diffuse together before excitation of the photosensitizer occurs. Consequently these reactants, which are said to react by *static quenching*, occupy approximately the same location during excitation and reaction. Measures of the reaction probability by static quenching are independent of diffusion and will not be limited by diffusion control no matter how probable (how fast) the reaction is.

A homologous series of photosensitive electron donors and one

electron acceptor were chosen to span a range of reaction exergonicities. The static quenching critical radius for each donor-acceptor pair was determined from samples containing high acceptor concentrations, providing a measure of reaction probability in the absence of diffusion. Bimolecular quenching constants were measured with the same samples so that rate-energy relationships with and without diffusion, obtained under identical experimental conditions, could be compared.

Chapter 1 summarizes the quantum mechanical origin of some fundamental concepts, discusses some of the practical difficulties encountered in investigating rate-energy relationships, and identifies the two rate-energy relationships which have found the widest support from studies of electron-transfer reactions.

Chapter 2 summarizes theory for electron transfer, emission quenching, and the reaction thermodynamics. Chapter 3 develops the rationale for the experimental work by reviewing relevant literature, discussing the principal conclusion drawn from the literature, and describing the experimental design which was adopted. Two new methods, developed to obtain the static quenching critical radius by measuring ET product concentrations, are presented. Chapter 4 describes reactant synthesis, identification, and sample preparation. Chapters 5, 6, and 7 discuss experimental methods, the experiments performed, results, and data analysis for the three techniques used: time-correlated single photon counting, emission spectroscopy, and electron paramagnetic resonance (EPR) spectroscopy. Chapter 8 discusses the rate-energy relationships obtained and the significance of these results with respect to current literature and theory.

1.2 Development of Energy and Kinetic Terms

1.2.1 Energy

The Heisenberg uncertainty principle states that it is impossible to specify precisely and simultaneously both the momentum and position of a particle.[1] The most complete description of a system that can be obtained is the wave function $\Psi(q,t)$ where q represents the set of coordinates necessary to describe the system. The physical interpretation of $\Psi(q,t)$ is that

$$\Psi^*(q,t)\,\Psi(q,t)\,dq_1\,dq_2\,\ldots\,dq_{3N} \qquad (1.1)$$

gives the probability at time t of finding the system between q_1 and $q_1 + dq_1$, q_2 and $q_2 + dq_2$, etc.

The wave functions and energies of a molecule are found by solving the Schrödinger equation[2]

$$\mathcal{H}\,\Psi(q_i,q_\alpha) = E\,\Psi(q_i,q_\alpha) \qquad (1.2)$$

where q_i and q_α represent the electronic and nuclear coordinates, respectively. $\mathcal{H}$ is the Hamiltonian operator and E is a scalar corresponding to the energy of the system. When the Hamiltonian includes operators for both nuclear energy and electronic energy then E is the total energy of the molecule.

If nuclei and electrons are regarded as point masses and relativistic interactions are neglected, then the molecular Hamiltonian is given by a sum of terms comprising the operators for the kinetic energy of the nuclei, the kinetic energy of the electrons, the repulsions between the nuclei, the attractions between the nuclei and electrons, and the repulsions between the electrons. Since the masses

of nuclei are much greater than those of electrons, nuclei move much slower than electrons and may be regarded as being fixed during electronic motion (the Born-Oppenheimer approximation). Then the nuclear kinetic energy term may be omitted and the Schrödinger equation for electronic motion is given by

$$(\mathcal{H}_{el} + V_{NN})\,\psi_{el} = U\,\psi_{el} \tag{1.3}$$

where ψ_{el} is a time independent wavefunction of the electronic q_i and nuclear q_α coordinates. The energy U is the electronic energy U_{el} plus the energy of nuclear repulsion. $\mathcal{H}_{el}$ is the purely electronic Hamiltonian

$$\mathcal{H}_{el} = -\frac{\hbar^2}{2m}\sum_i \nabla_i^2 - \sum_\alpha \sum_i \frac{Z_\alpha e^2}{4\pi\epsilon_o r_{i\alpha}} + \sum_j \sum_{i>j} \frac{e^2}{4\pi\epsilon_o r_{ij}} \tag{1.4}$$

The nuclear repulsion term V_{NN} is given by

$$V_{NN} = \sum_\alpha \sum_{\beta>\alpha} \frac{Z_\alpha Z_\beta e^2}{4\pi\epsilon_o r_{\alpha\beta}} \tag{1.5}$$

and is a constant for each nuclear configuration. $r_{\alpha\beta}$, r_{ij}, and $r_{i\alpha}$ refer to internuclear, interelectronic, and nuclear-electronic distances, respectively. Equation 1.5 may be calculated separately and the solution added to U_{el}.

When the Born-Oppenheimer approximation is invoked, the energy difference between two states, ΔU, is the difference between energies obtained by solving eq. 1.3.

1.2.2 Kinetics

The probability of a transition between two states has been

approximated by first-order time-dependent perturbation theory.[3]

The Hamiltonian for the system in the absence of the perturbation is $\mathcal{H}^{(0)}$. The Hamiltonian for the perturbed system is given by

$$\mathcal{H} = \mathcal{H}^{(0)} + \mathcal{H}^{(1)} \tag{1.6}$$

The time dependence of the system is contained in both the first-order perturbation correction to the Hamiltonian $\mathcal{H}^{(1)}$, which is small, and a time-dependent term in the wave function. The theory discussed here is developed for the case where the time dependence of both functions is harmonic. The eigenfunctions of $\mathcal{H}^{(0)}$ are $\Phi_n^{(0)}(q,t)$ and are assumed to be known. The solution to the general Schrödinger equation is found by approximating the eigenfunctions $\Phi_m(q,t)$ of $\mathcal{H}$ with a linear combination of the $\Phi_n^{(0)}(q,t)$ functions

$$\Phi_m(q,t) = \sum_n c_{mn}(t)\, \Phi_n^{(0)}(q,t) \tag{1.7}$$

$$= \sum_n c_{mn}(t)\, \psi_n^{(0)} \exp[-i\omega_n t] \tag{1.8}$$

where the time dependence is assumed to be given by the exponential term and $\omega_n = E_n^{(0)}/\hbar$. A transition between two levels is described by the time evolution of a mixture of states that initially comprises almost entirely one pure (unperturbed) state and at time t comprises almost entirely another pure state. By substituting eq. 1.8 and the solution of the unperturbed time-independent Schrödinger equation into the Schrödinger equation for the perturbed time-dependent system, one obtains an expression for the coefficients. If it is assumed that at $t = 0$ all the coefficients except c_{m1} are zero, then an expression is

obtained for $c_{mf}(t)$

$$c_{mf}(t) = \frac{1}{i\hbar}\int_0^t \exp[i\omega_{f1}t]\, H_{f1}^{(1)}(t)\, dt \qquad (1.9)$$

where ω_{f1} is $(E_f - E_1)/\hbar$ and $H_{f1}^{(1)}(t)$ is given by

$$H_{fi}^{(1)}(t) = \langle\psi_f^{(0)}(q)\left|\mathcal{H}^{(1)}(q,t)\right|\psi_1^{(0)}(q)\rangle \qquad (1.10)$$

The time dependence of $\mathcal{H}^{(1)}(t)$ is taken to be

$$\mathcal{H}^{(1)}(t) = \mathcal{H}_0^{(1)}(e^{i\omega t} + e^{-i\omega t}) \qquad (1.11)$$

and $H_{0,f1}^{(1)}$, which represents the time-independent first-order correction, may be placed in front of the integral sign in eq. 1.9.

The probability of finding the system in a state $\psi_f^{(0)}$ at time t if it was initially (at t = 0) in a state $\psi_1^{(0)}$ is

$$P_f(t) \equiv |c_{mf}(t)|^2 \qquad (1.12)$$

Substituting eqs. 1.9 and 1.11 into eq. 1.12 and integrating over time yields an expression which contains the square of the time-independent first-order perturbation matrix element and a time-dependent function.

$$P_f(t) \approx 4\left|H_{0,f1}^{(1)}\right|^2 \left\{\frac{\sin^2\tfrac{1}{2}(\omega_{f1} - \omega)t}{\hbar^2(\omega_{f1} - \omega)^2}\right\} \qquad (1.13)$$

If the transition is being made to a narrow range of states, the total transition probability is the sum of the probabilities for each state

$$P(t) = \Sigma_f P_f(t) \qquad (1.14)$$

Since the frequencies of the levels ν_f lie close together, the sum may be transformed into an integral over the number density of states $n(\nu)$ in the range ν to $\nu + d\nu$

$$P(t) = \int P_f(t) n(\nu_f)\, d\nu_f \tag{1.15}$$

After substituting eq. 1.13 into eq. 1.15 and integrating, the total transition probability is

$$P(t) \simeq (t\hbar^{-2}) |H^{(1)}_{0,fi}|^2 n(\nu_f) \tag{1.16}$$

In this example, the probability increases linearly with time. Therefore it is possible to define a constant transition rate w_{fi} from state i to state f as

$$w_{fi} = P(t)/t \tag{1.17}$$

The density of states is more commonly expressed as the number of states $\rho(\epsilon)$ in an energy range rather than a frequency range where

$$\rho(\epsilon) = n(\nu)/h \tag{1.18}$$

By substituting eqs. 1.16 and 1.18 into eq. 1.17, one obtains the expression known as Fermi's Golden Rule

$$w_{fi} = (2\pi\hbar^{-1}) |H^{(1)}_{0,fi}|^2 \rho(\epsilon_f) \tag{1.19}$$

which gives the probability of transition between two electronic states.

1.3 Linear Free Energy Relationships

The above discussion has shown that the energy of a state is determined by using the Hamiltonian operator $\mathcal{H}^{(0)}$ and that the transition rate between two states is proportional to the square of the

matrix element of t first-order time-independent perturbation that mixes the two states. There is no *a priori* relationship between $\varkappa^{(0)}$ and $\varkappa^{(1)}$. Consequently one might predict that no relationship should exist between the energy difference between two states and the rate of transfer between them. However, a number of empirical expressions have been developed which do relate rate and energy.[4] They are commonly termed Linear Free Energy Relationships (LFER) but would be better classed as correlation relationships since linearity is not universal, particularly over a wide range of variables, and physico-chemical properties other than thermodynamic quantities are sometimes employed.[5] Considerable effort has been invested in their development, based on the conviction that structure and function are intrinsically related.

The validity of all LFER's is based on the assumption that for a series of reactions only one independent variable changes. In this context a reaction series is defined as a set of homologous reactions in which structural changes in the reactants are limited to substitutions outside the formal reaction zone which act as small perturbations to the reaction zone.[6] To justify this assumption, the "separability postulate"[7] is invoked which states that for a function of two variables (e.g. structural change and reaction) the two variables can be separated when the higher terms of a Taylor expansion of the variables are small enough to be neglected. This is possible over a limited range and for functions of a certain "well-behaved" type.[5] The problem is one of differences and similarities. The reactions studied must be sufficiently similar to be classed as a series and different enough to provide a range of some variable. In practice, this is sometimes difficult to achieve and the criterion applied is based on pragmatism.

If the LFER holds, then the reactions under investigation are believed to comprise a series that is a function of one variable and all other parameters (*e.g.* the reaction mechanism) are constant. If the LFER is not followed, then the reactions are considered to be too disparate to be classed as a series.

The first LFER that found wide support was the Brønsted catalysis law[8]

$$\log k_{HA} = \alpha \log K_{HA} + \text{const} \qquad (1.20)$$

It relates the rate constant k_{HA} to the acid dissociation constant K_{HA} for a general acid catalysis reaction by acid HA. α is called the Brønsted constant.

For rate-equilibrium relationships similar to eq. 1.20 a major source of failure was pointed out by Eigen in 1964.[9] After the rate constant has reached its diffusion-controlled limit, further increase in the equilibrium constant can only level the curve at a diffusion-controlled plateau.

During the past two decades several LFER's specific to electron transfer reactions have been investigated. The widest experimental support has been found for an empirical relationship proposed by Rehm and Weller[10,11] (eq. 1.21) to explain bimolecular ET in solution. Although equations based on theory originated by Marcus[12,13,14] have found substantial confirmation, the LFER derived from this theory, eq. 1.22, has found less support. Both the Rehm-Weller and the Marcus relationships may be expressed in terms of the following standard Gibbs energies: the energy change ΔG°, the activation energy $\Delta G^{\ddagger}$, and the intrinsic barrier $\Delta G^{\ddagger}(0)$, which is the activation energy when ΔG° is zero.

The Rehm-Weller equation is

$$\Delta G^{\ddagger} = \frac{\Delta G^{\circ}}{2} + \left[\left(\frac{\Delta G^{\circ}}{2}\right)^2 + \left(\Delta G^{\ddagger}(0)\right)^2 \right]^{\frac{1}{2}} \qquad (1.21)$$

and the Marcus equation is

$$\Delta G^{\ddagger} = \Delta G^{\ddagger}(0)\left[1 + \frac{\Delta G^{\circ}}{4\Delta G^{\ddagger}(0)}\right]^2 \qquad (1.22)$$

When one of these expressions for activation energy is substituted into a rate equation for an electron-transfer reaction, the expression can be tested. Use of the Rehm-Weller equation predicts that as ΔG° becomes more negative, the rate constant will increase to a maximum and remain there; it is significant that the shape of this curve corresponds to that of a bimolecular reaction reaching a diffusion controlled plateau. The Marcus equation predicts that the ET rate constant will increase to a maximum and then decrease in what is known as the "inverted" or "anomalous" region.

CHAPTER 2. THEORY

In order to measure a reaction rate, it is necessary to define a reference time zero. Fast bimolecular reactions, like many ET reactions, must be studied under conditions that permit measurement of the ET reaction, not of solution mixing. A convenient method employs the reaction of electronically excited states; light initiates a reaction between species which do not react until light is absorbed. The reaction may be monitored by the decay of excited-state emission or by growth of a product. Time zero is defined as the time at which light impinges on the sample which is often equated with the time at which light is absorbed by the photosensitizer.

This chapter discusses the thermodynamics of excited-state electron-transfer reactions, electron-transfer theory, and emission quenching as it pertains to ET.

2.1 Reaction Thermodynamics

Electronically excited molecules, that have lifetimes longer than the time required for thermal equilibration in all degrees of freedom other than electronic relaxation ($\geq$ 1 ps in condensed media), may be treated as separate chemical species with corresponding equilibrium thermodynamic quantities.[15,16] If it is assumed that $\Delta S^{\circ} \approx 0$ and $\Delta V^{\circ} \approx 0$ for the excitation process, then standard reduction potentials may be defined for excited states in terms of the ground state potentials and the excitation energy. The assumption that $\Delta S^{\circ} \approx 0$ is equivalent to assuming that vibrational and rotational constants of the excited state are the same as those of the ground state. The assumption that $\Delta V^{\circ} \approx 0$ is reasonable for all but very small molecules.[15]

Changes in shape, size, and solvation of an excited state with respect to the ground state cause a shift between absorption and emission maxima (the Stokes shift). When the Stokes shift is small, it is valid to assume that $\Delta S^\diamond$ is zero. In this case, the reduction potential of a one electron excited state is reasonably approximated by

$$E^\diamond_{D^+,D^*} = E^\diamond_{D^+,D} - U_{o-o}(D-D^*) \qquad (2.1)$$

where $E^\diamond_{D^+,D^*}$ is the reduction potential of D^+ to D^*. $U_{o-o}(D-D^*)$ is the one electron potential corresponding to the spectroscopic energy difference between the zero vibrational levels of the excited state and the ground state.

Consequently, $\Delta G^\diamond$ for electron transfer from D^* to A is given by

$$\Delta G^\diamond = E^\diamond_{D^+,D} - E^\diamond_{A,A^-} - U_{o-o}(D-D^*) \qquad (2.2)$$

where $E^\diamond_{D^+,D}$ and $E^\diamond_{A,A^-}$ are the reduction potentials of D^+ (to D) and A, respectively.

$\Delta G^{\diamond\prime}$ is the Gibbs energy change between reactants separated by a distance R. It is related to $\Delta G^\diamond$ by

$$\Delta G^{\diamond\prime} = \Delta G^\diamond + w^p - w^r \qquad (2.3)$$

where w^r and w^p are the work terms for bringing the reactants and products from infinity to a separation distance R. w^r and w^p can be calculated from Debye-Hückel theory;[17] they are proportional to ion charge and are inversely proportional to the separation distance R and the static dielectric constant of the solvent. When both reactants are doubly charged and the products are singly and triply charged, the sum of the work terms is equal to that for neutral reactants undergoing

charge separation.

$$w^p - w^r \simeq -e^2/4\pi\epsilon_o\epsilon R_{DA} \qquad (2.4)$$

where ϵ is the dielectric constant of the solvent and R_{DA} is the center-to-center distance between the reactants.

The solvent dependence of $\Delta G^\ddagger$ may be treated by an equation derived by Weller[18] which is based on the Born equation for individual ion solvation. The Gibbs energy change for radical ion pair formation, ΔG_{rip}, in a solvent of dielectric constant ϵ^{sol}, is related to the donor and acceptor oxidation and reduction potentials in a reference solvent of dielectric constant ϵ^{ref} by

$$\Delta G_{rip} = \Delta G^\ddagger_{ref} + \frac{e'}{2\epsilon^{sol}}\left[\frac{1}{r_A} + \frac{1}{r_D} - \frac{2}{R_{DA}}\right] - \frac{e'}{2\epsilon^{ref}}\left[\frac{1}{r_A} + \frac{1}{r_D}\right] \qquad (2.5)$$

where r_A and r_D are the acceptor and donor radii, respectively, and e' represents the term $e^2/4\pi\epsilon_o$.

Further references to Gibbs energies will assume the inclusion of work and solvent correction terms.

2.2 Electron-Transfer Theory

The theory of electron-transfer reactions in solution has been discussed in numerous publications (*e.g.* 19,20,21,22). Section 2.2 summarizes the current state of relevant concepts and equations developed for outer-sphere bimolecular ET reactions. Outer-sphere ET reactions are those which occur when the reactants do not share a common atom or group or, more generally, when interaction between the relevant electronic orbitals of the two reaction centers is weak. The treatment presented here generally follows the 1985 review by Marcus and Sutin.[19]

2.2.1 Classical Theory

The classical description of outer-sphere ET is based on the activated complex theory developed by Marcus.[12,13,14] A fundamental idea was identified by Libby[23] who described the barrier to an ET reaction in terms of the solvent reorientation necessitated by a change in charge distribution. This concept had been developed by Franck with reference to excited-state transitions.[24]

The essence of the ET problem is the fact that the equilibrium nuclear configurations before and after electron transfer are different.[25] The configuration change involves changes in the vibrations and rotations of solvent dipoles and changes in the reactant bond lengths and bond angles. Since nuclei are much heavier than electrons, the time scale of nuclear motion (10^{-11} - 10^{-13} s) is much longer than electronic motion ($\simeq 10^{-15}$ s) and consequently the Franck-Condon principle applies: during the time of electron transfer, nuclei do not change their positions or momenta significantly. Therefore ET occurs at a nuclear configuration common to both reactants and products, which is termed the transition state or activated complex. The change in energy between the equilibrium reactant nuclear configuration and the transition-state configuration constitutes an activation barrier to the reaction.

Bimolecular ET reactions may be formulated as a sum of several steps. First the donor D and acceptor A diffuse together to form a precursor complex D|A. Then D|A reorganizes to the transition state $(D|A)^{\ddagger}$ and ET occurs to produce a successor complex $D^{+}|A^{-}$ which initially has the same nuclear configuration as $(D|A)^{\ddagger}$. The successor relaxes to a new equilibrium configuration and may dissociate into separated ions.

$$D + A \underset{k_{-D}}{\overset{k_D}{\rightleftharpoons}} D|A \qquad (2.6)$$

$$D|A \underset{k_{-ET}}{\overset{k_{ET}}{\rightleftharpoons}} D^+|A^- \qquad (2.7)$$

$$D^+|A^- \xrightarrow{k_{sep}} D^+ + A^- \qquad (2.8)$$

If the reverse ET rate is negligible relative to the rate of $D^+|A^-$ separation, then, using a steady-state approximation, the observed second-order rate constant k_{obs} is given by

$$\frac{1}{k_{obs}} = \frac{1}{k_D} + \frac{1}{K_A k_{ET}} \qquad (2.9)$$

where $K_A = k_D/k_{-D}$.

If $K_A k_{ET} \gg k_D$, then the observed rate is equal to the rate at which the reactants diffuse together and the reaction is diffusion controlled. Approximate bimolecular rate constants for diffusion controlled reactions may be obtained from a simplified Debye expression[26]

$$k_D = 8RT/3\eta \qquad (2.10)$$

where R is the gas constant, T is the temperature, and η is the viscosity of the solvent. Although the derivation of this equation depends on a number of simplifying assumptions (*e.g.* the diffusing species are spherical, of the same diameter, and with the same interaction radii), it succeeds reasonably well in predicting the maximum value of k_{obs} in a variety of solvents. In glycerol, for example, k_D is approximately 6.2×10^6 $M^{-1}s^{-1}$ at 25°C.

If $k_D \gg K_A k_{ET}$, then the $k_{obs} \simeq K_A k_{ET}$. A variety of models have been used to develop specific expressions for $K_A k_{ET}$ which is essentially equivalent to an equilibrium collision frequency in solution multiplied by a reaction efficiency term.[19] K_A may estimated[20] from the Eigen-Fuoss equation which includes a correction for ionic strength effects from Debye-Hückel theory.

$$K_A = (4\pi/3)N_A d^3 \exp[-w^r/RT] \qquad (2.11)$$

where N_A is Avogadro's number, d is the sum of reactant radii, assuming spherical reactants, and w^r is a work term described above. The first-order rate constant k_{ET} is taken to be[19] an effective frequency ν_n for motion along the reaction coordinate (referring to mainly vibrational motion but including solvational contributions) multiplied by a reaction efficiency term which incorporates $\Delta G^{\ddagger}$.

$$k_{ET} = \nu_n \kappa_{el} \exp[-\Delta G^{\ddagger}/RT] \qquad (2.12)$$

κ_{el} is an electronic transmission coefficient averaged over reactant separation distance and is the transmission probability for electron transfer per passage of the system through the transition-state configuration. In classical treatments κ_{el} is usually taken to be unity. When κ_{el} is unity, then ν_n is given as a weighted sum of nuclear frequencies ν_j when there are several vibrational motions contributing to ν_n and to λ, which is defined below ($\lambda = \Sigma_j \lambda_j$).

$$\nu_n = \left[\frac{\Sigma_j \lambda_j \nu_j^2}{\Sigma_j \lambda_j} \right]^{1/2} \qquad (2.13)$$

If systems held together by coulombic forces are represented approximately as harmonic oscillators, then the potential energy of the system is a quadratic function of nuclear configuration. When solvational motion, which is not harmonic, is included, the actual profile of a many-dimensional surface is more complicated. It is a less drastic approximation to assume[19] that the Gibbs energy surface is a quadratic function of coordinates since it is a Boltzmann-weighted profile statistically averaged over many coordinates. One-dimensional schematic representations of the many-dimensional energy surfaces are shown in Fig. 2.1 for ET in the normal and inverted regions. The surface P for the precursor complex plus surrounding medium intersects the surface S for the successor complex plus surrounding medium at a configuration corresponding to the activated complex in which ET occurs (where the dashed lines intersect in Fig. 2.1).

If one assumes that the force constants before and after ET are equal, then the Gibbs energy of activation $\Delta G^{\ddagger}$ is given by

$$\Delta G^{\ddagger} = \frac{(\lambda + \Delta G^{\circ})^2}{4\lambda} \qquad (2.14)$$

Equation 2.14 has been derived by several approaches[13,14,27] and may be confirmed by the geometrical properties of parabolas. It is this classical Marcus expression that is the source of the predicted quadratic relationship between k_{ET} and ΔG°, resulting in an inverted region when $-\Delta G^{\circ} > \lambda$.

λ is the Gibbs reorganization energy and is defined as the change in Gibbs energy on the precursor energy surface between the equilibrium configurations of the precursor and successor complexes. λ is given by the sum of two terms, the outer λ_o and inner λ_i contributions. λ_o

Figure 2.1: Potential energy surface overlap for electron transfer in the classical harmonic oscillator approximation for both normal (a) and inverted (b) regions. For clarity, the quantum mechanical electron coupling matrix element H_{ps} is included in this Figure to show the first order perturbation to the zero order energy surfaces.

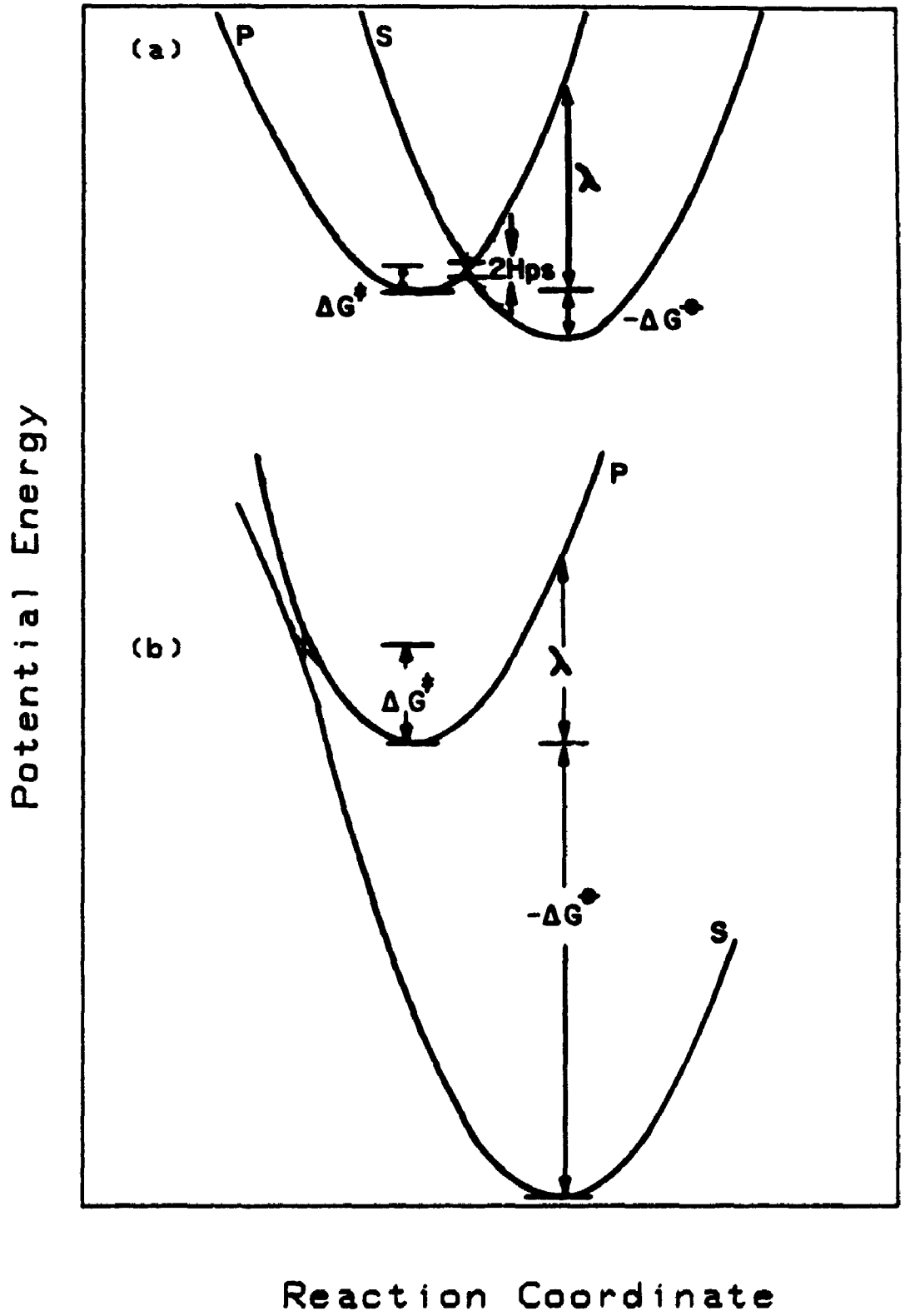
(a)
P
S
λ
2Hps
ΔG‡
-ΔG°
(b)
P
ΔG‡
λ
-ΔG°
S
Potential Energy
Reaction Coordinate

accounts for the changes in solvent orientation and λ_i for changes in bond lengths between the equilibrium states of the precursor and successor complexes.

When the reactant vibrations are treated as harmonic oscillators then

$$\lambda_i = \Sigma_j \frac{f_j^p f_j^s}{f_j^p + f_j^s} (\Delta q_j)^2 \qquad (2.15)$$

where f_j^p is the j^{th} normal mode force constant in the precursor and f_j^s is a similar term for the successor. Δq_j is the change in the equilibrium value of the j^{th} normal coordinate and the sum is taken over all significant vibrations.

An expression for λ_o has been derived using dielectric continuum theory,[13,14,19] where it is assumed that the dielectric polarization outside the coordination shells responds linearly to changes in charge, and consequently the Gibbs energy depends quadratically on charging parameters. This treatment allows the individual solvent dipoles to move very anharmonically.

$$\lambda_o = \frac{1}{2} \epsilon_o N_A \left[\frac{1}{\epsilon_{op}} - \frac{1}{\epsilon_s}\right] \oint_V \left[E^p - E^s\right]^2 dV \qquad (2.16)$$

where E^p and E^s are the electric fields exerted at each point dV by the precursor and successor complexes, respectively, *in vacuo*, and ϵ_{op} and ϵ_s are the optical (square of the refractive index[28]) and static dielectric constants, respectively, of the surrounding solvent.

Integration of eq. 2.16 requires the use of a specific model to determine appropriate boundary conditions. Outer-sphere ET is usually considered to occur between spherical ions that are far enough apart for

the fields around each one to be spherically symmetrical, but not so far apart that the Coulombic forces can be neglected. By assuming spherical, nonpenetrating reactants, and excluding the volume occupied by the reactants from the integration volume, integration of eq. 2.16 gives

$$\lambda_o = \frac{(\Delta e)^2}{4\pi\epsilon_o}\left[\frac{1}{2a_1} + \frac{1}{2a_2} - \frac{1}{R}\right]\left[\frac{1}{\epsilon_{op}} - \frac{1}{\epsilon_s}\right] \tag{2.17}$$

Δe is the charge transferred in the reaction, a_1 and a_2 are the radii of saturated dielectric spheres containing the donor and acceptor, respectively, and R is the center-to-center distance between them.

Other models have been suggested. For example, Cannon[29] replaced the two separated spheres by a prolate ellipsoid which yielded another expression proportional to $[1/\epsilon_{op} - 1/\epsilon_s]$.

2.2.2 Quantum Mechanical Theory

The presence of the electron acceptor site creates an electronic perturbation which mixes the electronic character of D and A. Application of time-dependent perturbation theory to the system gives the Golden Rule result derived in Chapter 1.

$$w_{ps} = 2\pi\hbar^{-1}\langle\Psi_s^\circ|\chi_{e1}|\Psi_p^\circ\rangle^2\rho(\nu_s) \tag{2.18}$$

If the Born-Oppenheimer approximation is valid, then the wavefunctions may be written as products of electronic and vibrational wavefunctions, *e.g.* $\Psi_{sj}^\circ = \chi_{sj}^\circ\psi_s^\circ$. Then

$$w_{p1,sj} = 2\pi\hbar^{-1}H_{ps}^2\,\langle\chi_{sj}^\circ|\chi_{p1}^\circ\rangle^2\rho(\nu_s) \tag{2.19}$$

where

$$H_{ps} = \langle \psi_s^\circ | \chi_{el} | \psi_p^\circ \rangle \qquad (2.20)$$

is called the electronic coupling coefficient. H_{ps} contains the reaction distance dependence which is usually taken as an exponential decrease with increasing reactant separation. When H_{ps} is very small (*e.g.* $H_{ps} \leq 0.025$ eV for a typical transition-metal system[30]) the reaction is said to be non-adiabatic. Larger values of H_{ps} yield adiabatic reactions which correspond to $\kappa_{el} = 1$ in eq. 2.12. For clarity, H_{ps} is illustrated on the classical energy surfaces in Fig 2.1. $\langle \chi_{sj}^\circ | \chi_{pi}^\circ \rangle$ is the vibrational overlap integral (Franck-Condon factor) of the vibrational and solvational wavefunctions. The reaction energy dependence is contained in this term. Figure 2.2 schematically represents vibrational overlap for reactions in the normal and inverted regions.

Equation 2.19 may also be written

$$w_{pi,sj} = 2\pi\hbar^{-1} H_{ps}^2 \Sigma_j \langle \chi_{sj}^\circ | \chi_{pi}^\circ \rangle^2 \delta(\epsilon_{sj} - \epsilon_{pi}) \qquad (2.21)$$

where the summation is over all vibrational levels j in the successor complex. ϵ_{sj} and ϵ_{pi} are the vibrational energies of level j in the successor state and level i in the precursor state, respectively, and δ is a Dirac delta function that ensures energy conservation.

The total transition rate is obtained by multiplying the rate for each vibrational level i in the precursor complex by its fractional population $\exp[-\epsilon_{pi}^\circ/k_BT]/\Sigma_i \exp[-\epsilon_{pi}^\circ/k_BT]$ and summing over all vibrational levels i. Then

Figure 2.2: Potential energy surface overlap in the normal (a) and inverted (b) regions showing overlap of the vibrational wavefunctions.

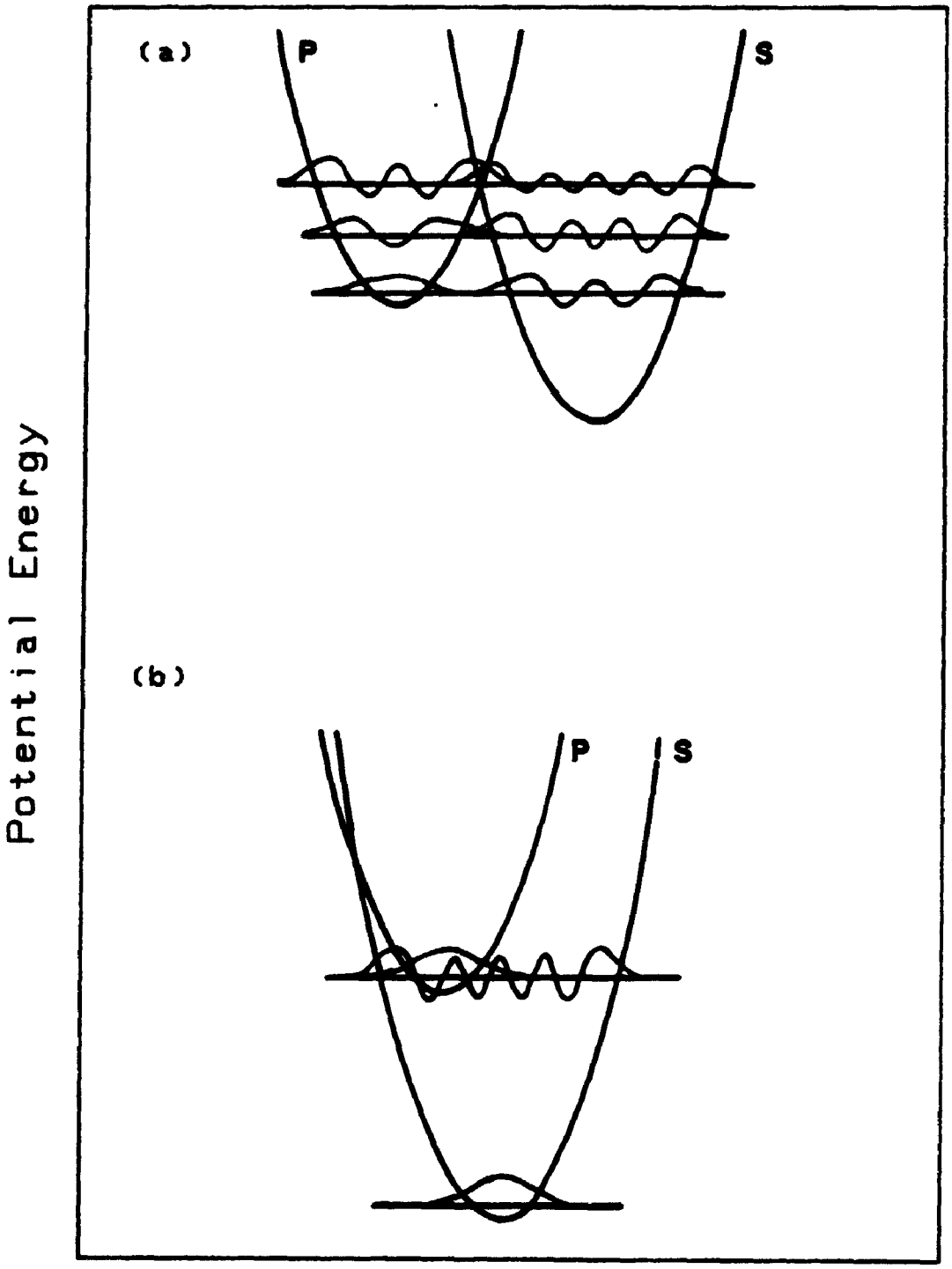
(a)
P
S
(b)
P
S
Potential Energy
Reaction Coordinate

$$k_{ET} = \frac{2\pi}{\hbar} H_{ps}^2 \sum_i \sum_j \frac{\langle \chi_{sj}^{\bullet} | \chi_{pi}^{\bullet} \rangle^2 \exp[-\epsilon_{pi}^{\bullet}/k_B T]}{\Sigma_j \exp[-\epsilon_{pi}^{\bullet}/k_B T]} \qquad (2.22)$$

Equation 2.22 has been solved for a variety of assumptions and limits. If the inner-shell coordinates are treated quantum mechanically as harmonic or anharmonic (Morse) oscillators but the solvent motion (orientational and vibrational) outside the inner coordination shell is treated classically, then eq. 2.22 may be written

$$k_{ET} = \frac{2\pi}{\hbar} H_{ps}^2 \sum_i \sum_j \frac{1}{(4\pi\lambda_o k_B T)^{\frac{1}{2}}} \exp\left[\frac{(-\Delta G^{\bullet} + \Delta\epsilon_\nu + \lambda_o)^2}{4\lambda_o k_B T}\right] FC \qquad (2.23)$$

where FC is the Boltzmann weighted Franck-Condon factor as given in eq. 2.22 for the non-classical motion and $\Delta\epsilon_\nu$ is the vibrational energy of the successor minus that of the precursor for the set of vibrational quantum numbers i and j. This is one of several expressions which have been termed semi-classical. In the high temperature limit or when all of the vibrational frequencies are small ($h\nu \ll k_B T$) this reduces to

$$k_{ET} = \frac{2\pi}{\hbar} H_{ps}^2 \frac{1}{(4\pi\lambda k_B T)^{\frac{1}{2}}} \exp\left[\frac{-(\Delta G^{\bullet} + \lambda)^2}{4\lambda k_B T}\right] \qquad (2.24)$$

resulting in a quadratic relationship between k_{ET} and $\Delta G^{\bullet}$ similar to the classical expression (eqs. 2.12 and 2.14).

When H_{ps} = 0.025 eV and $-\Delta G^{\bullet} = \lambda$ at T = 298 K, then a maximum rate of approximately 10^{13} s^{-1} is predicted from eq. 2.24.

In the inverted region, where $-\Delta G^{\bullet} > \lambda$, the vibrational overlap is far greater than in the normal region (see Fig. 2.2) as the presursor potential curve becomes "embedded" in the successor curve.[20] This

increase is further enhanced by the fact that as the quantum number of the successor vibration becomes larger (as ΔG° becomes more negative) the vibrational wavefunction amplitudes increase in magnitude near the potential-energy curve. The situation becomes analogous to that of non-radiative decay of an excited state which is described by an energy-gap law such as that derived by Siebrand[31] or Robinson and Frosch.[32] The energy-gap law predicts that in the inverted region $\ln k_{ET}$ should decrease linearly as ΔE becomes more negative. This analogy has been supported by calculations made by Siders and Marcus.[33,34,35] Two high frequency internal modes were included in their calculation of the Franck-Condon sum using single mode harmonic oscillator overlap integrals. Under this condition $\ln k_{ET}$ decreases approximately linearly with increasing $-\Delta G^\circ$ in the inverted region.

It is interesting to note that a rate-energy curve which exhibits similar asymmetry in ΔG° may be calculated from classical parabolic energy surfaces if the successor complex is represented by a parabola with a smaller directrix than the precursor (*i.e.* the successor system is modeled by a harmonic oscillator with a greater force constant). If k_2 and k_1 are the force constants of the successor and precursor complexes, respectively, then

$$\Delta G^\ddagger = \frac{k_1}{2}\left(\frac{q^2 + 2\Delta G^\circ/k_2}{2q}\right)^2 \qquad (2.25)$$

ΔG° and $\Delta G^\ddagger$ are related to the potential energy surfaces as shown in Fig. 2.1. q is the separation between the precursor and successor equilibrium configurations and $\lambda = \frac{1}{2}k_1q^2$. The degree of asymmetry in a rate-energy curve calculated using eq. 2.25 depends on the magnitude of the difference between k_1 and k_2; when $k_2 \approx 3k_1$ a curve resembling the

quantum mechanical prediction of Siders and Marcus[34] is obtained.

Asymmetry in rate-energy plots is also found with a relatively simple expression for k_{ET} used by Miller, Beitz, and Huddleston[36] based on a simplification of a semi-classical theory derived by Kestner, Logan, and Jortner.[37]

$$k_{ET} = \left(\frac{\pi}{\hbar^2 \lambda_s k_B T}\right)^{1/2} H_{ps}^2 \sum_{w=0}^{\infty} \frac{e^{-S} S^w}{w!} \exp\left[\frac{-(\Delta G^\circ + \lambda_s + w\hbar\omega)^2}{4\lambda_s k_B T}\right] \qquad (2.26)$$

where the sum is over w, the number of vibrational quanta of the high-frequency vibrations in the product state. This expression incorporates two types of vibrational modes that are rearranged by electron transfer: low-frequency (< 10 cm^{-1}) polarization modes of the solvent and high-frequency (300-3000 cm^{-1}) skeletal vibrations of the reactants.[38] The low-frequency modes are treated classically and the high-frequency modes are assumed to span a narrow range of frequencies, permitting them to be represented by one average frequency ω. The reorganization energies for each ion are defined by

$$\lambda_s = \tfrac{1}{2}\Sigma_i \Delta_i^2 \hbar\omega_i \qquad (2.27)$$

summed over all solvent modes and

$$\lambda_v = \tfrac{1}{2}\Sigma_i \Delta_i^2 \hbar\omega_i \qquad (2.28)$$

summed over all the high frequency modes. The reduced displacements Δ_i are given by

$$\Delta_i = (\mu_i \omega_i / 2\hbar)^{1/2} \Delta R_i \qquad (2.29)$$

where μ_i and ΔR_i are the reduced mass and the displacement in configuration space for the i^{th} vibration, respectively. The electron-

vibration coupling strength S is

$$S = \lambda_v/\hbar\omega \qquad (2.30)$$

Rate-energy curves calculated using classical (eq. 2.24) and semi-classical (eq 2.26) treatments of nuclear motion are shown in Fig. 2.3.

2.3 Excited State Emission Quenching

If it is assumed that the pathways by which an electronically excited molecule decays in the absence of additional solutes are undisturbed by the presence of additional solutes, then excited-state emission quenching may be used to investigate the rate of the quenching reaction. The theories of emission quenching discussed here were developed for energy-transfer reactions. However, in the context of this thesis it will be assumed that electron transfer is the only mechanism causing emission quenching.

2.3.1 Dynamic Bimolecular Quenching

The simplest analysis[26] of bimolecular quenching of emission in solution assumes the following mechanism

	rate	
$D \xrightarrow{h\nu} D^*$	fI'	(2.31)
$D^* \longrightarrow D + h\nu$	$k_1[D^*]$	(2.32)
$D^* \longrightarrow D$	$k_2[D^*]$	(2.33)
$D^* + Q \longrightarrow D^+ + Q^-$	$k_q[D^*][Q]$	(2.34)

The rate of production of the fluorescent state D^* of the photosensitive solute D is constant and equal to the product of the incident irradiance I' and the efficiency of light absorption f. k_2 represents the sum of the rate constants for decay of D^* by all processes other than emission

Figure 2.3: The relationship between log k_{ET} and ΔG_{rip} for classical and quantum mechanical models of electron transfer. The classical relationship (a) was calculated from eq. 2.24 using H_{ps} = 0.025 eV and λ = 1.0 eV. The (semi-classical) quantum mechanical relationship (b) was calculated from eq. 2.26 using H_{ps} = 0.025 eV, λ_s = 0.8 eV, λ_v = 0.2 eV, and $\hbar\omega$ = 1800 cm^{-1}.

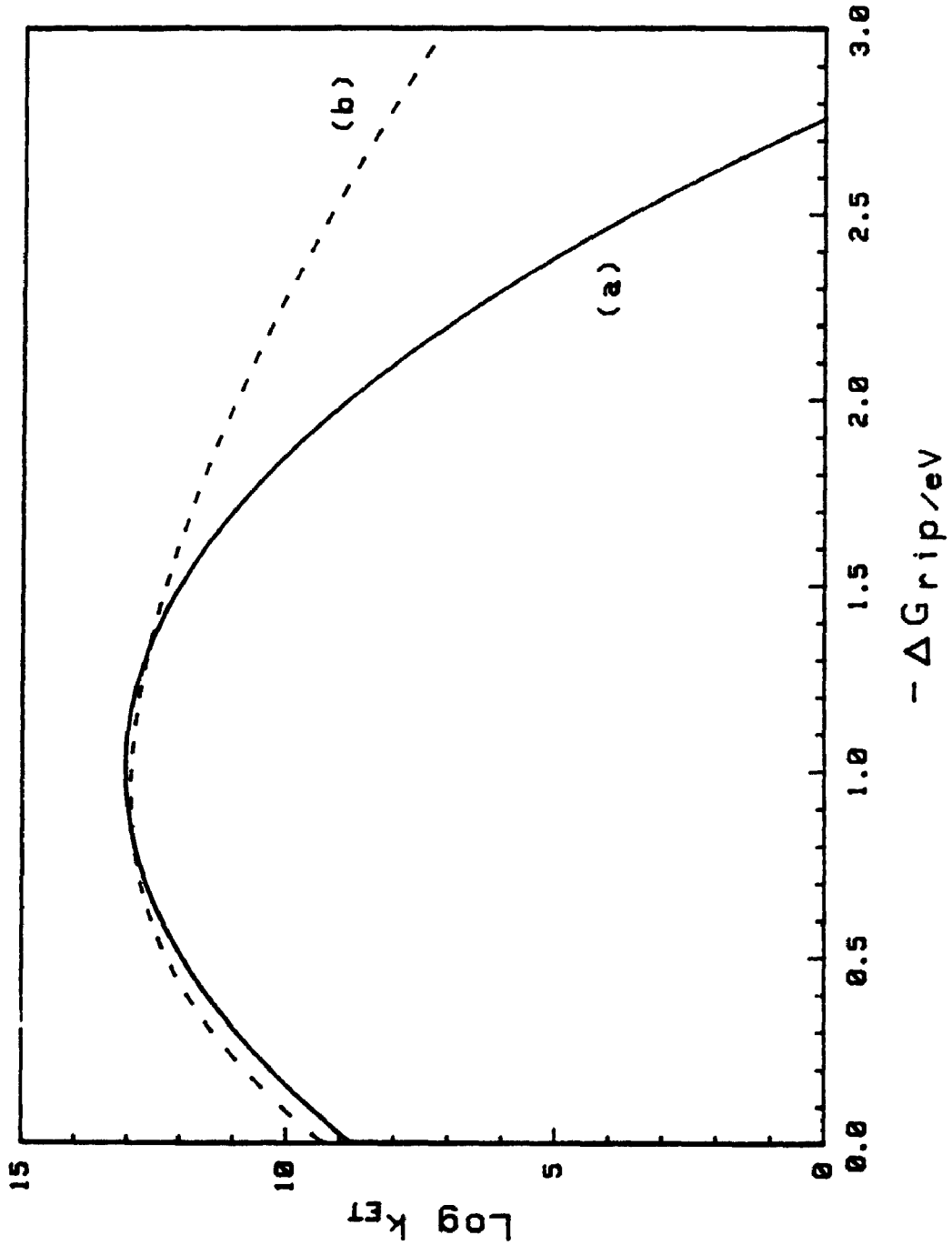
Log k_{ET}
15
10
5
0
0.0
0.5
1.0
1.5
2.0
2.5
3.0
$-\Delta G_{rip}$/eV
(a)
(b)

and bimolecular quenching reactions with a quencher Q.

If one makes the steady-state approximation

$$d[D^*]/dt = 0 \tag{2.35}$$

then in the absence of Q

$$fI' = (k_1 + k_2)[D^*] \tag{2.36}$$

and in the presence of Q

$$fI' = (k_1 + k_2 + k_q[Q])[D^*] \tag{2.37}$$

The emission quantum yield ϕ may be defined as the ratio of the rate of emission to the rate of production of emitting states.

$$\phi = k_1[D^*]/fI' \tag{2.38}$$

In the absence of Q the quantum yield ϕ_o is

$$\phi_o = k_1/(k_1 + k_2) \tag{2.39}$$

and in the presence of Q the quantum yield ϕ_Q is

$$\phi_Q = k_1/(k_1 + k_2 + k_q[Q]) \tag{2.40}$$

From eqs. 2.39 and 2.40 the ratio of quantum yields is

$$\phi_o/\phi_Q = 1 + k_q\tau_o[Q] \tag{2.41}$$

where $\tau_o = 1/(k_1 + k_2)$ and is the lifetime of D^* in the absence of Q (*i.e.* the time required for $[D^*]$ to decay to e^{-1} of an initial value). A frequently used expression that is equivalent to eq. 2.41 is

$$I_o/I = 1 + k_q\tau_o[Q] \tag{2.42}$$

where I is the emission intensity.

Equations 2.41 and 2.42 are known as the Stern-Volmer equations because of their similarity to the equation first formulated by Stern and Volmer[39] for bimolecular collisional quenching in gases.

The assumptions[40] made in the derivation of eqs. 2.41 and 2.42, apart from those always implicit in the steady-state assumption (*i.e.* $[D^*]$ is not significantly changed by the quenching reaction), are (*i*) that the radiation absorbed by D is constant over the period of reaction, (*ii*) that Q reacts only with the state of D^* which contributes to product formation, and (*iii*) that the product is formed only from the state of D^* quenched by Q.

Assumption (*i*) is met if the reduction in [D] caused by reaction is insignificant in comparision to the initial value of [D], or if [D] has a much greater extinction coefficient at the excitation wavelength than any products formed and is present in sufficient concentration to absorb all of the radiation. It is usually preferable to use a small conversion percentage of D which results in a low product concentration that will not interfere with light absorption or the reaction pathway. Failure to meet assumptions (*ii*) and (*iii*) has been discussed in detail.[40] In both cases non-linear Stern-Volmer plots may be observed.

If D^* and Q collide via diffusion, at a rate which is independent of time,

$$D^* + Q \rightleftharpoons D^*Q \qquad (2.43)$$

then it has been shown[41] that the quenching reaction is described by eq. 2.42 at all concentrations of Q. This process is frequently called *dynamic quenching.* However, if D and Q collide, forming a complex before excitation,

$$D + Q \quad \rightleftharpoons \quad DQ \xrightarrow{h\nu} D^*Q \qquad (2.44)$$

the Stern-Volmer plot is no longer linear and the situation is described as *static quenching.* In practice, formation of DQ complexes prior to excitation may be prevented by using low concentrations of Q. However, since transient measurements are independent of the ground state equilibrium,[42] another variation of the Stern-Volmer equation is unaffected by static quenching.

$$\tau_o/\tau = 1 + k_q\tau_o[Q] \qquad (2.45)$$

where τ_o and τ are the emitter lifetimes in the absence and presence of quenchers, respectively, and the condition of low [Q] is not required to obtain k_q.

2.3.2 The Perrin Model of Static Quenching

The phenomenon of energy transfer was originally investigated as a problem in luminescence self-quenching. In 1909 Bruninghaus[43] published a description of the concentration dependence of manganese luminescence in solid calcium phosphate solutions in which he identified an optimum concentration. The intensity of emitted light I was found to fit the expression

$$I = Kc \exp[-kc] \qquad (2.46)$$

where c is the concentration of the photoactive material and K and k are constants.

Studies of liquid solutions by F. Perrin[44] and Wawilow[45] (*i.e.* Vavilov) found that the fluorescence intensity was given by an expression of the same form as eq. 2.46, although their experimental

results and theoretical expressions for emission at small concentrations did not agree. Perrin determined that fluorescence intensity from a very thin sample is proportional to an exponential function of concentration c and some constant k. He concluded that the constant is the inverse of the concentration c_m which yields optimum fluorescence. Consequently, the fluorescent power ϕ, which was defined as the fluorescence intensity per unit mass of fluorophor, tends towards a limit ϕ_o as the concentration approaches zero and

$$\phi = \phi_o \exp[-c/c_m] \tag{2.47}$$

The Vavilov expression

$$K = K_o \exp[-\alpha(c - c_o)] \tag{2.48}$$

identifies a critical concentration c_o necessary to cause a decrease of the absolute fluorescence yield K_o. K_o is determined at low concentrations and α is a constant. Both F. Perrin and Vavilov base their theoretical discussion on one of the two suggestions made earlier by J. Perrin[46] to explain a decrease in luminescence at higher concentrations: when two active molecules are sufficiently close together, their fields overlap and they are coupled in such a way as to diminish their power of responding to excitation. J. Perrin later described the concentration dependence in terms of "deactivating impacts".[47]

The effect of diffusion was discussed by both F. Perrin[44] and Vavilov.[45] F. Perrin concluded that diffusion decreased the observed value of c_m. Vavilov developed his analysis of quenching in terms of collision frequency; c_o is therefore determined by the lifetime of the

excited state τ and the diffusion coefficient D of the emitting species.

In 1926 these ideas were developed in a more quantitative form by Merritt[48] who stated that, if two active molecules are separated by a certain distance ρ, then their luminescence is either completely destroyed or greatly reduced. The probability that molecule B will not lie within a sphere of radius ρ around molecule A is $(V - v)/V$, where V is the total volume and v is the volume of the sphere of radius ρ. The probability that all of the other molecules lie outside v is $(1 - v/V)^N$ where N is the total number of active molecules. The number of active molecules that are free to radiate is $N(1 - v/V)^N$, and, after excitation, the intensity of luminescence is

$$I = \mathcal{I}N(1 - v/V)^N \tag{2.49}$$

$$= \mathcal{I}N \exp[-gN] \tag{2.50}$$

where

$$g = -\ln[1 - v/V] \tag{2.51}$$

and $\mathcal{I}$ is a constant. When v/V is small, g is approximately equal to v/V, and

$$I = \mathcal{I}N \exp[-(v/V)N] \tag{2.52}$$

Energy transfer between molecules of different species was also considered by Sveshnikoff[49] in studies of fluorescence quenching of dyes. In his extension of the Smoluchowski theory of diffusion control to bimolecular reactions he combined Vavilov's notion of an active sphere surrounding a photoexcited donor with the Smoluchowski radius of closest approach,[50] at which reaction occurs instantaneously.

The Perrin model of energy transfer, as it is now known,[51] is

applied specifically to solid media, although, as described above, the concepts were originally developed for liquid solutions. It is named[52] for J. Perrin who first recognized that direct "electrodynamic mutual exchange" between an excited molecule and its neighbor can cause a transfer of excitation energy. The Perrin model assumes that[51]

1. The donor and acceptor are fixed in space during the lifetime of the excited donor D^*.

2. There exists a quenching sphere about D^* of radius R_c and volume v within which an acceptor A will deactivate D^* with unit efficiency.

3. If A is located outside the sphere, then D^* is unquenched.

The quenchers that do not cause quenching must be located in the volume (V - v) where V is the total solution volume. The number of quenching molecules is the product of the quencher concentration [Q], Avogadro's constant N_A, and the total solution volume V. The probability of "not quenching" (*i.e.* emission) P_E is

$$P_E = [(V - v)/V]^{[Q]N_A V} \tag{2.53}$$

$$= \exp\{[Q]N_A V \ln(1 - v/V)\} \tag{2.54}$$

$$= \exp\{-vN_A[Q]\} \qquad \text{for } v/V \ll 1 \tag{2.55}$$

The intensity of emission I in the presence of quenchers is found from the probability of emission and the intensity of emission in the absence of quenchers I_o

$$I = P_E I_o \tag{2.56}$$

Consequently (from eqs. 2.55 and 2.56)

$$I/I_o = \exp\{-\nu N_A[Q]\} \qquad (2.57)$$

In 1931 Frank and Vavilov[53] combined the concept of a quenching sphere with the probability of collision and the probability of emission, and derived a more general relation

$$I_o/I = (1 + k_q\tau_o[Q]) \exp\{\nu N_A[Q]\} \qquad (2.58)$$

Most subsequent models of quenching lead to relations which are similar in form or approximate to eq. 2.58.[54]

2.4 The Application of Static Quenching to Electron Transfer

The capture volume model was applied to electron-transfer reactions by Miller.[55] Since ET reactions initiated by a pulsed electron beam continued for several minutes following each pulse, he modified the model to incorporate a time dependent reaction radius. It was assumed that during a period of time t all electrons trapped less than the distance R(t) from a scavenger would travel to the scavenger. Electrons trapped at larger distances were assumed to remain in the traps. R(t) was defined as the distance at which $k(R)_{ET} = t^{-1}$. This model was revised[56] when it was found that the data were better fit by taking $k(R)_{ET} = (gt)^{-1}$ where g is dimensionless constant with a value of 1.9.

Miller and coworkers[36,56,57] expressed the rate constant for electron transfer (*e.g.* eq. 2.22) as

$$k(R)_{ET} = 2\pi\hbar^{-1} H_{ps}^2 F\rho \qquad (2.59)$$

where $F\rho$ is a thermally averaged, Frank-Condon-weighted density of

states term, equivalent to the double sum in eq. 2.22. They used a common approximation[58] for the electronic coupling coefficient H_{ps}

$$H_{ps} = H_{ps}(R_o) \exp[-(R - R_o)/2a] \tag{2.60}$$

where R_o is the sum of donor and acceptor radii, R is the center-to-center ET reaction distance, and a is a range parameter that determines the steepness of the rate-distance dependence. Then $k(R)_{ET}$ is approximately

$$k(R)_{ET} = \nu_o F \exp[-(R - R_o)/a] \tag{2.61}$$

where

$$\nu_o \equiv 2\pi\hbar^{-1}H_{ps}(R_o)^2\rho \tag{2.62}$$

Initially,[56] F and ρ were separated for simplicity, but later versions[36,57] retained the product $F\rho$ as the thermally averaged Franck-Condon-weighted density of states (FCWD).

Since, by definition, $k(R)_{ET}$ is equal to $(gt)^{-1}$ when the reactants are separated by R(t), eq. 2.61 may be rearranged to solve for R(t)

$$R(t) = R_o + a\,\ln[g\nu_o Ft] \tag{2.63}$$

Consequently, R(t) is a logarithmic function of the Franck-Condon factor which contains the reaction energy dependence.

In analogy to eq. 2.57, R(t) is found from

$$A(t)/A_o(t) = \exp\{-(4/3)\pi c[R(t)^3 - R_o^3]\} \tag{2.64}$$

A(t) and $A_o(t)$ are the time dependent absorbances of the electron donor, with and without acceptors, respectively; $A(t)/A_o(t)$ gives the fraction of donors which have not transferred electrons at time t. c is the

number of acceptors per unit volume.

Since the data[36] could not be fitted by a time-independent Franck-Condon factor, the rates of different reactions at the same time were compared. The relative Franck-Condon factors, F_i, for two reactions were found by manipulating eq. 2.63.

$$F_2/F_1 = \exp[R_2(t) - R_1(t)]/a \qquad (2.65)$$

The relationship between k_{ET} and R_c is established more clearly for emission quenching experiments. An exact mathematical model of luminescence quenching was developed by Inokuti and Hirayama[59] for processes obeying the rate equation 2.66

$$k(R) = \frac{1}{\tau_o} \exp\left[\frac{2R_q}{L}\left(1 - \frac{R}{R_q}\right)\right] \qquad (2.66)$$

L is a positive constant called the effective Bohr radius, τ_o is the excited-state lifetime in the absence of added quenchers, and R_q is the Dexter[60] donor-acceptor separation distance at which the rate of energy transfer is equal to the rate of unquenched luminescent decay. Inokuti and Hirayama derived a decay function of donor luminescence and concluded that the relative luminescence yield I/I_o approaches Perrin model behavior as R_q becomes much larger than L (*e.g.* at $R_q \simeq 10^2 L$). Consequently, for critical radii much larger than L, the Perrin radius R_c and the Dexter-Inokuti-Hirayama radius R_q are equivalent. This has been confirmed[61] by fluorescence and phosphorescence quenching studies from which critical radii were calculated according to both models and found to be almost identical.

Miller, Peeples, Schmitt, and Closs[62] recognized that since eq. 2.61 has the same form as eq. 2.66, Inokuti and Hirayama's result

may be applied to electron-transfer reactions. They obtained time-independent measures of R_q from fluorescence quenching in rigid solutions by defining R_q as the distance at which the ET quenching rate equals the normal fluorescence decay rate τ_o. Then, from eq. 2.61

$$R_q = R_o + a\,\ell n[\nu_o \tau_o F] \tag{2.67}$$

Since $R_q \simeq R_c$, R_q was obtained from eq 2.68

$$I_o/I = \exp\{(4\pi/3)[A]N_A R_q^3\} \tag{2.68}$$

and related to ΔG^* contained in the Franck-Condon factor F by eq. 2.67. A correction for finite molecular volume is given by

$$(R_q')^3 = (R_q\text{-observed})^3 + R_o^3 \tag{2.69}$$

Since the value of R_q depends on the emitter lifetime (see eq. 2.67), R_q must also be normalized (by manipulating eq. 2.67) to some lifetime characteristic of the series of emitters used in the experiment.

$$R_q\text{-corr} = R_o + a\,\ell n\{\exp[(R_q' - R_o)/a]/n\} \tag{2.70}$$

where n is a normalizing factor determined by τ_o for each emitter.

Figure 2.4 shows R_q and k_{ET} as a function of ΔG_{rip}. Both measures of rate were calculated from eq. 2.26 using the same parameters. The calculation of R_q also used eq. 2.67 with a typical[75] value for the range parameter a = 0.75 Å.

Figure 2.4: Rate-energy relationships comparing log k_{ET} (- - -) and R_q (———). Both are calculated from eq. 2.26 using H_{ps} = 0.001 eV, λ_s = 0.1 eV, λ_v = 0.6 eV, and $\hbar\omega$ = 400 cm^{-1}. The calculation of R_q also uses eq. 2.67 with τ_o = 1 μs, a = 0.75 Å, and R_o = 10 Å.

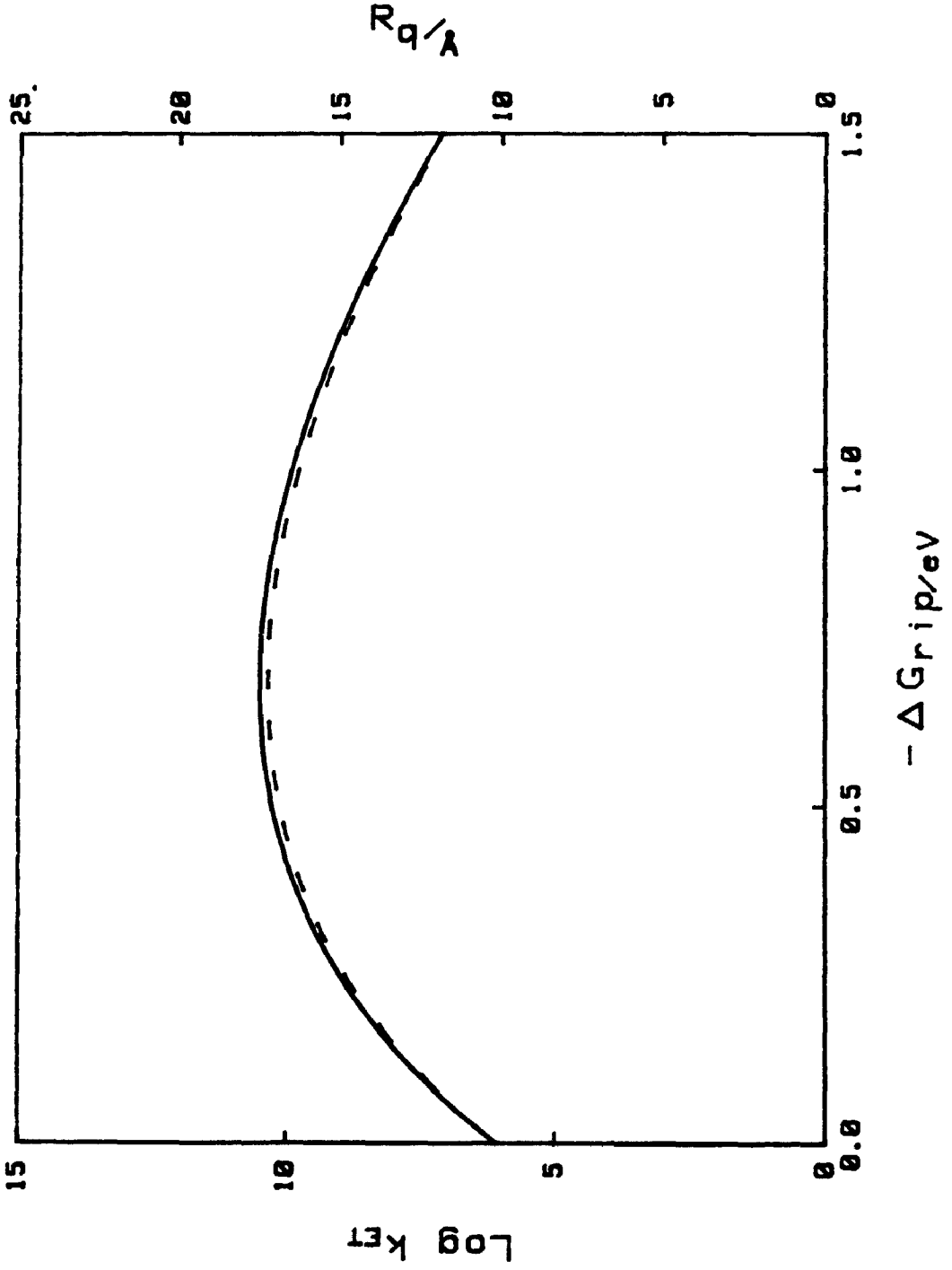
$R_{q/Å}$
25.
20
15
10
5
0
1.5
1.0
0.5
0.0
$-\Delta G_{rip/eV}$
Log k_{ET}
15
10
5
0

CHAPTER 3 LITERATURE REVIEW AND EXPERIMENTAL DESIGN

Chapter 3 describes the rationale on which the work presented in this thesis was based. Recent literature is summarized and used to identify the essential experimental condition required to observe inverted behavior. The experimental design that was chosen to achieve this condition is described and new methods to obtain R_c are presented.

3.1 Literature Review

Several predictions made by Marcus theory, for example, the cross relation, have found considerable support.[19] However, the prediction that ET rates will decrease at high exergonicities has been less successful until recently.

Numerous emission quenching studies of bimolecular ET reactions in solution (for example, refs. 11,63,64,65,66) have failed to demonstrate the predicted rate decrease at high exergonicities. Rate constants are observed to increase to a maximum at moderate exergonicities (-0.3 to -0.6 eV) and remain there to the highest exergonicities attainable ($\approx$ -3.0 eV).

The leveling effect which diffusion control exerts on the rate constants of very fast reactions is well known.[*e.g.* 9,55] In addition to this phenomenon, a variety of explanations have been suggested to account for the apparent absence of inverted behavior. They include (i) competing mechanisms at large $-\Delta G^{\circ}$, such as H-atom transfer,[33] formation of products in excited electronic states,[56] or exciplex formation,[67] (ii) quantum effects such as nuclear tunneling[68], (iii) a modifying effect caused by the range of distances over which ET occurs,[33] and (iv) the increase of λ with distance in case (iii),

thereby reducing the extent of inversion.

Several small indications ("vestiges") of decreased rates at high exergonicities have been reported.[69,70,71,72,73] More recently, clear evidence of inverted behaviour has been seen in a limited number of specially designed experiments.

Miller et al.[36] examined ET between aromatic molecules in methyltetrahydrofuran (MTHF) at 77 K. Biphenyl radical anions, created by pulse radiolysis, reacted with 28 different acceptors such as naphthalene or phenanthrene. The reactions were monitored by measuring the time-dependent absorbance of the biphenyl radical anion at 650 nm. R(t) and relative Franck-Condon factors were obtained from eqs. 2.64 and 2.65, respectively, as described in section 2.4. Plots of F_2/F_1 against $-\Delta G^{\ddagger}$ showed maxima at approximately 0.8 eV and 1.1 eV for $t = 10^{-6}$ s and 10^2 s, respectively. The inverted region decrease resembled a linear rather than a quadratic function of $-\Delta G^{\ddagger}$ and the data were fitted with a semiclassical expression for k_{ET} (eq. 2.26) using $\lambda_s = 0.4$ eV and $\lambda_v = 0.4$ eV for $t = 10^{-6}$ s, and $\lambda_s = 0.76$ eV and $\lambda_v = 0.4$ eV for $t = 10^2$ s.

The same experimental design was used by Kira[74] in a study of ET from amines and aromatic hydrocarbons to radiation induced cations, trapped holes, and solute cations in *sec*-butyl chloride glasses at 77 K. A different method of data analysis took the survival probability of acceptor cations to be

$$\frac{A(t)}{A_o(t)} = \exp\left\{-[D]\int_0^{\infty}\{1 - \exp[\nu(R)FCt]\}4\pi R^2\, dR\right\} \qquad (3.1)$$

where $\nu(R)$ is a function of donor trap depth. FC and t in eq. 3.1 were said to be "mathematically equivalent" leading to eq. 3.2, from which

the Franck-Condon factor was found.

$$\Delta \log(FC) = -\Delta \log(t) \qquad (3.2)$$

A plot of FC against ΔG° showed a maximum at about -0.8 eV and an almost horizontal plateau between -0.8 eV and -3.0 eV.

Miller et al.[62] obtained R_q from eq. 2.68 by emission quenching with 20 organic donors and 3 acceptors in rigid room-temperature *trans*-1,5-decalindiol and in ethanol at 77 K. A plot of R_q-corr against $-\Delta G^{\circ}$ showed an increase in R_q-corr to 15.5 Å as $-\Delta G^{\circ}$ increased to the most exergonic system at -1.57 eV.

Equation 2.68 was used also by Guarr, McGuire, Strauch, and McLendon[75] to measure R_q for a series of polypyridine ruthenium donors and the acceptor methyl viologen, dispersed in glycerol and cooled to between 248 K and 276 K. The maximum R_q-corr = 15.5 Å was found at ΔG° = -0.7 eV. One further point showed a decrease to 14.2 Å at 1.0 eV. λ was estimated to be approximately 0.8 eV.

Another method to achieve rigid matrices was used by McLendon and Miller.[76] Porphyrin and metalloporphyrin redox sites were embedded in protein matrices and pseudo-unimolecular ET between active sites was induced by pulse radiolysis or flash photolysis. The four data points were fitted by a classical Marcus expression for k_{ET} with λ = 0.8 eV. The most exergonic datum at approximately -1.2 eV showed a decrease from the maximum k_{ET} by *ca* 50 fold.

Miller, Calcaterra, and Closs[77] used pulse radiolysis (in MTHF at 296 K) to add electrons to either end of large molecules which were synthesized by connecting members A and B of the desired redox couples to rigid, saturated hydrocarbon spacers. Electrons were captured by A

or B with almost statistical probability and photometric absorption measured the rate at which the initial distribution achieved equilibrium. Four points were found in the inverted region and the data were fitted with eq. 2.26 using λ_s = 0.75 eV and λ_v = 0.45 eV.

Wasielewski, Niemczyk, Svec, and Pewitt[78] used emission decay to obtain unimolecular rate constants for ET between porphyrins and quinones joined by a rigid chemical linkage. The reactants were dissolved in butyronitrile or in toluene at 294 K. Rate constants for the forward (light-induced) reaction appeared in the normal portion of the curve while those for reverse reactions (decay of product biradicals to ground-state reactants) decreased in the inverted region. A maximum occurred at approximately $k_{ET} = 2.5 \times 10^{11}$ s^{-1} and ΔG_{rip} = -0.9 eV.

Another experiment using rigidly linked reactants was performed by Irvine, Harrison, Beddard, Leighton, and Sanders.[79] They observed photoinduced ET in complexes formed by porphyrins capped with methyl viologen or quinone groups in several solvents. Both charge separation and charge recombination were observed and log rate was plotted as a function of ΔG_{rip}. In the inverted region k_{ET} fell from 3×10^{11} s^{-1} at ΔG° = -0.7 eV to 4×10^{9} s^{-1} at -2.07 eV. Data were reasonably well fit by a quantum mechanical expression for k_{ET}.

An elegant experiment was designed by Ohno, Yoshimura, and Mataga.[80] In order to observe bimolecular electron transfer in solution in the absence of diffusion, they observed the back reaction within geminate ion pairs. It was assumed that successor complexes $D^+|A^-$ have two options: they may diffuse apart, yielding separated products D^+ and A^-, or back electron transfer to the ground state reactants may occur, yielding D and A. Ruthenium polypyridine donors and aromatic amine acceptors were dispersed in acetonitrile or acetonitrile-water mixtures.

Concentrations of the photo-excited states and ET products were determined spectroscopically immediately after laser excitation and after complete decay of the excited state. k_q was found from emission quenching. Hence the fraction f of bimolecular quenching which produced free radicals was calculated. f is related to the rate constant for the back reaction k_b and the rate constant for geminate pair dissociation k_{dis} by

$$k_b/k_{dis} = (1/f) - 1 \qquad (3.3)$$

Plots of $\log(k_b/k_{dis})$ against $\Delta G^{\ddagger}$ show a bell-shaped curve with a maximum at -1.7 eV.

A similar approach by Gould, Moser, Ege, and Farid[81] obtained smoother curves in the inverted region. This study used 9,10-dicyanoanthracene and 2,6,9,10-tetracyanoanthracene as photosensitive acceptors and biphenyl, diphenylacetylene, and naphthalene derivatives as electron donors. 4,4'Dimethoxystilbene (DMS) was added to scavenge the radical cations which escaped from the photo-product radical ion pair and the resulting DMS radical cation was monitored spectroscopically. The relative yields of product ion formation for the different redox couples were converted to absolute yields ϕ_{sep} by using the benzophenone triplet state as an actinometer. k_{ET} for the back reaction was found from

$$\phi_{sep} = k_{sep}/(k_{sep} + k_{ET}) \qquad (3.4)$$

Steady-state product analysis studies determined k_{sep} to be approximately 5×10^8 s^{-1}. k_{ET} was calculated and plotted against $\Delta G^{\ddagger}$. The data all appear in the inverted region and do not quite reach the

maxima of curves calculated with λ = 1.9 or 1.75 eV.

Another variation of this experiment by Vauthey, Suppan, and Haselbach[82] determined the ion yield by photoconductivety measurements, avoiding the added complication of scavengers. Photocurrents were calibrated by monitoring the product absorption of one system to determine the ion yield. k_{sep} was taken to be approximately constant at 5×10^8 s^{-1} and k_{ET} for the back reaction was calculated from

$$k_{ET} = k_{sep}(1 - \phi_{sep})/\phi_{sep} \qquad (3.5)$$

Data from the photosensitive acceptor 9,10-dicyanoanthracene and a range of 21 electron donors spanned nearly 2 eV. The rate maximum occurred at approximately -1.6 eV and the data were fitted best with a semiclassical expression for k_{ET}.

3.2 Experimental Design

The inverted region has been clearly demonstrated (by the presence of more than datum point) in three types of experimental design: (i) forward ET between reactants dispersed in low- or room-temperature glasses,[36] (ii) intramolecular ET in forward,[77] reverse,[78] or a combination of both,[79] reactions and (iii) reverse ET in geminate ion pairs.[80,81,82] The characteristic common to these experiments is that diffusion is excluded from the reaction sequence. k_{obs} is thus independent of diffusion and cannot be diffusion controlled. The conclusion drawn from these examples is that inverted behavior has not been observed in bimolecular ET because fast reactions are rate-limited by diffusion. The top of the rate-energy curve is masked by diffusion control and rate decreases are expected in systems of sufficient exergonicity or if diffusion is eliminated from the reaction mechanism.

Diffusion is eliminated in the present work by using the condition of high acceptor concentration which results in static quenching. The critical quenching distance R_q is calculated as a diffusion-independent measure of ET rate.

R_q is found from eq. 2.58 by emission quenching (using the Inokuti and Hirayama conclusion $R_c \simeq R_q$) and from eqs. 3.13 and 3.14, described below, by EPR spectroscopy. Single photon counting is used to measure quenched and unquenched lifetimes and k_q is found from eq. 2.45.

Thus static and dynamic measures of reaction rate (R_q and k_q, respectively) are obtained from the same samples under identical conditions.

3.3 New Methods to Obtain R_c

In addition to the use of donor emission quenching, ET reactions may be investigated by observing the formation of acceptor radicals. Two methods described here permit the calculation of R_c from the concentration of product radicals. Any technique capable of measuring an observable that is a known function of the radical concentration may be employed. Both methods require the use of an electron source or sacrificial donor which is able to reduce the photosensitive primary donors after they are photo-oxidized, blocking the reverse ET reaction.

3.3.1 The Saturation Method

The first method applies only to solutions that are sufficiently rigid to prevent reactant diffusion during the time of the experiment. Solutions of the donor D, acceptor A, and sacrificial donor S are cooled to achieve the desired rigidity. The following reaction sequence is initiated by irradiation

$$D + h\nu \longrightarrow D^* \quad (3.6)$$

$$D^* + A \longrightarrow D^+ + A^- \quad (3.7)$$

$$D^+ + S \longrightarrow D + S^+ \quad (3.8)$$

S^+ decomposes irreversibly. Continuous irradiation causes this sequence to repeat until all the acceptors within R_c of each donor are reduced, which is indicated by saturation of the product signal. The product concentration is determined from a standard curve relating concentration to signal size. The volume occupied by reduced acceptors is calculated from the product concentration and the original acceptor concentration. The volume per donor is found, and R_c is the radius of this volume.

Preliminary experiments using this method are described in Appendix 6. The project was not completed because of time and money limitations.

3.3.2 The Probability Method

The second method may be used with liquid or solid solutions. The probability that excited donors will be unquenched by electron transfer is related to the fraction of sample volume occupied by the "active sphere" volume in solid media (*i.e.* eq. 2.57).

$$I/I_o = \exp\{-vN_A[Q]\} \quad (3.9)$$

Equation 3.9 may be written

$$D_u/D_o = \exp\{-vN_A[Q]\} \quad (3.10)$$

where D_o is the concentration of excited donors in the absence of quencher, and D_u is the concentration of excited donors unquenched by added acceptors. Equivalently

$$1 - D_q/D_o = \exp\{-vN_A[Q]\} \quad (3.11)$$

where D_q is the concentration of excited donors quenched by added acceptors. Since each donor quenched by electron transfer yields one product radical, D_q is equal to the concentration of radicals produced in a given irradiation time t. D_o is found by increasing the acceptor concentration until there is an acceptor within R_c of every excited donor during t. The product concentration is then independent of acceptor concentration and D_o is equal to the product concentration at time t.

All experimental techniques useful with this method must measure some observable that is related to D_q or D_o by a proportionality constant. The constants cancel in eq. 3.11 and need not be known.

Experiments determine the product signal size P as a function of acceptor concentration for constant D and S concentrations and an arbitrary irradiation time. Signal size values are selected from the ranges where P depends on acceptor concentration (P_d) and where P is independent of acceptor concentration (P_{ind}). Then

$$1 - (P_d/P_{ind}) = \exp\{-vN_A[Q]\} \quad (3.12)$$

This method may be used in fluid media by employing an equation analogous to eq. 2.58

$$[1 - (P_d/P_{ind})]^{-1} = (1 + k_q\tau_o[Q]) \exp\{vN_A[Q]\} \quad (3.13)$$

Finally

$$R_c = [(3/4\pi)\, v]^{1/3} \quad (3.14)$$

CHAPTER 4 MATERIALS AND SAMPLE PREPARATION

Chapter 4 describes the choice and suitability of the chemical systems, donor synthesis and identification, reactant purification, and sample preparation.

4.1 Choice of Materials

The choice of reactants was determined by suitability and availability. The reactants were required to react by photoinduced electron transfer which limited the systems to species where either the donor or the acceptor showed a unique optical absorption. The series of systems was also required to be homologous and to span as wide a range as possible of ΔG° values.

A homologous series of ruthenium(II) polypyridines was chosen as photosensitive ET donors because the photophysical and electron transfer properties of these compounds are known in detail.[16] Since the excited states consist of a manifold of several substates of varying singlet and triplet character, radiative excited state decay is termed emission rather than fluorescence or phosphorescence.

1,1′-dimethyl-4,4′-bipyridinium dication, which is more commonly known as the methyl viologen dication (MV^{2+}), was chosen as the electron acceptor for a number of reasons. When reverse ET is blocked, the methyl viologen radical is stable in degassed glycerol and detectable by EPR or by absorption spectroscopy. The redox chemistry and electronic structure of MV^{2+} have been fully characterized[83] and the energy of the lowest MV^{2+} excited state is 20,000 cm^{-1}.[84] Consequently, RuL_3^{2+*} deactivation can occur only by electron transfer and not by energy transfer. With the RuL_3^{2+} complexes available, MV^{2+} provides a useful range of ΔG_{rip} values (see Table 4.3).

Ethylenediaminetetraacetic acid (EDTA) is a convenient sacrificial electron donor since its function as a sacrificial donor in the RuL_3^{2+}-MV^{2+} system (eqs. 3.6 to 3.8) is well known.[85] Although there is some evidence that the EDTA oxidation products reduce MV^{2+} thermally,[86] the number of $MV^{+\cdot}$ radicals produced by this mechanism would be proportional to the number of EDTA molecules oxidized, and therefore proportional to the number of $MV^{+\cdot}$ radicals produced by photoinduced ET. The proportional increase in the product signal would cancel in eq. 3.13, and the calculated value of R_q would be unaffected.

Since MV^{2+} and EDTA are known[87] to form complexes in aqueous solution, complexation in glycerol was investigated by optical absorption spectroscopy. Difference spectra were obtained (see section 4.3.1 for a description of the spectrophotometer) by adding individual spectra and subtracting the spectrum of a solution containing a mixture of the system components. Peaks in the difference spectra indicate the presence of a new species (a complex) in the mixture solution. Difference spectra show that complexation did not occur between ruthenium complexes and MV^{2+} or between the ruthenium complexes and $EDTA^{3-}$, but did occur between $EDTA^{3-}$ and MV^{2+}. A sample difference spectrum is shown in Fig. 4.1.

In an attempt to reduce the extent of MV^{2+}-$EDTA^{3-}$ complexation, EDTA was preciptated as a complex of Fe^{3+}, Al^{3+}, or Ca^{2+}, all of which have high equilibrium constants for the complex formation reaction (1.3×10^{25}, 1.3×10^{16}, and 5.0×10^{10} M^{-1}, respectively[88]). The iron complex absorbed light in the ruthenium compound absorption range and the aluminum complex was gelatinous and difficult to collect, but the calcium complex was white and easy to handle. However, difference

Figure 4.1: A difference spectrum shows the difference (·····) between the absorption spectrum (———) of a sample containing two species and the sum of spectra (- - -) of samples each containing one species. The concentration of MV^{2+} is 0.25 M and the concentration of $EDTA^{3-}$ is 0.15 M.

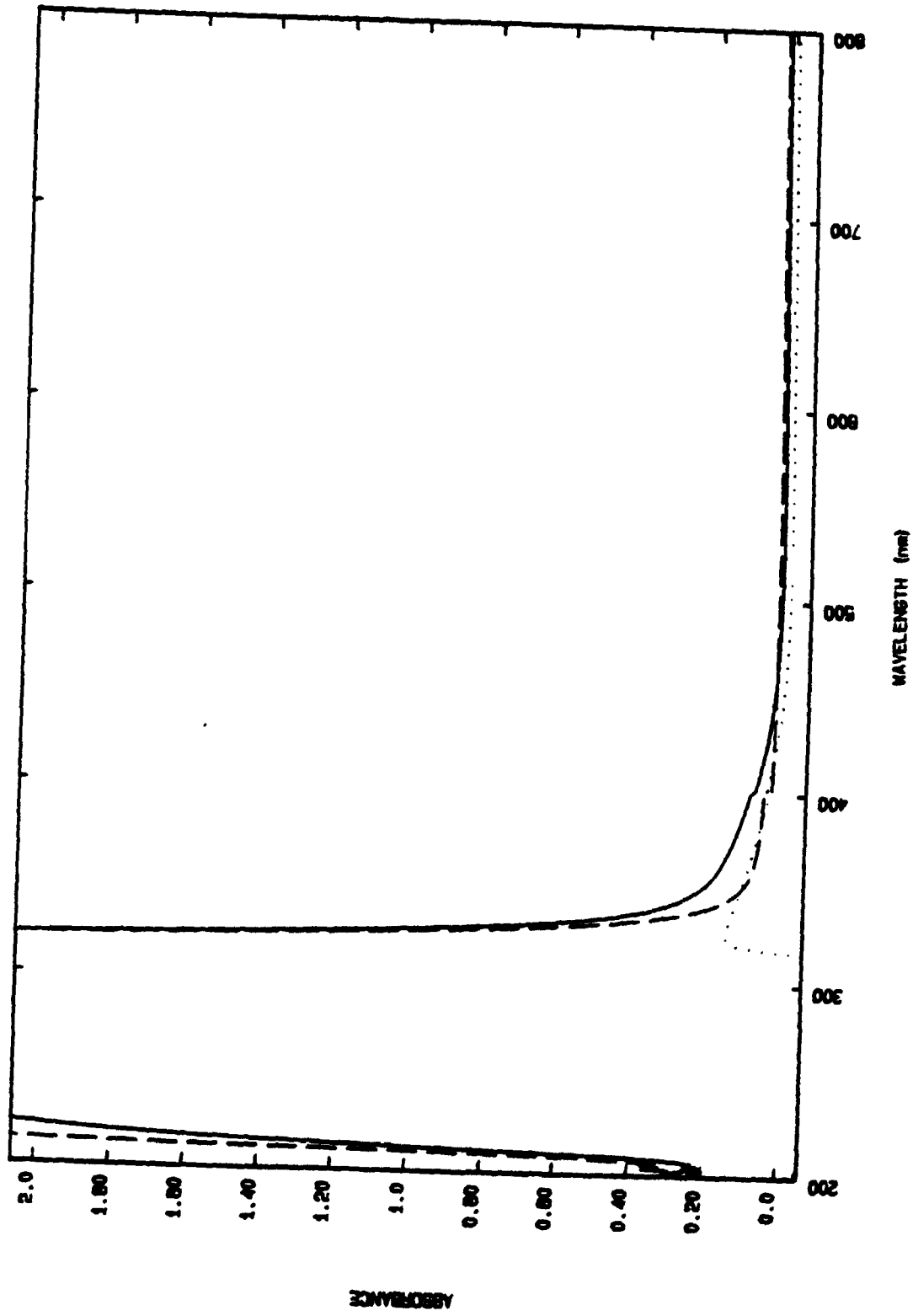
800
700
600
500
400
300
200
WAVELENGTH (nm)
2.0
1.80
1.60
1.40
1.20
1.0
0.80
0.60
0.40
0.20
0.0
ABSORBANCE

spectra showed that further complexation with MV^{2+} was similar to the complexation seen with the sodium salt. Since nothing was gained by this approach, it was abandoned.

Several other sacrificial donors were investigated. Sodium ascorbate was only sparingly soluble in glycerol. MV^{2+} was thermally reduced by triethanolamine, sodium ascorbate, phenylhydrazine, and methylhydrazine. Difference spectra showed complexation between MV^{2+} and cysteine, sodium pyruvate and mercaptoethanol. Glyoxylic acid, dinitrodiphenylhydrazine, and N,N-dimethylglycine did not appear to function as sacrificial donors since no light-induced product signals were found in solutions containing them and $Ru[bpy]_3^{2+}$. It was decided to further investigate $EDTA^{3-}$-MV^{2+} complexation and the function of $EDTA^{3-}$ in the redox system to determine whether or not $EDTA^{3-}$ interfered with the photo-induced results.

A Benesi-Hildebrand[89] plot was constructed from the absorbance at 380 nm in glycerol solutions containing 0.0478 M MV^{2+} and a range of $EDTA^{3-}$ (from the sodium salt) concentrations between 0 and 0.0875 M. Assuming the concentration of $EDTA^{3-}$ (before complexation) is much greater than the complex concentration, then, from the complex formation equilibrium equation and Beer's law

$$1/\Delta A = 1/(\epsilon \ell [M]) + 1/(K_{eq} \epsilon \ell [M][E]) \qquad (4.1)$$

where ΔA is the change in absorbance between solutions with and without $EDTA^{3-}$ at a wavelength where complex absorption occurred. ϵ is the extinction coefficient of the complex absorption, and [M] and [E] are the concentrations of MV^{2+} and $EDTA^{3-}$, respectively, before complexation occurs. From the slope and intercept, K_{eq} for the formation of MV^{2+}-$EDTA^{3-}$ complexes was found to be 30.3 M^{-1} (see Fig. 4.2). This is less

Figure 4.2: A Benesi-Hildebrand plot determines the equilibrium constant of the MV^{2+}-$EDTA^{3-}$ complex to be 30.3 M^{-1}.

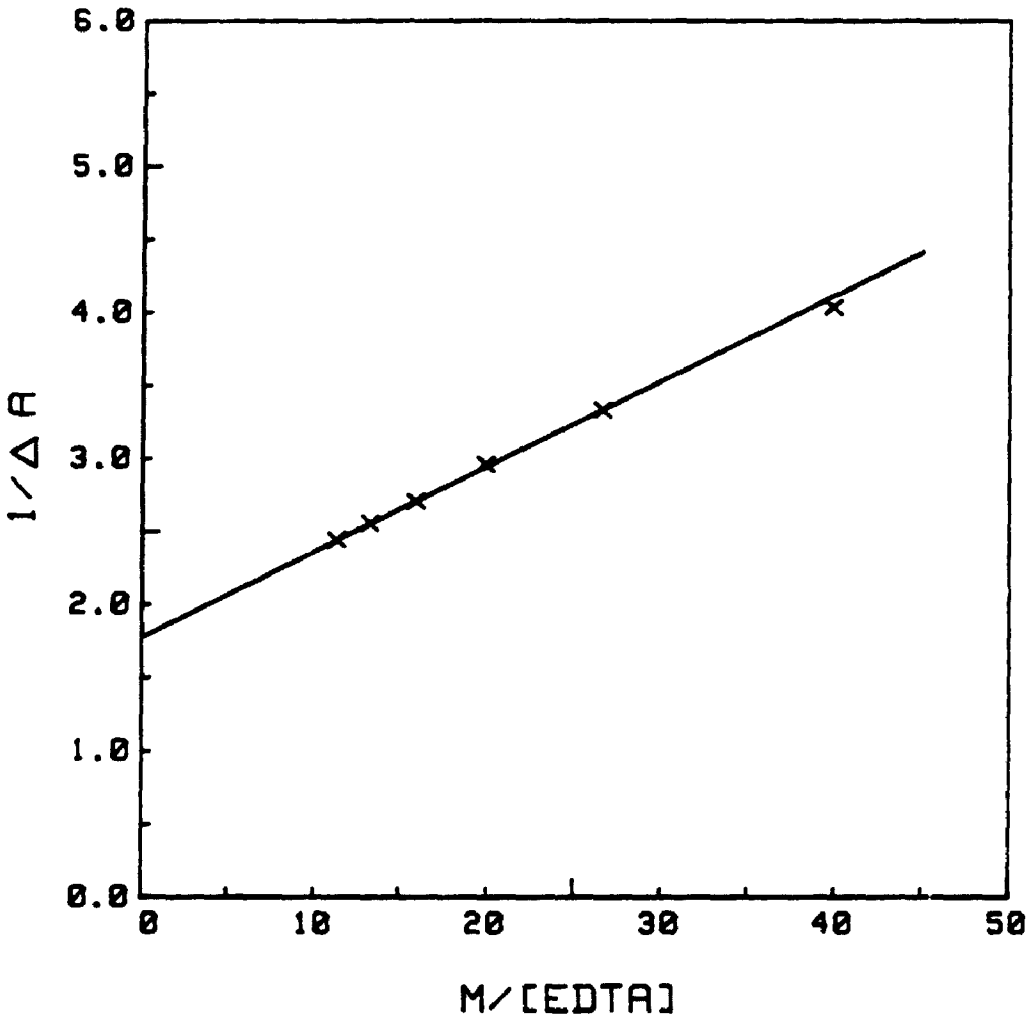
6.0
5.0
4.0
3.0
2.0
1.0
0.0
1/ΔA
0
10
20
30
40
50
M/[EDTA]

than the value of 68 M^{-1} reported for K_{eq} in aqueous solutions,[90] from which it was concluded that, since complexation was less in glycerol solutions, interference in the redox system by EDTA would be less. However, it must be noted that the aqueous solution value of K_{eq} was found at pH = 11.2 and a decrease was reported to occur in less alkaline solution, although values were not given for pH = 8.2.

Although considerable MV^{2+}-$EDTA^{3-}$ complexation clearly occurred, extensive investigations by EPR determined that a range of $EDTA^{3-}$ concentrations existed for which the photoinduced ET results were constant, demonstrating that complexation did not interfere with the ET reaction. Two examples are shown in Fig. 4.3. Both plots span $EDTA^{3-}$ concentrations above and below the MV^{2+} concentration used, demonstrating that, not only was the photoproduct signal independent of [$EDTA^{3-}$], but it was also independent of the relative magnitudes of the $EDTA^{3-}$ and MV^{2+} concentrations. Other experiments determined the [$EDTA^{3-}$]-independent range up to MV^{2+} concentrations of 0.239 M. Here the photoproduct signal was independent of [$EDTA^{3-}$] between concentrations of 0.04 and 0.09 M for irradiation times of 4 min. An $EDTA^{3-}$ concentration of 0.06 M was chosen for all EPR and selected emission quenching test experiments, as well as some preliminary experiments in which $MV^{+\cdot}$ was detected by optical absorption spectroscopy. It was concluded that photoinduced signals were independent of [$EDTA^{3-}$] at this concentration and that EDTA was a useful sacrificial donor.

The ruthenium, MV^{2+}, and EDTA system components were suitable optically because the ruthenium complexes showed an absorption maximum in the region of 450 nm that is distant from the short wavelength (< 380

Figure 4.3: EDTA dependence of light induced EPR signals in systems containing 2.00×10^{-3} M $Ru[bpy]_3^{2+}$ and 0.0253 M MV^{2+} (x) or 2.00×10^{-3} M $Ru[3,4,7,8\text{-}(CH_3)_4phen]_3^{2+}$ and 0.1073 M MV^{2+} (o).

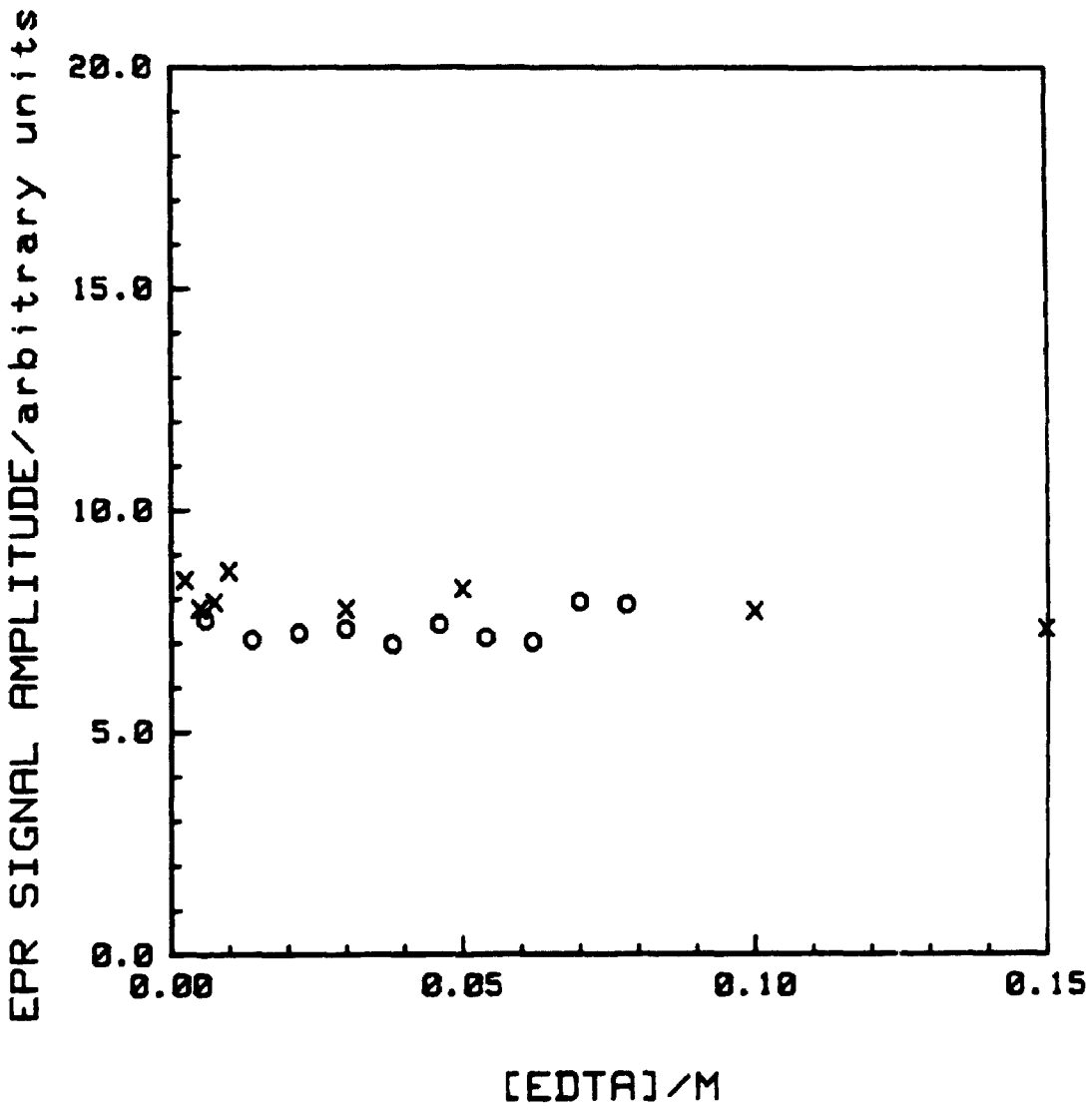
EPR SIGNAL AMPLITUDE/arbitrary units
20.0
15.0
10.0
5.0
0.0
0.00
0.05
0.10
0.15
[EDTA]/M

nm) absorptions of MV^{2+} and $EDTA^{3-}$. An example of the absorption spectra of a system is shown in Fig. 4.4.

All the reactants were soluble in glycerol which was chosen originally so the early low temperature results could be compared to literature values. Glycerol was useful for the liquid media experiments since its use resulted in Perrin plots that showed more shallow curvature than in water and were easier to reproduce.

The above information indicated that the ruthenium complexes, methyl viologen, and EDTA dispersed in glycerol were suitable chemical systems for the proposed experiments. All the materials were available commercially or by synthesis from published methods.

4.2 Synthesis and Purification

Unless otherwise stated all chemicals were reagent grade and were used as received.

In the complexes used, Ru^{2+} is octahedrally coordinated with one or more of the following ligands (L) or substituted ligands: 2,2′-bipyridine (bpy), 1,10-phenanthroline (phen), 2,2′:6′,2′′-terpyridine (tpy), cyanide (CN), N-methylimidazole (NMI), and ammonia (NH_3). In most cases the dichloride salt was prepared; however, several compounds required more massive counterions and were precipitated as a diiodide (complexes 13 and 30 in Table 4.1) or as a diphosphoroushexafluoride (19 and 23).

Tris(2,2′-bipyridine)ruthenium(II) dichloride was purchased (ICN). All other ruthenium complexes were synthesized according to literature methods. Table 4.1 lists the compounds prepared (including precursors) and cites the reference in which the method is described. Starting materials were used as received: $RuCl_3 \cdot 3H_2O$ (Strem), K_2RuCl_6 (ICN),

Figure 4.4: Absorption spectra for the $Ru[bpy]_3^{2+}$ - MV^{2+} system. The components are represented by (———), $Ru[bpy]_3^{2+}$; (- - -). MV^{2+}; (·····), EDTA; and (-·-·-), $MV^{1+\cdot}$.

ABSORBANCE
4.0
3.50
3.0
2.50
2.0
1.50
1.0
0.50
0.0
200
300
400
500
600
700
800
WAVELENGTH (nm)

Table 4.1 Synthesis and Identification by Absorption Spectroscopy

Compound (Precursor)	% Yield	λ_{max}/nm[a] (lit.)	λ_{max}/nm[a] (exptl.)
2. $K_2RuCl_5 \cdot H_2O$[92] ($RuCl_3 \cdot 3H_2O$)	91.0	—	—
3. Ru[4,4′-$(CH_3)_2$bpy]$_3Cl_2$[93] (2.)	74.0	460[93,b]	458
4. Ru[4,4′-$(C_6H_5)_2$bpy]$_3Cl_2$[93] (2.)	15.8	445,474[93]	460.474[c]
5. Ru[3,4,7,8-$(CH_3)_4$phen]$_3Cl_2$[93] (2.)	41.9	438[93]	436
6. Ru[4,7-$(CH_3)_2$phen]$_3Cl_2$[93] (2.)	30.0	425,445[93]	428,444
7. Ru[5,6-$(CH_3)_2$phen]$_3Cl_2$[93] (2.)	67.0	425,453[93]	426,452
8. Ru[4,7-$(C_6H_5)_2$phen]$_3Cl_2$[93] (2.)	36.6	460[93]	458
9. Ru[5-CH_3phen]$_3Cl_2$[93] (2.)	75.5	420,450[93]	422,448
10. Ru[5-C_6H_5phen]$_3Cl_2$[93] (2.)	24.7	420,448[93]	422.450
11. Ru[phen]$_3Cl_2$[93] (2.)	95.7	421,447[93]	420,448
12. Ru[5-Clphen]$_3Cl_2$[93] (2.)	82.7	422,447[93]	422,448
13. Ru[5-NO_2phen]$_3I_2$[93] (2.)	73.4	449[93]	452
14. Ru(bpy)$_2C_2O_4$[94] (K_2RuCl_6)	32.2	—	—
15. cis-Ru(bpy)$_2$(CN)$_2$[95] (14.)	30.6	≈456[96,d]	454[d]
16. Ru(phen)$_2C_2O_4$[94] (K_2RuCl_6)	22.4	—	—
17. cis-Ru(phen)$_2$(CN)$_2$[95] (16.)	23.3	≈448[96,d]	450[d]
18. cis-Ru(bpy)$_2Cl_2$[97] ($RuCl_3 \cdot 3H_2O$)	81.3	550[97,d]	550[d]
19. cis-Ru(bpy)$_2$(NMI)$_2$(PF_6)$_2$[98] (18.)	60.2	483[99,e]	492[e]
20. Ru(tpy)Cl_3[100] ($RuCl_3 \cdot 3H_2O$)	84.9	—	—

(continued)

Table 4.1 (continued)

21. [Ru(tpy)(bpy)Cl]Cl[101] (20.)	81.3	—	—
22. Ru(tpy)(bpy)(OH_2)(ClO_4)$_2$[102] (21.)	64.3	—	—
23. Ru(tpy)(bpy)(NH_3)(PF_6)$_2$[102] (22.)	30.9	482[106]	482
24. 2,2′-bpy-N,N′-O_2[103] (bpy)	81.5	—	—
25. 4,4′-(NO_2)$_2$bpy(O)$_2$[103] (24.)	42.5	—	—
26. 4,4′-Cl_2bpy(O)$_2$[103] (25.)	76.9	—	—
27. 4,4′-(NEt_2)$_2$bpy[104] (26.)	48.7	—	—
28. Ru[4,4′-(NEt_2)$_2$bpy]$_3Cl_2$[93] (27.)	≈70.0	518[105,f]	518[f]
29. 4,4′-(OEt)$_2$bpy[104] (25.)	45.9	—	—
30. Ru[4,4′-(OEt)$_2$bpy]$_3I_2$[93] (29.)	85.4	477[105,f]	476[f]

(a) In water unless otherwise noted.

(b) Perchlorate salt.

(c) Acetonitrile

(d) Methanol

(e) CH_2Cl_2

(f) Ethanol:Methanol 4:1 v/v

2,2′-bpy (Aldrich), 4,4′-$(CH_3)_2$bpy (Aldrich), 4,4′-$(C_6H_5)_2$bpy (ICN), 1,10-phen (Aldrich), 5-Clphen (ICN), 5-NO_2phen (Aldrich), 5-CH_3phen (Aldrich), 5-C_6H_5phen (Sigma), 4,7-$(CH_3)_2$phen (ICN), 5,6-$(CH_3)_2$phen (ICN), 4,7-$(C_6H_5)_2$phen (ICN), 3,4,7,8-$(CH_3)_4$phen (Aldrich), NMI (Aldrich), and 2,2′:6′,2′′-tpy (Aldrich). The final products used in the ET reactions were purified by column chromatography on basic alumina (BDH or Fisher) with acetonitrile or dimethylformamide. Then they were recrystallized from doubly distilled water or 95% ethanol, washed with diethyl ether, and air dried.

Methyl viologen (Aldrich) was precipitated as a dichloride salt from spectroscopic grade methanol by the addition of spectroscopic grade acetone and dried at ≈70°C for 48 hours.

EDTA functions as an electron donor when one or both of the nitrogen atoms are unprotonated.[105] If the EDTA skeleton is represented as Y, then the useful species are the monoprotonated form HY^{-3} and the completely unprotonated Y^{-4}. Since it was found that Y^{-4} reduces MV^{2+} under visible light, the donor of choice was the trianion. The fraction of EDTA in the trianionic form is maximized at a pH of 8.21 (see Appendix 1). However, precipitation of EDTA from a solution adjusted to pH = 8.21 (by adding HCl or NaOH) yielded a solid which, when redissolved, gave a solution of pH = 6.2. It was determined empirically that when EDTA precipitates from a solution adjusted to pH = 8.43, it redissolves to give a solution of pH = 8.21. Consequently EDTA (Fisher) was routinely purified by repeated precipitation of the trisodium salt until a small amount of the solid dissolved to produce a solution of the desired pH. The remainder of the solid was dried for a week at ≈70°C and ground into a powder with a morter and pestle.

Glycerol (BDH) was dried over 4A molecular sieves (BDH) and

distilled under vacuum.

4.3 Ruthenium Compound Identification

The ruthenium complexes used as ET donors were identified by optical absorption spectroscopy and by fast atom bombardment (FAB) mass spectrometry.

4.3.1 Optical Absorption Spectroscopy

Optical absorption spectra were obtained on a Hewlett Packard 8450A diode array spectrophotometer. Literature and experimental values of λ_{max} are listed in Table 4.1. Data for intermediates in the syntheses are given where literature values were available.

4.3.2 Fast Atom Bombardment Mass Spectrometry

Traditional mass spectrometry techniques are not useful with non-volatile or thermally labile compounds. However, the large molecular weight complexes under examination in the present work were found to produce interpretable fast atom bombardment mass spectra.

4.3.2.1 FAB Technique[106,107]

In conventional mass spectrometry, a vaporized sample is bombarded by a stream of high energy electrons, converting some molecules to ions. The ions are accelerated in an electric field and are separated according to their mass to charge ratio by varying the magnetic field.

The kinetic energy of an accelerated ion is

$$\tfrac{1}{2}mv^2 = eV \qquad (4.2)$$

where m is the mass of the ion, v is its velocity, e is its charge, and V is the potential difference between the accelerating plates. In the

presence of magnetic field, a charged particle will travel in a curved flight path.

$$r = mv/eB \tag{4.3}$$

where r is the radius of curvature of the path and B is the strength of the magnetic field. From eqs. 4.2 and 4.3

$$m/e = B^2r^2/2V \tag{4.4}$$

which relates the mass to charge ratio to the path curvature radius, the magnetic field strength, and the electric field strength.

A detector counts the number of ions of a particular m/e, and a recorder prints out a mass spectrum which is a graph of the number of particles detected as a function of mass-to-charge ratio.

This method is limited to chemical species which are volatile below their decomposition temperature.

FAB mass spectrometry bombards the sample with a stream of neutral atoms (argon or xenon). The atoms collide with sample molecules creating ions by momentum transfer in a process known as sputtering. The advantage of this method lies in its ability to generate ions from solutions of relatively non-volatile liquid matrices (glycerol or thioglycerol) and permits the recording of both positive and negative ion spectra of polar molecules, ionic complexes, and high molecular-weight organometallic molecules, all of which are essentially non-volatile or thermally labile under conventional electron impact source conditions.

The spectra reported here were obtained on a Finnigan Matt 8230 double-focusing, sector field mass spectrometer. The FAB gun operated at 4 kV and 0.2 mA with xenon gas. All application programs were

performed by a Digital Corporation PDP 11 central computer.

The compounds were ground to a fine powder and dissolved in approximately 5 μL of glycerol (MW 92.11). Glycerol contributed a regular pattern of peaks to the spectra at 92n + 1 (n = 1,2,3...) in the positive mode and at 92n - 1 (n = 1,2,3...) in the negative mode.

4.3.2.2 FAB Results

The ruthenium complexes belong to three categories: (1) ionic complexes with an acidic proton, (2) ionic complexes without an acidic proton, and (3) neutral complexes. Three mechanisms were proposed[108] to account for the appearance of singly charged molecular ions

$$\text{I.} \quad [M^{2+} - H^{+}]^{1+} \tag{4.5}$$

$$\text{II.} \quad [M^{2+} + e^{-}]^{1+} \tag{4.6}$$

$$\text{III.} \quad [M^{0} + H^{+}]^{1+} \quad \text{or} \quad [M^{2+} + 2e^{-} + H^{+}]^{1+} \tag{4.7}$$

It was expected that complexes of type (1) would react by mechanism I, type (2) would react by II, and type (3) would react by III. Although it was found[108] that the spectra were best fitted by combinations of all three mechanisms, in most cases one mechanism was dominant. Table 4.2 lists the compounds analysed, the mechanisms found, and the m/e peaks expected and found.

Several discrepancies between the results presented here and those in reference 108 likely result from the loss or gain of a proton. Two experiments with complex 11 showed molecular ion peaks differing by 1 dalton, indicating that differences in proton gain or loss could occur readily in different experiments. The expected molecular ion peaks were found (±1) for all complexes except 10 and 13. Reference 108 (which

Table 4.2 FAB Results

Ion	Dominant Mechanism[108]	Molecular Ion Peak	
		Expected	Found
1. $Ru[bpy]_3^{2+}$	II	570	570
3. $Ru[4,4'-(CH_3)_2bpy]_3^{2+}$	I	654	653
4. $Ru[4,4'-(C_6H_5)_2bpy]_3^{2+}$	II	1026	1026
5. $Ru[3,4,7,8-(CH_3)_4phen]_3^{2+}$	I	810	809
6. $Ru[4,7-(CH_3)_2phen]_3^{2+}$	I	726	725
7. $Ru[5,6-(CH_3)_2phen]_3^{2+}$	II	726	726
8. $Ru[4,7-(C_6H_5)_2phen]_3^{2+}$	II,III	1098	1098
9. $Ru[5-CH_3phen]_3^{2+}$	II	684	684
10. $Ru[5-C_6H_5phen]_3^{2+}$	II,III	870	884
11. $Ru[phen]_3^{2+}$	II,III	642	641,642
12. $Ru[5-Clphen]_3^{2+}$	III	745	745
13. $Ru[5-NO_2phen]_3^{2+}$	—	777	756
15. $cis-Ru(bpy)_2(CN)_2$	III	466	467
17. $cis-Ru(phen)_2(CN)_2$	III	514	515
19. $cis-Ru[(bpy)_2(NMI)_2]^{2+}$	—	578	578
23. $Ru[(tpy)(bpy)(NH_3)]^{2+}$	—	508	507
28. $Ru[4,4'-(NEt_2)_2bpy]_3^{2+}$	II	996	996
30. $Ru[4,4'-(OEt)_2bpy]_3^{2+}$	II	834	834

used the compounds prepared for this thesis) found the expected peak for complex 10.

4.4 Sample Preparation

It was concluded that all the desired complexes had been synthesized with the exception of complex 13, about which doubts existed although its optical absorption maximum was reasonably close to the literature value. All the complexes listed in Table 4.2 were accepted for ET experiments. Values of ΔG_{rip} with relevant oxidation potentials are listed in Table 4.3, in the order of increasing $-\Delta G_{rip}$, for all compounds for which experiments were attempted. Time limitations prevented the use of all the donors listed in Table 4.2.

Stock solutions of the three reaction components were prepared by dissolving precisely weighed amounts of the solid (using an analytical balance for $MVCl_2$ and Na_3EDTA and a microbalance for the ruthenium compounds) in aliquots of glycerol measured by a 10.00 mL Trutest Precision syringe (Trudell Co.). Solutions containing MV^{2+} were wrapped with tin foil and handled under reduced light.

EPR samples were prepared by combining aliqots of the stock solutions measured with 0.250, 0.500, and 1.000 mL syringes to achieve the desired concentrations of the three reactants in a total volume of 1.000 mL. Deaeration time dependence experiments determined that the photoproduct signal was independent of deaeration time after 30 min. so, to ensure the rigorous removal of all oxygen, the samples were bubbled with prepurified nitrogen for one hour. Then they were transferred under a nitrogen atmosphere in a glove bag to Suprasil tubes (i.d. 2.0 mm, o.d. 3.0 mm). The tubes were capped with rubber septa and evacuated on a rotary pump line for two hours. Samples were prepared and handled

Table 4.3 Energetics

Ion	$E^{\circ}_{D^+,D^*}$/eV[a,b]	ΔG_{rip}/eV[c]
13. $Ru[5\text{-}NO_2phen]_3^{2+}$	-0.67	-0.24
12. $Ru[5\text{-}Clphen]_3^{2+}$	-0.77	-0.34
1. $Ru[bpy]_3^{2+}$	-0.84	-0.41
11. $Ru[phen]_3^{2+}$	-0.87	-0.44
9. $Ru[5\text{-}CH_3phen]_3^{2+}$	-0.90	-0.47
7. $Ru[5,6\text{-}(CH_3)_2phen]_3^{2+}$	-0.93	-0.50
3. $Ru[4,4'\text{-}(CH_3)_2bpy]_3^{2+}$	-0.94	-0.51
6. $Ru[4,7\text{-}(CH_3)_2phen]_3^{2+}$	-1.01	-0.58
19. $cis\text{-}Ru[(bpy)_2(NMI)_2]^{2+}$	-0.81[d]	-0.65
5. $Ru[3,4,7,8\text{-}(CH_3)_4phen]_3^{2+}$	-1.11	-0.68
15. $cis\text{-}Ru(bpy)_2(CN)_2$	-1.06[e]	-0.94
17. $cis\text{-}Ru(phen)_2(CN)_2$	-1.07[e]	-0.95
30. $Ru[4,4'\text{-}(OEt)_2bpy]_3^{2+}$	-1.09[f,g] to -1.14[f,h]	-0.93 to -0.98
23. $Ru[(tpy)(bpy)(NH_3)]^{2+}$		-1.00[i]
28. $Ru[4,4'\text{-}(NEt_2)_2bpy]_3^{2+}$	-1.30[f,g]	-1.14

Notes to Table 4.3

(a) Standard reduction potentials vs NHE for $RuL_3^{3+} + e^- \rightarrow RuL_3^{2+*}$.

(b) Values are cited in water from ref. 93 unless otherwise noted.

(c) Calculated from eq. 2.5 using an average of the reduction potentials given in refs. 109 (measured vs SCE and corrected to NHE) and 110 (measured vs Ag/AgCl and corrected to NHE) for $MV^{2+} + e^- \rightarrow MV^{+\cdot}$ in each of three reference solvents: -0.427 V (H_2O), -0.208 V (acetonitrile), and -0.168 V (DMF). Average radii were taken to be 7 Å for the ruthenium compounds,[111] 3 Å for MV^{2+},[112] and a contact distance of 10 Å.

(d) In acetonitrile; calculated from the value in ref. 98 versus SSCE.

(e) In DMF from ref. 84.

(f) In acetonitrile from ref. 113.

(g) U_{o-o} is calculated from the emission maximum with a correction factor added.

(h) U_{o-o} is calculated from low-temperature magnetic circular dichroism and luminescence spectra.

(i) Ref. 76

under reduced light; sample tubes were wrapped with tin foil and stored in a dark container.

The samples for static and dynamic emission experiments were prepared by combining aliquots of donor and acceptor stock solutions to obtain the desired reactant concentrations in a total volume of 3.000 mL. The sample bottles were agitated on a shaker for several hours before the samples were transferred to long-necked, square, 1.00 cm, Suprasil emission cuvettes (Hellma). The samples were bubbled with prepurified nitrogen for one hour. Then the cells were capped with rubber septa and the samples were evacuated on a rotary pump line for four hours. Samples were prepared and handled under reduced light. The cuvettes were wrapped with tin foil and stored a dark container.

CHAPTER 5 TRANSIENT EMISSION EXPERIMENTS AND RESULTS

Values for k_q and τ_o were obtained from time-correlated single photon counting experiments. Chapter 5 describes this technique, the experiments that were performed, the method of data analysis, and the results.

5.1 Transient Emission

5.1.1 Time-Correlated Single Photon Counting[114]

The fundamental assumption of the single photon counting experiment is that the emission probability distribution of a single photon is equivalent to the time distribution of emitted light intensity following excitation. The probability distribution is constructed by measuring the time at which the first photon is emitted after an excitation flash under the condition of low light intensity. Repeated flashes build a histogram of counts versus time, which represents the decay curve of the emitter.

The reference time zero is set by an electrical pulse generated by the flash-lamp discharge. Each time the lamp flashes, a synchronization pulse is sent to the time-to-amplitude converter (TAC) which initiates charging of a capacitor. The first emission photon to reach the emission photomultiplier tube (PMT) generates a stop pulse which stops the TAC capacitor charging. The voltage on the capacitor, which is proportional to the elapsed time between the start and stop pulses, is processed by an analog-to-digital converter, and a count is recorded in the appropriate channel of the multichannel analyzer (MCA). The analyzer channels represent increments in time and the counts in each channel are proportional to the probability for fluorescence emission from the sample between t and $t + \Delta t$ where Δt is the time width of each

channel.

5.1.2 Single-Photon Counting Apparatus

The excitation light source was a Coherent picosecond laser system[115] consisting of a Model CR-8 argon ion laser pumping a Model 590 dye laser equipped with a Model 7200 cavity dumper. Rhodamine 6G was used in the dye laser to provide an excitation maximum at 580 nm. The pulse width was less than 300 ps.

The temperature of the sample holder was controlled to 25.0°C by a Neslab Eric 44 temperature controller.

A PRA International, Inc. 3000 Nanosecond Spectrofluorimeter performed the single photon counting experiments. Figure 5.1 shows a schematic diagram of the spectrofluorimeter.

The system was directly interfaced to a DEC MINK-II computer for data analysis.

5.2 Transient Emission Experiments

A set of either 8 or 4 samples was prepared for each ruthenium donor, containing the same concentration of donor and varying concentrations of MV^{2+} from 0 M to some maximum.

The donor concentration was usually approximately 4×10^{-5} M, at which concentration the absorbance at λ_{max} was 0.3 or less. The concentration range between 1×10^{-5} M and 2×10^{-4} M was tested with $Ru[bpy]_3^{2+}$ and the lifetimes found differed by no more then 2%.

The maximum MV^{2+} concentration was specific to each donor and chosen to span the curve found by eq. 2.58. The maximum concentrations ranged between 0.04612 M for $Ru[5\text{-}CH_3phen]_3^{2+}$ and 0.3159 M for $Ru[(tpy)(bpy)(NH_3)]^{2+}$.

Figure 5.1: Schematic diagram of the time-correlated single photon counting apparatus. LAMP is the irradiation source, PMT is the photoultiplier tube, MONO is the monochromater, DISC is the discriminator, TAC is the time-to-amplitude converter, ADC is the anologue-to-digital converter, MCA is the multichannel analyzer, and COMP is the computer.

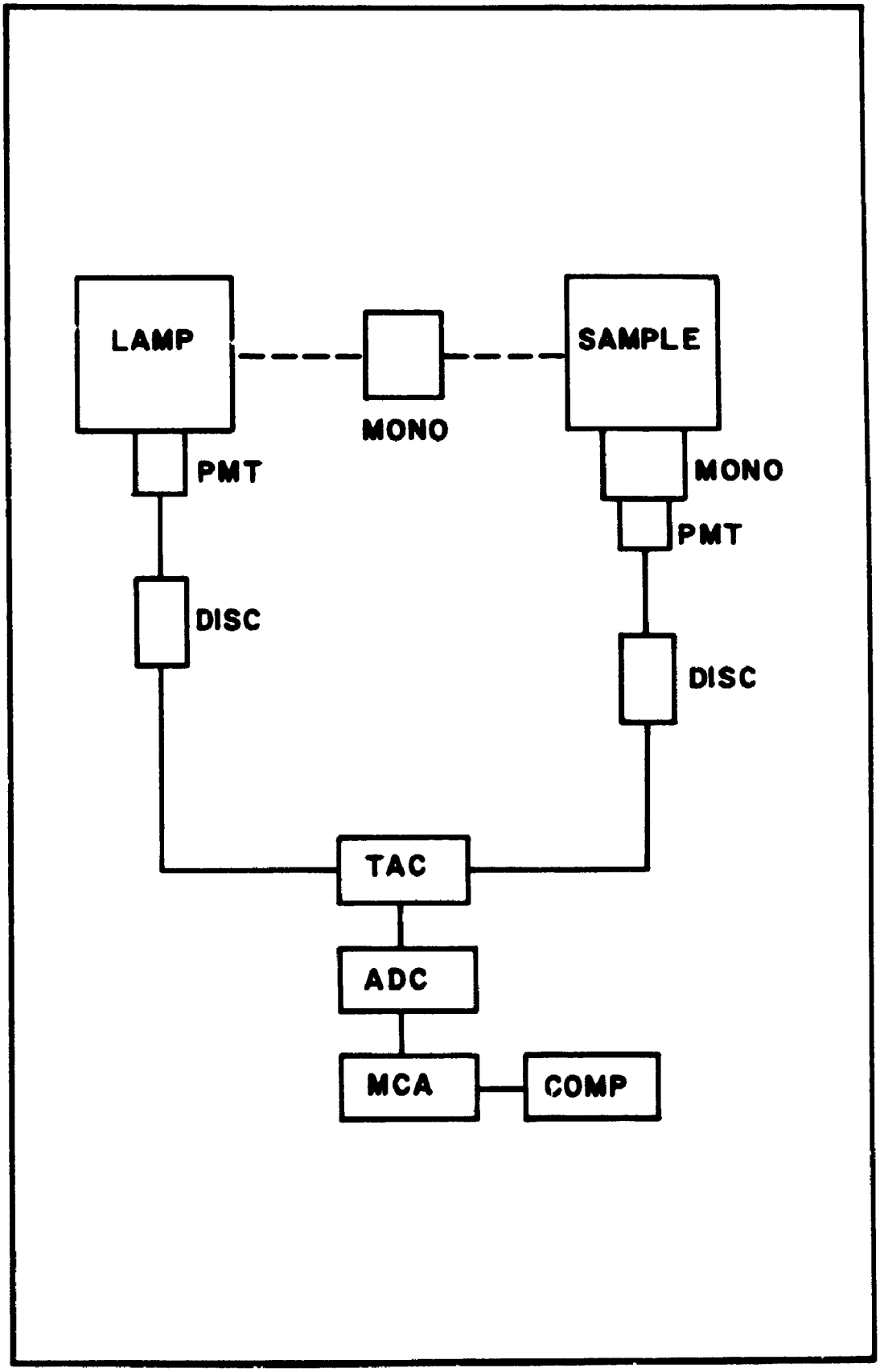
LAMP
MONO
SAMPLE
PMT
MONO
PMT
DISC
DISC
TAC
ADC
MCA
COMP

The emission wavelength was chosen for each donor to maximize emission intensity. Filters were placed in the incident light path to reduce the intensity until the emission count rate was less than 3% of the incident light count rate. A time scale was chosen so that the decay trace spanned approximately 3 lifetimes. Data were typically recorded until the effective peak channel contained 50,000 counts.

Data were obtained for 13 of the donors listed in Table 4.3. Time limitations prevented experiments with the remaining compounds.

5.3 Data Analysis and Results

The decay curves were analyzed by iterative reconvolution[116] using a sum of up to four exponentials. In all cases where multiple exponentials were used, only one of the longer decays had a significant pre-exponential factor. Control experiments found that a very short lifetime (< 5 ns) was due to MV^{2+}. The χ^2 test and the appearance of random residuals at the 95% confidence level were used as the criteria for goodness of fit. Figure 5.2 shows two decay curves of $Ru[bpy]_3^{2+}$, with and without MV^{2+}.

Values of $1/\tau$ and [Q] were input into the Basic program SVCALC (see Appendix 2) which calculated k_q as the slope from eq. 5.1 (which is a rearrangement of eq. 2.45).

$$1/\tau = 1/\tau_o + k_q[Q] \qquad (5.1)$$

An example, using the experiment from which the spectra in Fig. 5.2 were taken, is shown in Fig 5.3.

The values of k_q and τ_o are shown in Table 5.1, arranged in the order of increasing system exergonicity. Standard deviations, while not statistically valid on such small sample sizes, are included to provide

Figure 5.2: Time-resolved emission decay of $Ru[bpy]_3^{2+}$ in glycerol showing (a) unquenched and (b) quenched spectra. The concentration of MV^{2+} in the quenched sample is 0.1631 M. The hatched line is the excitation source profile and the data are obscured by the solid line fit. Residuals to the fit are shown above the decay. (a) is fit with τ_o = 0.997 μs (χ^2 = 1.163) and (b) is fit with τ = 0.868 μs (χ^2 = 1.034).

Time Resolved Emission

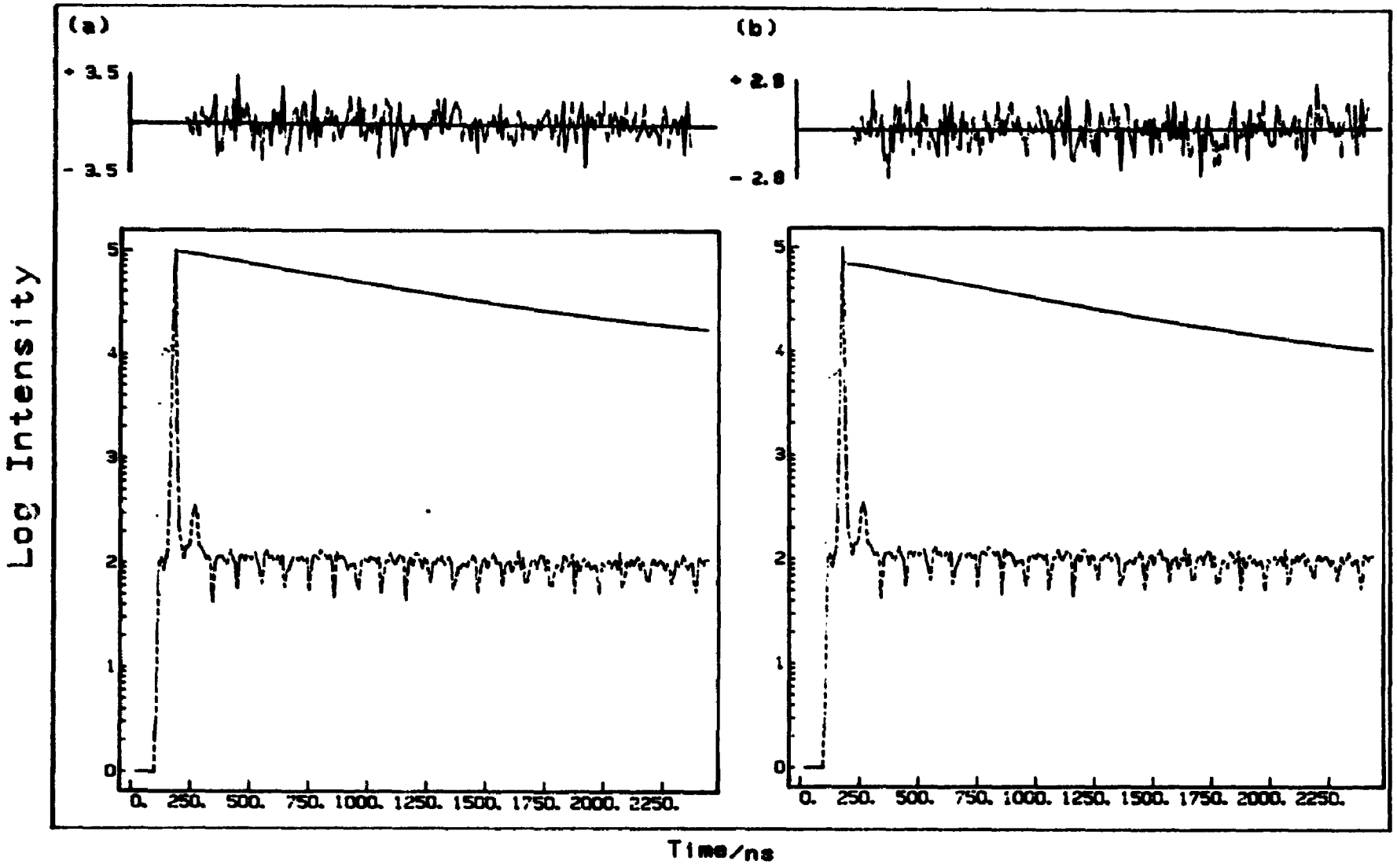

Figure 5.3: k_q is determined from eq. 5.1 by the program SVCALC. This example shows data from the $Ru[bpy]_3^{2+}$ experiment for which transient decay spectra are shown in Figure 5.2. k_q is 8.3×10^6 $M^{-1}s^{-1}$.

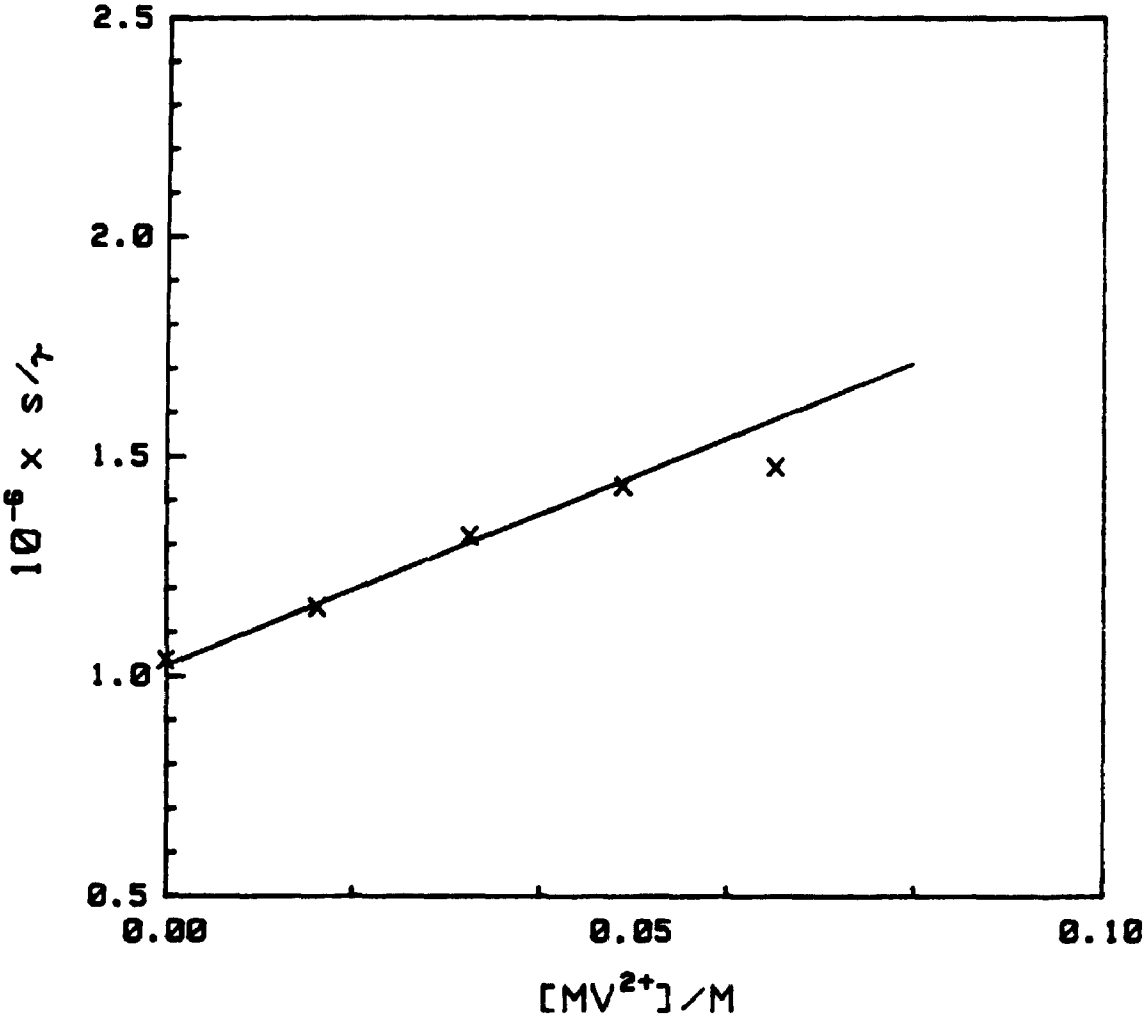
2.5
2.0
1.5
1.0
0.5
$10^{-6} \times s/\tau$
0.00
0.05
0.10
$[MV^{2+}]/M$

Table 5.1 Lifetimes and Bimolecular Quenching Constants

Ion	N	$\tau_o/\mu s$	S.D.	$10^{-7} \times k_q/M^{-1}s^{-1}$	S.D.
12. $Ru[5\text{-}Clphen]_3^{2+}$	2	1.43	0.21	0.74	0.42
12. with EDTA	1	1.22	—	0.73	—
1. $Ru[bpy]_3^{2+}$	3	0.92	0.04	0.94	0.07
1. with EDTA	2	0.86	0.01	0.85	0.0?
11. $Ru[phen]_3^{2+}$	3	0.74	0.07	1.10	0.32
9. $Ru[5\text{-}CH_3phen]_3^{2+}$	3	1.23	0.02	0.55	0.37
9. with EDTA	1	1.24	—	0.24	—
7. $Ru[5,6\text{-}(CH_3)_2phen]_3^{2+}$	2	2.12	0.03	0.71	0.22
3. $Ru[4,4'\text{-}(CH_3)_2bpy]_3^{2+}$	1	0.76	—	1.45	—
6. $Ru[4,7\text{-}(CH_3)_2phen]_3^{2+}$	3	1.68	0.19	1.17	0.35
6. with EDTA	2	1.81	0.92	0.87	0.16
5. $Ru[3,4,7,8\text{-}(CH_3)_4phen]_3^{2+}$	4	0.59	0.06	1.43	0.17
5. with EDTA	2	0.59	0.02	1.43	0.17
15. $cis\text{-}Ru(bpy)_2(CN)_2$	1	0.45	—	1.42	—
17. $cis\text{-}Ru(phen)_2(CN)_2$	2	1.24	0.05	1.20	0.42
30. $Ru[4,4'\text{-}(OEt)_2bpy]_3^{2+}$	3	0.17	0.005	1.89	0.15
23. $Ru[(tpy)(bpy)(NH_3)]^{2+}$	2	0.034	0.001	1.24	0.40
28. $Ru[4,4'\text{-}(NEt_2)_2bpy]_3^{2+}$	2	0.053	0.002	1.13	0.09

an estimate of the error ranges.

Data are reported for five systems with and without EDTA. The presence of EDTA results in only small variations of both the unquenched excited state lifetime and the bimolecular quenching constant. Although four of the values of k_q are smaller in systems containing EDTA, the differences are within the error ranges found. It was concluded that it was valid to use τ_o and k_q obtained in the absence EDTA with data from systems containing EDTA (i.e. EPR results).

CHAPTER 6 STEADY STATE EMISSION

6.1 Steady State Emission Apparatus

Steady state emission measurements were performed on a Perkin Elmer 650-40 Fluorescence Spectrophotometer in the ratio mode interfaced with a Perkin Elmer 3600 Data Station. An Oxford VWR 1140 temperature controller maintained a constant 25.0°C temperature in the sample holder.

6.2 Steady State Emission Experiments

These experiments were performed with the same samples that were prepared for the transient emission experiments.

The excitation wavelength and excitation and emission slit widths were chosen to maximize the donor emission intensity while minimizing the acceptor emission intensity. The emission wavelengths were chosen for each donor to span the emission maximum and the preceding minimum. Control spectra from samples containing only the acceptor were obtained under identical conditions and were subtracted from the experimental spectra so that the emission intensity minimum was constant for each set of samples (containing the same donor and a range of acceptor concentrations). An example of unquenched, quenched, and control-corrected spectra are shown in Fig. 6.1.

Data were obtained for the same systems that were used in the transient decay experiments.

6.3 Data Analysis and Results

For each experimental set (one donor) the emission intensities at the emission maxima of the spectra, corrected for acceptor emission, were input, with the acceptor concentrations, into the Basic program

Figure 6.1: Sample emission spectra are shown for $Ru[bpy]_3^{2+}$ without (a) and with MV^{2+} before (b) and after (c) the correction for MV^{2+} emission. The concentration of $Ru[bpy]_3^{2+}$ is 6.6×10^{-5} M and the concentration of MV^{2+} is 0.06115 M. The normalized intensities at the emission maximum (608 nm) are (a) 0.2790, (b) 0.1613, and (c) 0.1589.

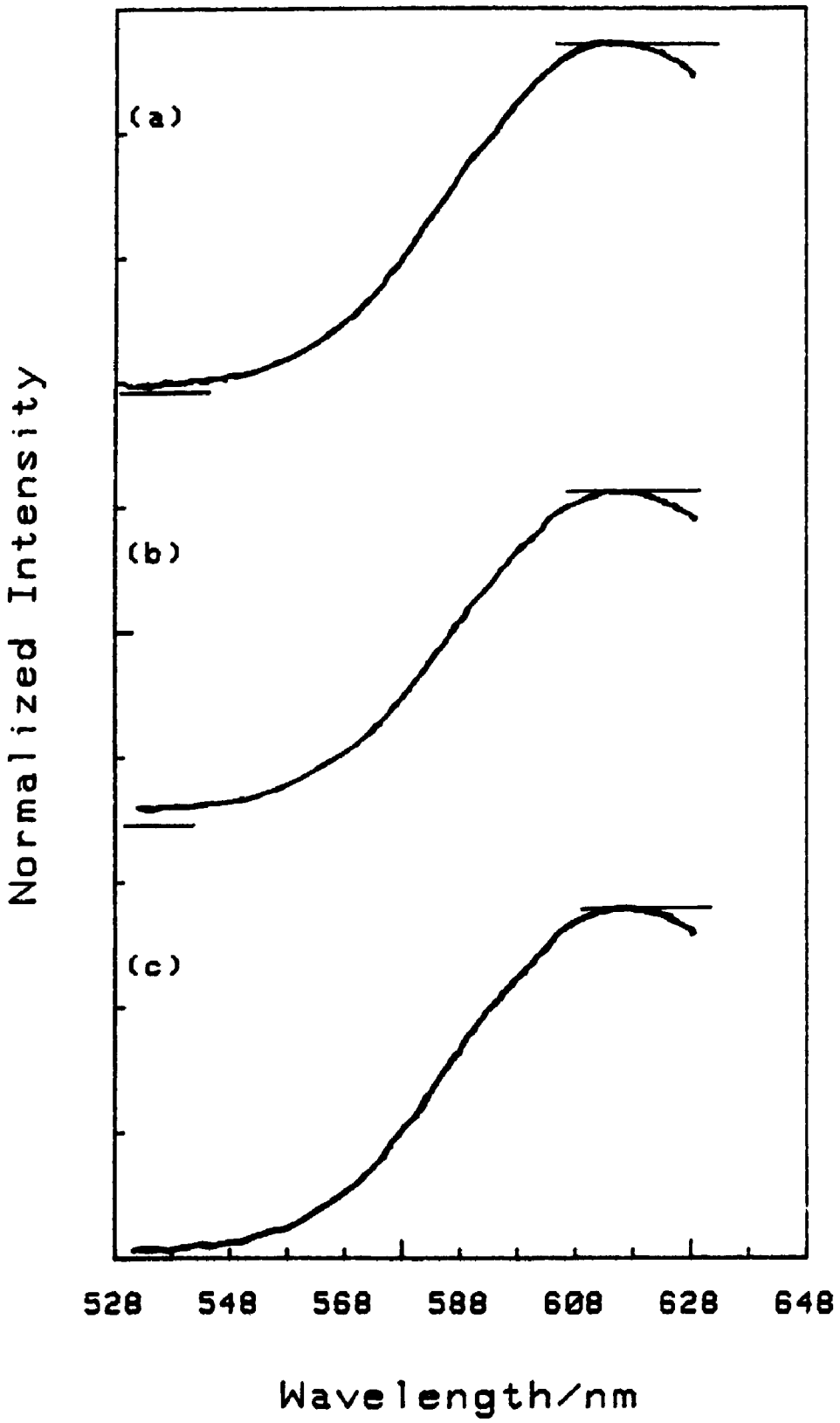
(a)
(b)
(c)
Normalized Intensity
528
548
568
588
608
628
648
Wavelength/nm

Figure 6.2: Emission quenching results are shown for (a) $Ru[bpy]_3^{2+}$, (b) $Ru[4,7\text{-}(CH_3)_2phen]_3^{2+}$, and (c) $Ru[4,4'\text{-}(NEt_2)_2bpy]_3^{2+}$. The lines of best fit were calculated from eq. 2.58 by the program PER_EM using (a) 11.8 Å, (b) 19.9 Å, and (c) 17.4 Å.

(a)

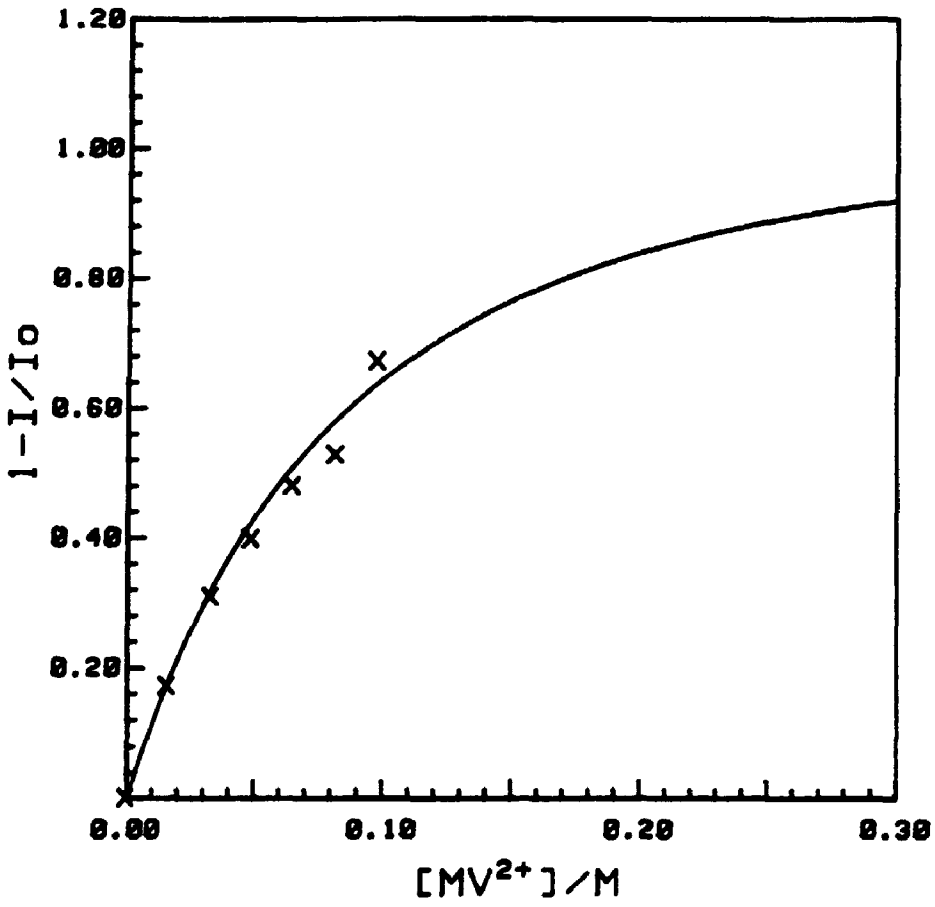

Residuals

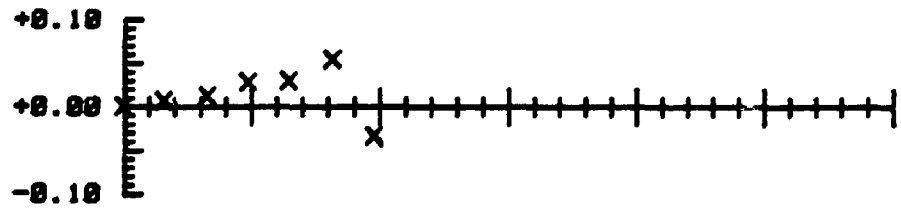

(b)

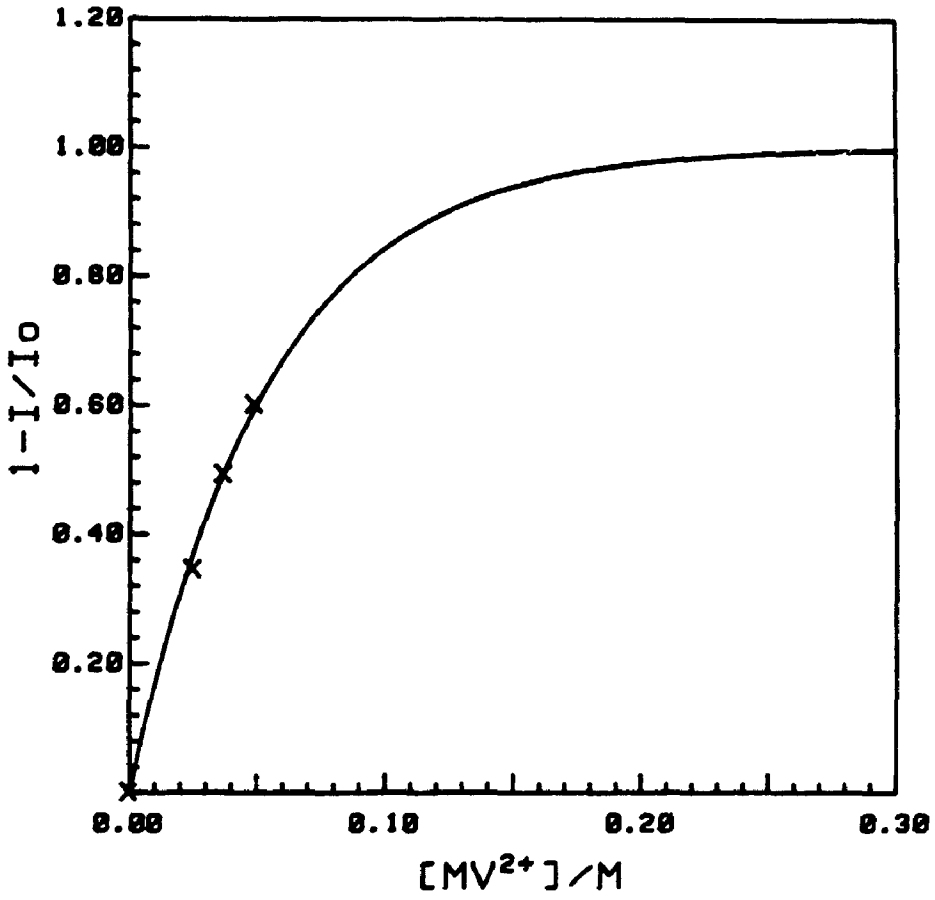

Residuals

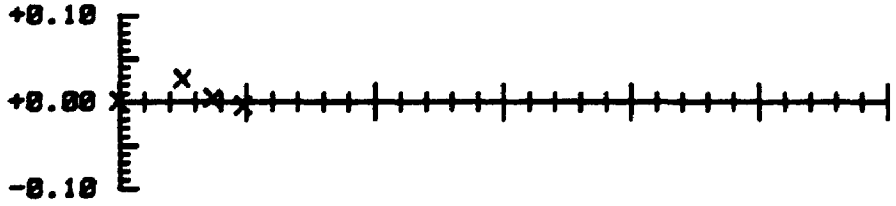

(c)

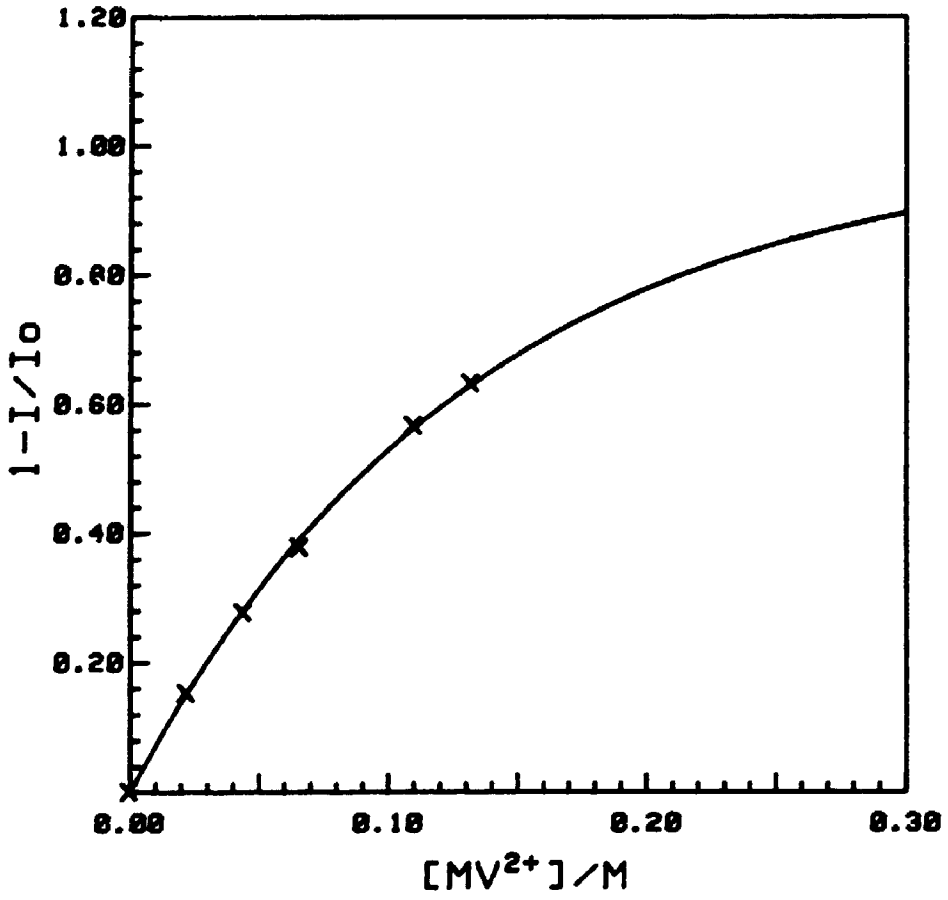

Residuals

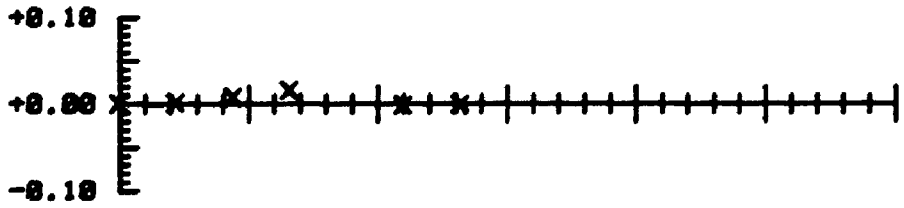

PER-EM (see Appendix 3). The values of k_q and τ_o reported in section 5.3 were also input. R_q and R_q-corr were calculated from eqs. 2.58 and 2.70. Three examples, chosen from systems at the outer limits and the middle of the range of ΔG_{rip} available, are shown in Figure 6.2. Data are plotted as $1 - I/I_o$, for easy comparison to the EPR data curves.

Values of R_q and R_q-corr are listed in Table 6.1 with sample sizes and standard deviations.

Table 6.1 R_q Calculated From Emission Quenching

Ion	N[a]	R_q/Å	S.D.	R_q-corr/Å	S.D.
12. $Ru[5\text{-}Clphen]_3^{2+}$	3	0.0	0.0	10.0	0.0
1. $Ru[bpy]_3^{2+}$	2	8.8	0.2	12.0	0.1
1. with EDTA	2	12.9	0.5	14.7	0.4
11. $Ru[phen]_3^{2+}$	2	10.3	0.3	13.0	0.2
9. $Ru[5\text{-}CH_3phen]_3^{2+}$	2	12.9	0.3	14.5	0.3
9. with EDTA	2	17.2	0.6	18.1	0.6
7. $Ru[5,6\text{-}(CH_3)_2phen]_3^{2+}$	2	13.4	0.08	14.6	0.06
3. $Ru[4,4'\text{-}(CH_3)_2bpy]_3^{2+}$	1	16.2	—	17.6	—
6. $Ru[4,7\text{-}(CH_3)_2phen]_3^{2+}$	2	19.3	0.1	19.8	0.1
6. with EDTA	1	19.9	—	20.3	—
5. $Ru[3,4,7,8\text{-}(CH_3)_4phen]_3^{2+}$	3	16.2	1.8	17.7	1.7
5. with EDTA	2	17.7	3.6	19.2	3.3
15. $cis\text{-}Ru(bpy)_2(CN)_2$	1	17.7	—	19.3	—
17. $cis\text{-}Ru(phen)_2(CN)_2$	2	19.6	0.4	20.2	0.4
30. $Ru[4,4'\text{-}(OEt)_2bpy]_3^{2+}$	3	9.8	0.6	13.4	0.4
23. $Ru[(tpy)(bpy)(NH_3)]^{2+}$	3	6.4	0.7	12.0	0.4
28. $Ru[4,4'\text{-}(NEt_2)_2bpy]_3^{2+}$	2	14.6	0.5	17.9	0.5

CHAPTER 7 EPR EXPERIMENTS

7.1 Electron Paramagnetic Resonance Spectroscopy Theory

Permanent magnetic dipoles arise from net electronic or nuclear angular momentum. The electronic magnetic dipoles arise from net spin or net orbital angular momenta or from a combination of these. For free radicals which have a very small orbital angular momentum, the spin-orbit interaction is very small; consequently attention may be focused on the spin angular momentum.

In the absence of a magnetic field the magnetic dipole energy levels are degenerate. Application of a static magnetic field splits the degeneracy and transitions between states may be induced by absorption of the magnetic component of electromagnetic radiation in the microwave region.

The magnetic dipole moment μ is defined by

$$W = -\mu \cdot B \tag{7.1}$$

$$= -\mu B \cos\theta \tag{7.2}$$

where W is the energy of a magnetic dipole of moment μ in a field B, and θ is the angle between the vector quantities μ and B.

The component of the electron spin magnetic moment μ_z along the direction of the magnetic field B is

$$\mu_z = -g\beta M_s \tag{7.3}$$

where M_s is the spin quantum number, β is the Bohr magneton, and g is a factor required for all cases other than those involving pure orbital angular momentum. β is a ratio of constants required to convert angular

momentum to magnetic moment and equals[118] $9.2740154(31) \times 10^{-24}$ JT^{-1}. For a free electron $g_e = 2.00232$ and for many free radicals g is approximately 2.

Substitution of eq. 7.3 into eq. 7.2 gives

$$W = g\beta BM_s \tag{7.4}$$

The possible values of M_s are $+\frac{1}{2}$ and $-\frac{1}{2}$. Consequently the energy level separation ΔW is

$$\Delta W = g\beta B \tag{7.5}$$

Transitions between the two levels are induced by electromagnetic radiation of frequency ν such that

$$h\nu = g\beta B_r \tag{7.6}$$

where B_r is the resonant magnetic field.

In practice, it is convenient to employ a fixed microwave frequency and scan an EPR spectrum by a linear variation of the static magnetic field. When the resonance condition (eq. 7.6) is met, a change in the detector current produces an absorption signal. Integration of the full absorption curve yields the intensity of the line which is proportional to the number of paramagnetic centers giving rise to the signal. In practice, it is simpler to measure the peak-to-peak amplitudes of the derivative lines which are proportional to their intensities under constant conditions (e.g. constant line width).

7.2 The EPR Apparatus

An EPR spectrometer comprises a klystron which emits monochromatic radiation, a cavity system which includes a sample holder and a

waveguide to direct and control the microwave beam to and from the sample, detection and modulation systems which monitor, amplify, and record the signal, and a magnet which provides a stable, linearly variable and homogeneous magnetic field. Figure 7.1 shows a schematic diagram.

EPR spectra were recorded on a Varian E-12 spectrometer at ambient temperatures of between 22.0 and 25.0°C.

Light from a 150 watt tungsten halogen lamp (Cole Parmer model 9741-50) was filtered by a 15 cm aqueous saturated sodium nitrite solution and by Corning glass filters CS 3-73 and CS 4-96. From 50 to 68% of the incident light was transmitted between 430 and 538 nm. Outside this range, transmission decreased sharply to zero.

7.3 EPR Experiments and Results

The $MV^{+\cdot}$ radical is the product measured by all EPR experiments. The EPR signal was identified with a sample of $MV^{+\cdot}$ prepared by reducing MV^{2+} in the presence of short wavelength irradiation ($\approx$ 350 nm) from sunlight in the method used by Johnson and Gutowsky.[119] The radical was identified optically by λ_{max} at 399 and 608 nm which were compared to literature values[120] of 395.7 nm and 604.4 in aqueous solutions prepared by reducing MV^{2+} with sodium dithionite. 100 kHz modulated EPR detection was employed with 10.0 mT modulation amplitude and 1 mW microwave power at $\approx$ 9.02 GHz. The g factor was calculated to be 2.0037 using the standard α,α'-diphenyl-β-picrylhydrazyl (DPPH) for which the g factor is 2.0037 $\pm$0.0002.[117] Although g factors are not usually determined for viologen radicals, values in the range of 2.003 to 2.004 have been reported.[121] The peak-to-peak line width was 1.65 mT.

The measured observable in these experiments was the peak-to-peak

Figure 7.1: A schematic diagram of the EPR spectrometer.

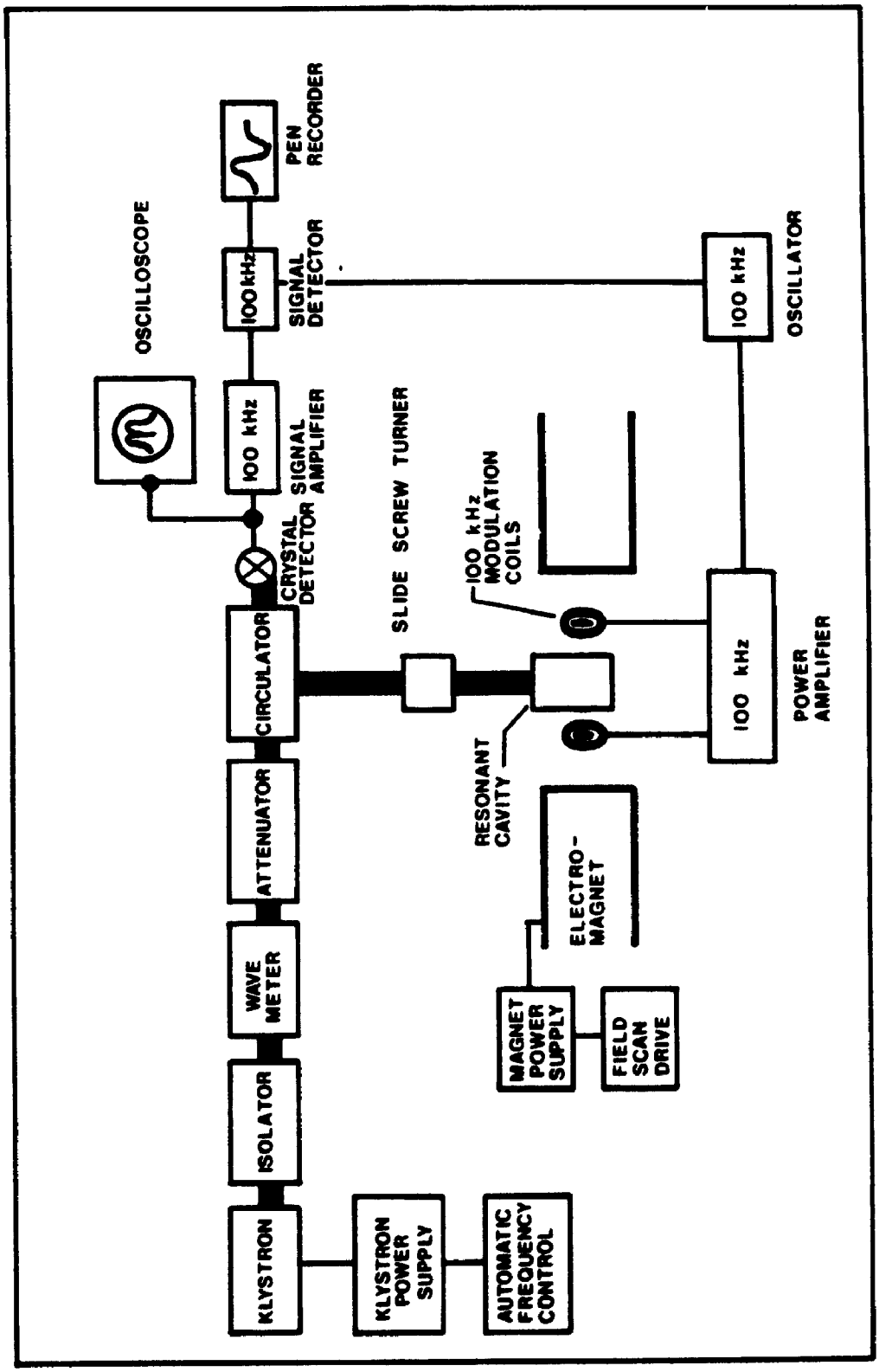
KLYSTRON
KLYSTRON POWER SUPPLY
AUTOMATIC FREQUENCY CONTROL
ISOLATOR
WAVE METER
ATTENUATOR
CIRCULATOR
CRYSTAL DETECTOR
100 kHz SIGNAL AMPLIFIER
100 kHz
SIGNAL DETECTOR
PEN RECORDER
OSCILLOSCOPE
SLIDE SCREW TURNER
100 kHz MODULATION COILS
RESONANT CAVITY
ELECTRO-MAGNET
MAGNET POWER SUPPLY
FIELD SCAN DRIVE
100 kHz
POWER AMPLIFIER
100 kHz
OSCILLATOR

EPR signal amplitude A. A and A_{max} provide measures of P_d and P_{ind} in eq. 3.13.

Preliminary experiments determined that an $EDTA^{3-}$ concentration of 0.0600 M was sufficient to reduce ruthenium photoproducts for a wide range of MV^{2+} concentrations (e.g. see Figure 4.3 and the discussion in section 4.1). At constant $EDTA^{3-}$ and MV^{2+} concentrations, light-induced signals were linear with ruthenium concentration up to 2×10^{-3} M and with irradiation time up to 1 minute when MV^{2+} concentrations were as high as 0.3 M. For concentrations of MV^{2+} up to 0.3 M and moderate ruthenium concentrations (e.g. 5×10^{-4} M), photoproduct signals were linear with irradiation time up to 15 min. Consequently, for each experiment, donor concentrations and irradiation times were chosen between 5×10^{-5} and 4×10^{-4} M and 30 s to 4 min, respectively, to obtain signals with minimum noise when A_{max} filled the chart recorder page.

Each experiment consisted of a set of 10 samples at constant donor and EDTA concentrations and varying MV^{2+} concentrations designed to define the Perrin plot curve and give three measures of A_{max}. Maximum MV^{2+} concentrations ranged between 0.06498M for $Ru[5,6\text{-}(CH_3)_2phen]_3^{2+}$ and 0.5805 M for $Ru[(tpy)(bpy)(NH_3)]^{2+}$.

EPR spectra were recorded before and after irradiation. Signal amplitudes were measured manually and light-minus-dark amplitudes were calculated. Control samples containing the highest MV^{2+} concentration in each set were treated identically. Figure 7.2 shows an example of one set of data. If the light-induced signal in the control sample was greater than 2% of the signal from the corresponding sample containing ruthenium, then a set of control samples was prepared and the light-

Figure 7.2: Double trace EPR signals are shown for a set of samples containing 1.94×10^{-3} M $Ru[5\text{-}Clphen]_3^{2+}$ and increasing concentrations of MV^{2+}. The dark signal appears approximately in the middle of each light-induced signal. The two almost flat signals at the lower left show the light-induced signals from the control samples for this set.

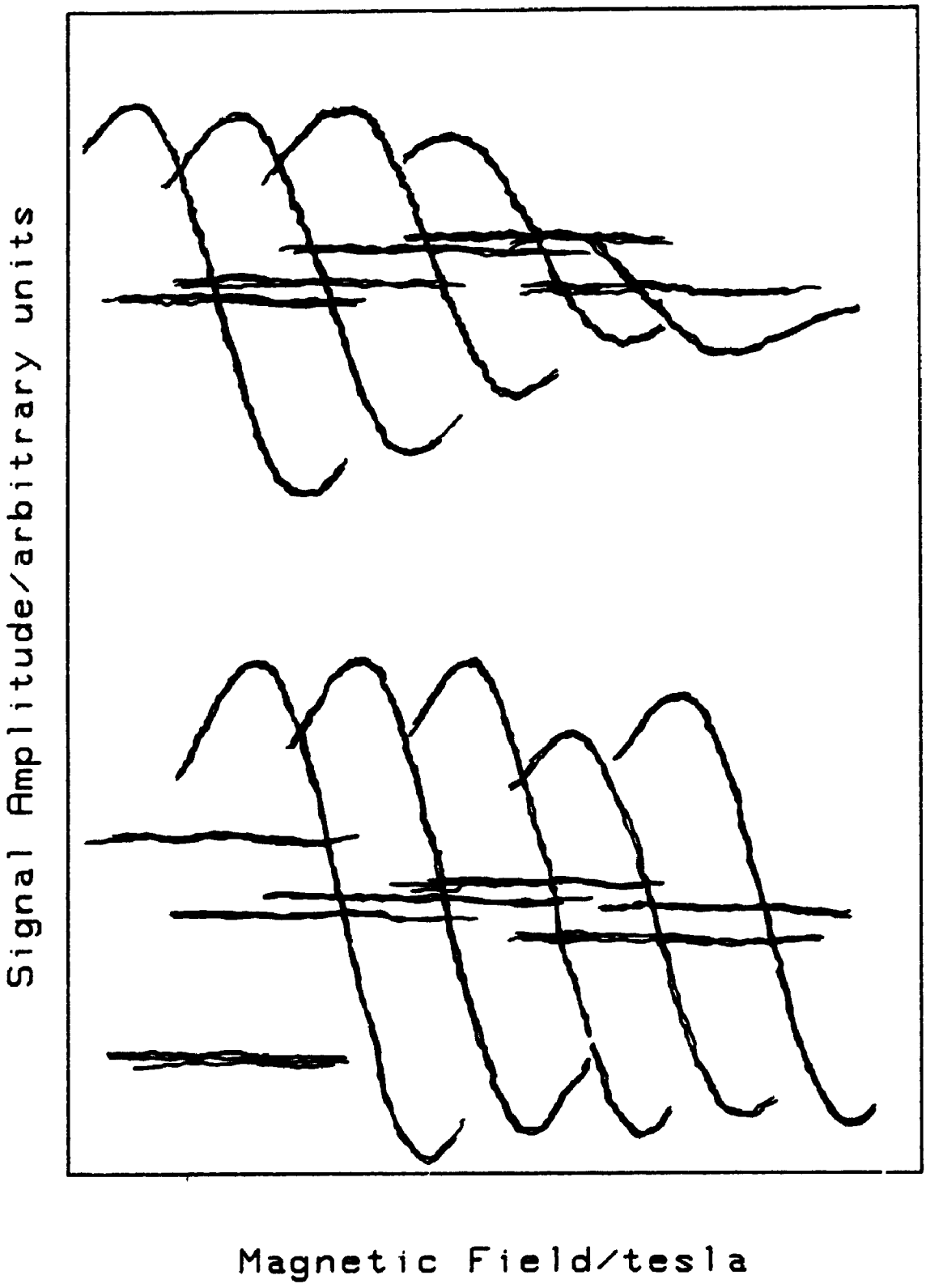
Signal Amplitude/arbitrary units
Magnetic Field/tesla

induced signal amplitudes from the control set were subtracted from the light-induced signal amplitudes from the corresponding experimental samples. This correction was necessary for $Ru[5\text{-}NO_2phen]^{2+}$, $Ru[(bpy)_2(NMI)_2]^{2+}$, $Ru[4,4'\text{-}(NEt_2)_2bpy]_3^{2+}$, and $Ru[(tpy)(bpy)(NH3)]^{2+}$. Corrected signal amplitudes from the first three of these compounds were extremely small (1 cm or less for all samples) and the data were discarded.

Corrected signal amplitudes, acceptor concentrations, and the values of k_q and τ_o from section 5.3 were input into the Basic program PER-EPR (see Appendix 4) which calculated R_q and R_q-corr for each donor from eqs. 3.13 and 2.70. Since some of the data analyses found rather large χ^2 and non-random residuals, PER-EPR was modified to vary A_{max} as well as R_q, in order to obtain the best fit. This procedure was viewed with mistrust, however, since several analyses obtained wildly improbable values of A_{max}. Particularly in cases where only a small range of $[MV^{2+}]$ was spanned, the procedure of minimizing χ^2 compressed the curve identified by A/A_{max} until the curvature was clearly a function of the fitting procedure and did not reflect the real value of R_q. The values of R_q reported were obtained with the fixed values of A_{max} determined by experiment. Figure 7.3 shows examples of EPR data plotted as A/A_{max} for 3 systems at the outer limits and in the middle of the range of ΔG_{rip} values available.

Average values of R_q and R_q-corr are listed in Table 7.1 with the number of experiments used in the calculation of the average and the standard deviation.

Figure 7.3: Typical EPR results are shown for (a) $Ru[5\text{-}Clphen]_3^{2+}$, (b) $Ru[(bpy)_2(CN)_2]$, and (c) $Ru[(tpy)(bpy)(NH_3)]^{2+}$. The lines of best fit were calculated from eq. 3.13 by the program PER_EPR using (a) 19.4 Å, (b) 24.2 Å, and (c) 18.3 Å.

(a)

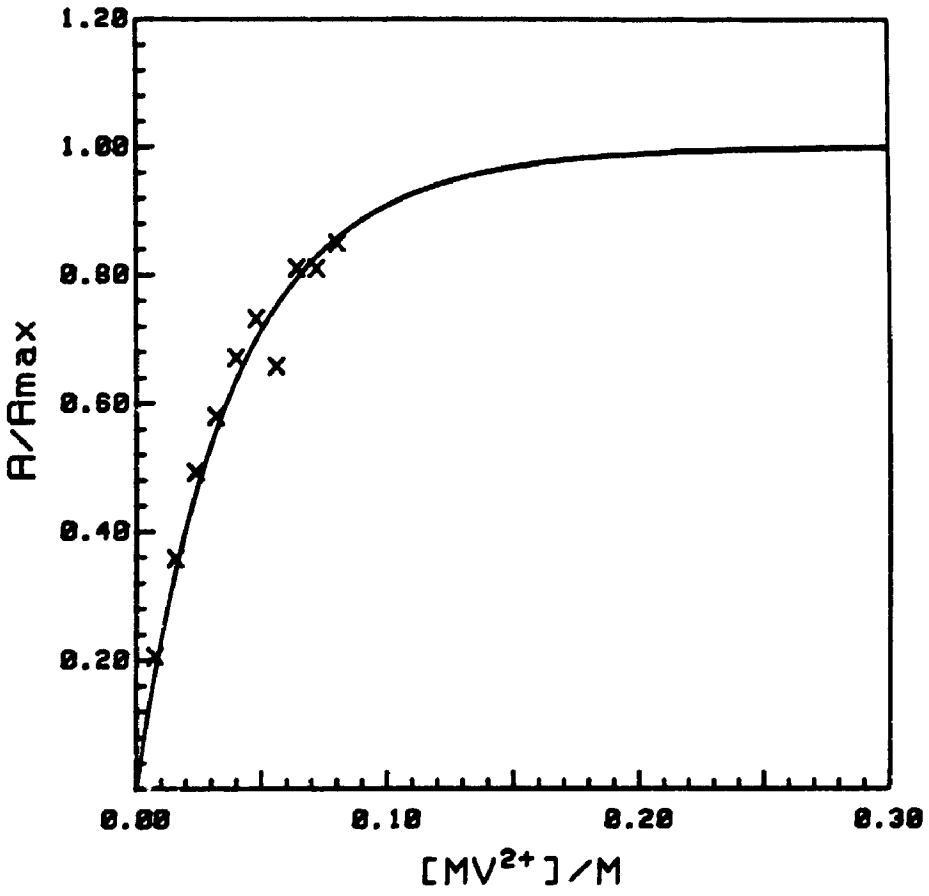
1.20
1.00
0.80
0.60
0.40
0.20
A/Amax
0.00
0.10
0.20
0.30
[MV2+]/M

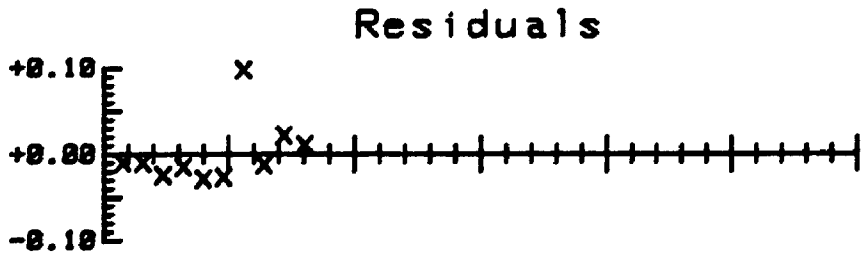
Residuals
+0.10
+0.00
-0.10

(b)

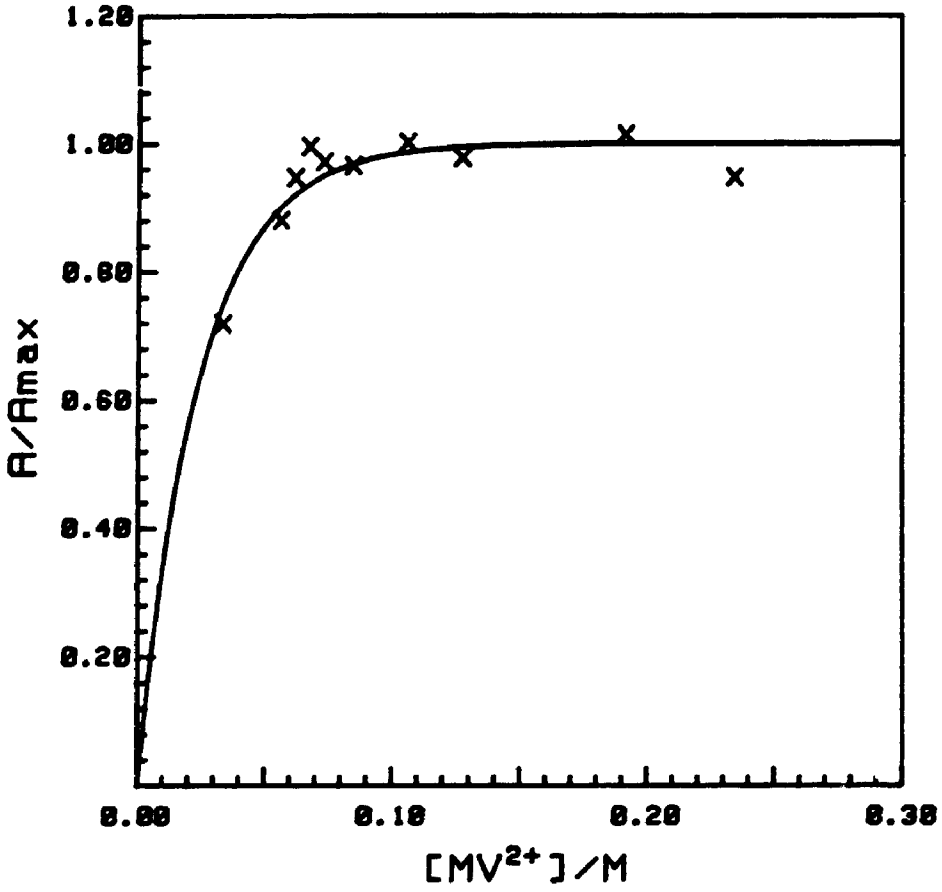

Residuals

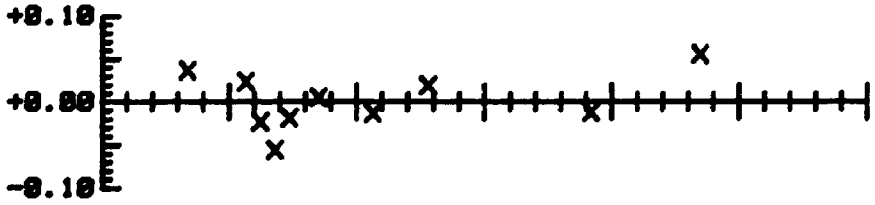

(c)

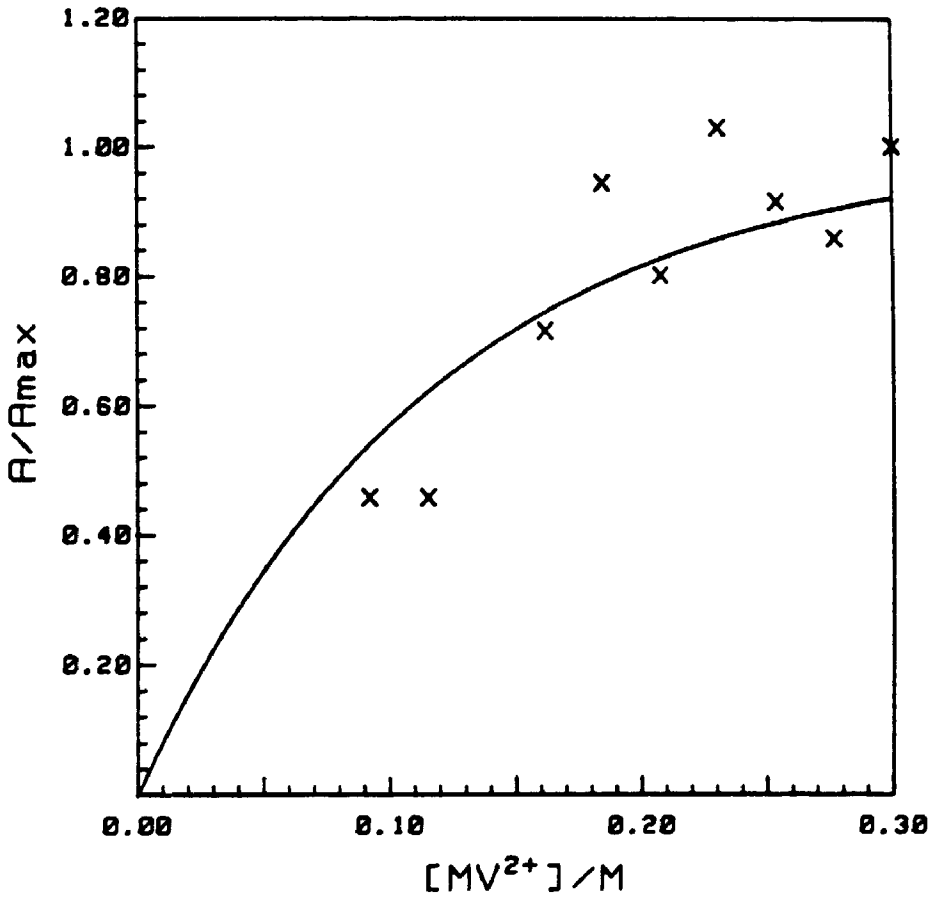
1.20
1.00
0.80
0.60
0.40
0.20
A/Amax
0.00
0.10
0.20
0.30
[MV2+]/M

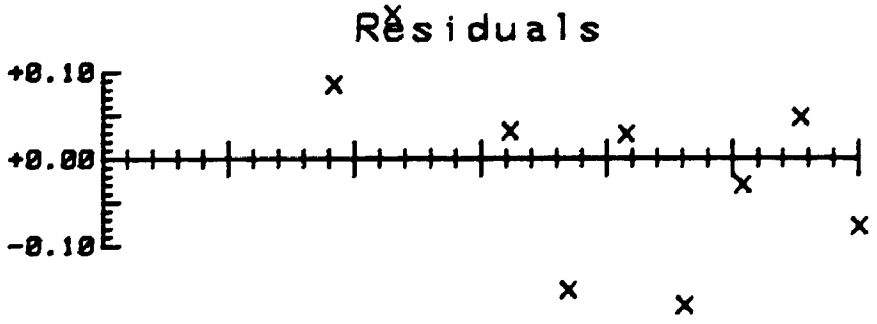
Residuals
+0.10
+0.00
-0.10

Table 7.1 R_q Calculated from EPR Data

Ion	N	R_q/Å	S.D.	R_q-corr/Å	S.D.
13. $Ru[5\text{-}NO_2phen]_3^{2+}$	3	—			
12. $Ru[5\text{-}Clphen]_3^{2+}$	5	19.6	1.3	20.1	1.2
1. $Ru[bpy]_3^{2+}$	5	20.7	1.9	21.8	1.8
11. $Ru[phen]_3^{2+}$	4	21.9	0.6	22.8	0.6
9. $Ru[5\text{-}CH_3phen]_3^{2+}$	4	24.3	2.4	24.8	2.3
7. $Ru[5,6\text{-}(CH_3)_2phen]_3^{2+}$	3	25.4	0.6	25.4	0.6
3. $Ru[4,4'\text{-}(CH_3)_2bpy]_3^{2+}$	4	25.8	0.9	26.7	0.9
6. $Ru[4,7\text{-}(CH_3)_2phen]_3^{2+}$	2	28.9	0.4	29.1	0.4
19. $cis\text{-}Ru[(bpy)_2(NMI)_2]^{2+}$	2	—			
5. $Ru[3,4,7,8\text{-}(CH_3)_4phen]_3^{2+}$	4	20.9	1.0	23.1	0.5
15. $cis\text{-}Ru(bpy)_2(CN)_2$	5	23.6	0.8	24.6	1.0
17. $cis\text{-}Ru(phen)_2(CN)_2$	4	25.9	1.3	26.3	1.3
30. $Ru[4,4'\text{-}(OEt)_2bpy]_3^{2+}$	6	20.3	1.9	22.3	1.7
23. $Ru[(tpy)(bpy)(NH_3)]^{2+}$	5	13.8	1.3	17.5	1.1
28. $Ru[4,4'\text{-}(NEt_2)_2bpy]_3^{2+}$	2	—			

Chapter 8 Discussion

8.1 The Rate-Energy Relationship

8.1.1 The Relationship Between R_q and ΔG_{rip}

Figure 8.1 shows the values of R_q-corr obtained from emission quenching experiments plotted against ΔG_{rip}. Although there is some scatter in the region of high exergonicity, a clear increase and then decrease in R_q with increasing exergonicity is evident.

For a = 0.75 Å, the value of the range parameter used in these calculations, an increase by 1.7 in R_q represents a rate increase of approximately one order of magnitude. The increase in R_q from 10.0 Å to 20.2 Å shown in Fig. 8.1 is roughly equivalent to an increase in rate of six orders of magnitude.

The maximum rate possible of approximately 10^{13} s^{-1} (see section 2.2.2) is equivalent to an R_q, when $\tau_o \simeq 1$ μs, of 22 Å (from eq. 2.67). This reflects an adiabatic reaction for which H_{ps} is approximately 0.025 eV. The maximum value of R_q found here of 20.2 Å may not identify the real maximum of the series since the donor ($Ru[(phen)_2(CN)_2]$) is a neutral species. If the series is restricted to the doubly charged homologues then the maximum is 19.7 Å found for $Ru[4,7\text{-}(CH_3)_2phen]_3^{2+}$ at ΔG_{rip} = -0.58 eV.

Fig. 8.1 shows a decrease in rate of approximately 4.5 orders of magnitude at high exergonicities, with the scatter previously noted.

The curvature observed is much sharper than that seen in other data (e.g. refs. 36, 77, 78, 81, 82) and more closely resembles the relationship obtained by Guarr et. al.[75] Sharp curvature in the rate-energy relationship given by eqs. 2.26 and 2.67 may be obtained by using very small values of $\hbar\omega$ or very large values of a. Since reasonable

Figure 8.1: The relationship between ΔG_{rip} and R_q-corr found from emission quenching data. The line of best fit is calculated from eqs. 2.26 and 2.67 using H_{ps} = 0.01 eV, λ_s = 0.16 eV, λ_v = 0.75 eV, $\hbar\omega$ = 80 cm^{-1}, τ_o = 1 μs, a = 0.75 Å, and R_o = 10 Å. Using an average standard deviation of 0.5 Å, a range of two standard deviations is shown for each R_q-corr.

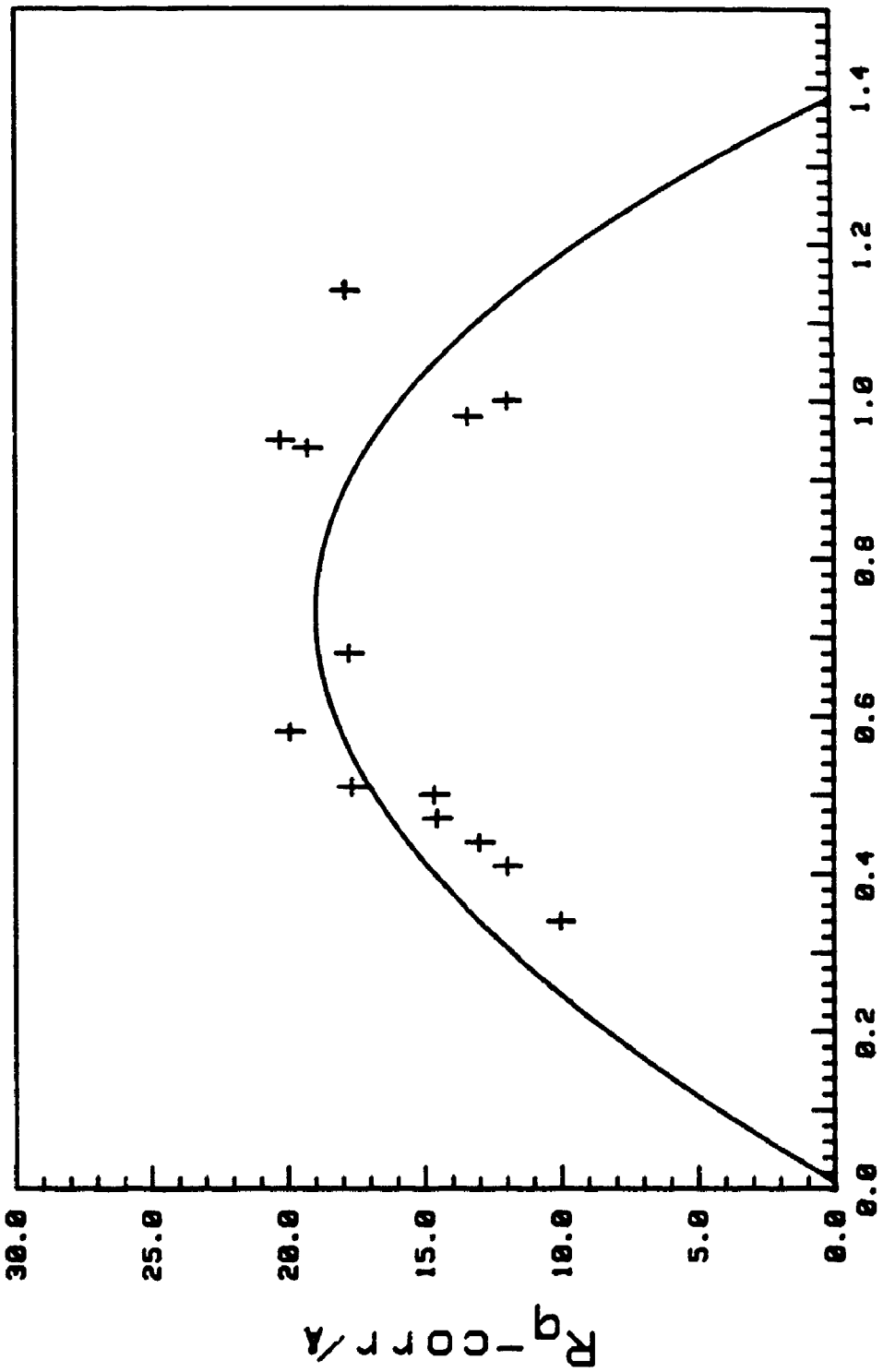
30.0
25.0
20.0
15.0
10.0
5.0
0.0
0.0
0.2
0.4
0.6
0.8
1.0
1.2
1.4
R_q-corr/Å
$-\Delta G_{rip}$/eV

values of the range parameter *a* have been established to vary between 0.4 and 0.9 Å[35], it is not physically realistic to fit the data with large *a*. The alternative is to use a small value of $\hbar\omega$. The average high frequency was expected to fall in the 200-600 cm^{-1} range corresponding to the metal-ligand vibrational frequencies, or in the 1000-3000 cm^{-1} range, corresponding to the C-C and C-H modes of aromatic hydrocarbons.[38] The low temperature data obtained by Miller et al.[36] in MTHF glasses showed shallow curvature and the low temperature data obtained by Guarr et al.[75] using ruthenium polypyridines in glycerol glasses showed sharp curvature. The room temperature data obtained by Ohno et al.[80], who also used ruthenium polypyridines showed extremely sharp curvature. Therefore it is concluded that the sharp curvature seen in Figure 8.1 results from a small "high frequency" $\hbar\omega$ which is related to the nature of the reactant structure. It is significant that such sharp curvature also demands a small value of λ_s.

The fitting line shown in Figure 8.1 was calculated from eqs. 2.26 and 2.67 (using the Basic program SCDATAFIT, see Appendix 5) with an average high frequency vibration $\hbar\omega$ = 80 cm^{-1}, H_{ps} = 0.01 eV, λ_s = 0.16 eV, and λ_v = 0.75 eV.

Calculations by Marcus and Siders[35] fitted ET rate data obtained from a series of ruthenium bipyridyls with a semiclassical expression for k_{ET}. They estimated H_{ps} to vary between 0.0054 and 0.023 eV. The value of H_{ps} obtained here falls within this range and indicates slightly nonadiabatic activity.

The value of ΔG_{rip} at the maximum rate is related to the reorganization energy barrier to the reaction. Values of λ for electron exchange reactions between ruthenium complexes containing bpy and NH_3

have been reported to range between 0.62 and 1.06 eV.[122] Guarr et al.[75] estimated $\lambda \approx 0.8$ eV for a series of polypyridine ruthenium donors and methyl viologen in low temperature glycerol. λ_o calculated from eq. 2.17 is 0.87 eV, assuming an average radii of 7 Å[111] for all the donors and 3 Å[112] for methyl viologen and a contact distance of 10 Å. This value for λ_s would decrease slightly if the contact distance were less than the sum of the reactant radii; if, for example, the plane of one of the ligands were parallel and adjacent to the plane of one of the aromatic rings of methyl viologen. λ_i, the internal reorganization energy is expected to be very small since the change in ruthenium-nitrogen bond length which occurs on oxidation has been estimated to be very small (0.04 Å for $Ru[NH_3]_6^{2+}$ [123] or 0 Å for $Fe[phen]_3^{2+}$ [124]). If the change in ruthenium-nitrogen bond length is taken to 0.04 Å, then, using $\hbar\omega = 80$ cm^{-1}, λ_v is 0.0029 eV for $Ru[bpy]_3^{2+}$ and 0.0034 eV for $Ru[phen]_3^{2+}$ (from eq. 2.28). If it is assumed that the changes in bond lengths on reduction of MV^{2+} are negligible, then the magnitude of λ_v in this system is negligible.

Although the value found here for λ is reasonable, ($\lambda_s + \lambda_v = 0.91$ eV), there is an apparent reversal of prediction seen in the values obtained for λ_s and λ_v which may be related to the nature of the solvent. Hydroxylic solvents display a broad range of vibrational modes ranging from low-frequency librations to high-frequency ν(OH) vibrations at approximately 3400 cm^{-1}.[125] On the basis of kinetic isotope effects, it has been suggested that contributions to the activation barrier for $Fe[H_2O]_6^{3+/2+}$ self-exchange ET may arise from high-frequency modes of the bound solvent as well as from low-frequency librations.[124] Studies of excited-state decay in hydroxylated and non-hydroxylated solvents found differences between deuterated and non-deuterated solvents which

could not be explained on the basis of eq 2.17 since the dielectric constant and refractive index are essentially unaffected by deuteration.[125,126] Anomalies in non-radiative decay rate constants were explained in terms of a "special" effect related to the vibrational trapping energy. In the present system, the trihydroxy solvent provides ample possibilities for hydrogen bonding with other species in the system. It may be significant that the small values of λ_v reported recently[78,81,82] were found in non-hydroxylic solvents such as acetonitrile and toluene. With this model it is also reasonable to imagine that solvent dipole reorientation (librational motion) would be considerably restricted by the extent and location of hydrogen bonds.

Gould et al.[81] have clearly demonstrated the extreme sensitivity of rate-energy relationships to reactant structure. They fitted k_{ET} for reverse ET within geminate ion pairs to eq. 2.26 for series of organic donors containing either one or two aromatic rings and found different values for the electronic coupling matrix element (0.00133 eV and 0.00098 eV) and for λ_s (1.6 eV and 1.45 eV) for the two series. λ_v was constant at 0.3 eV. It was concluded that the size of the aromatic nucleus was important, not the overall size of the molecule, and that differences in H_{ps} and λ_s resulted from differences in charge distribution and the degree of delocalization.

The apparent anomalies in the results presented here may be accounted for by structural differences which initially were thought to be relatively small. Figure 8.2 shows separate fits of eq. 2.26 to values of R_q including the two neutral donors, and excluding them. The electronic coupling matrix elements still show slight non-adiabaticity (both are 0.01 eV). Values of λ_s are rather small (0.16 eV) and those

Figure 8.2: Two fits to the emission quenching values of R_q-corr are calculated from eqs. 2.26 and 2.67. (a) includes the two neutral donors (compounds 15 and 17 at ΔG_{rip} = -0.94 eV and -0.95 eV, respectively) and the fitting parameters were H_{ps} = 0.01 eV, λ_s = 0.16 eV, λ_v = 0.84 eV, and $\hbar\omega$ = 100 cm^{-1}. (b) uses H_{ps} = 0.01 eV, λ_s = 0.16 eV, λ_v = 0.78 eV, and $\hbar\omega$ = 74 cm^{-1}. Both calculations used τ_o = 1 μs, a = 0.75 Å, and R_o = 10 Å.

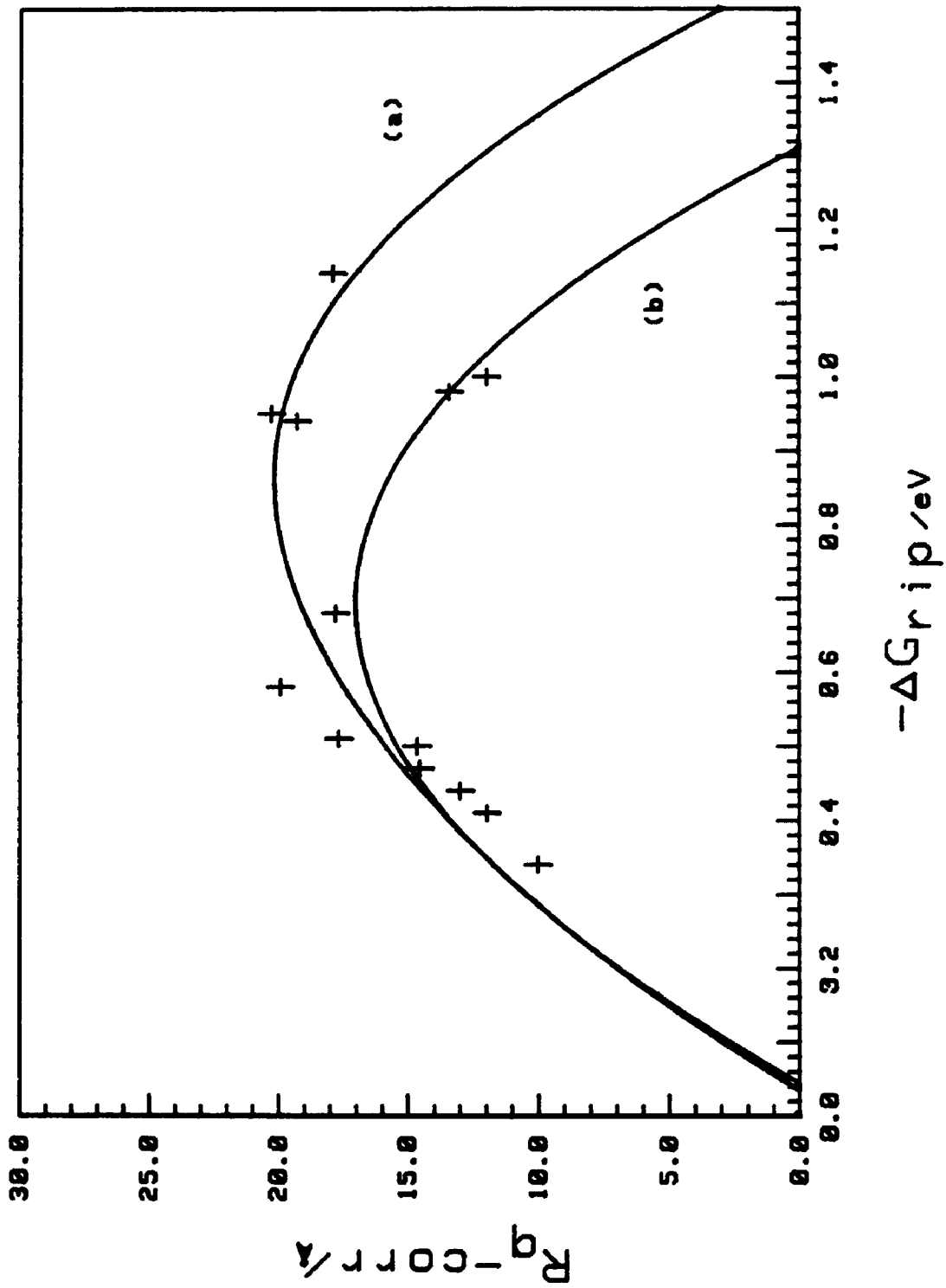
(a)
(b)
30.0
25.0
20.0
15.0
10.0
5.0
0.0
0.0
0.2
0.4
0.6
0.8
1.0
1.2
1.4
R_{q-corr}/Å
$-\Delta G_{rip}$/eV

for λ_v are rather large (0.84 eV and 0.78 eV). The best fits appear to be obtained using slightly different values for the average high-frequency vibration: the series including the neutral donors was fitted with 100 cm^{-1} and the other series with 74 cm^{-1}.

In the quantum mechanical model of electron transfer, the rate (probability) of ET is proportional to the overlap of vibrational wave functions. As previously noted in section 2.2, the overlap is greater as one potential surface becomes embedded in the other (see Fig 2.2). The exact location of vibrational wave function amplitude is clearly a defining parameter of ET probability and, clearly, this parameter is determined by structure. One might expect that rate constants in the inverted region would show much greater sensitivity to structure than those in the normal region and that this sensitivity would be expressed as variations in the average high-frequency vibration and in the vibrational reorganization energy.

Since coulombic repulsion between the uncharged donors and MV^{2+} is less than that between the charged donors and MV^{2+}, the measured R_q is expected to be larger than an R_q at the same ΔG_{rip} obtained with a charged donor. The experimentally determined values are rather large (see Fig. 8.2) and, although numerical corrections are difficult to estimate, even a small correction results in a more clear demonstration of inverted rate decreases. In this approximation, the most exergonic system is more obviously anomalous.

8.1.2 Comparison of k_q and R_q

Figure 8.3 shows both k_q and R_q-corr as a function of ΔG_{rip}. k_q is clearly diffusion controlled and close to the value estimated by eq. 2.10 for k_D in glycerol (6.2×10^6 $M^{-1}s^{-1}$). The difference between k_q

Figure 8.3: Comparison of k_q (x) and R_q-corr (o) (from emission quenching results).

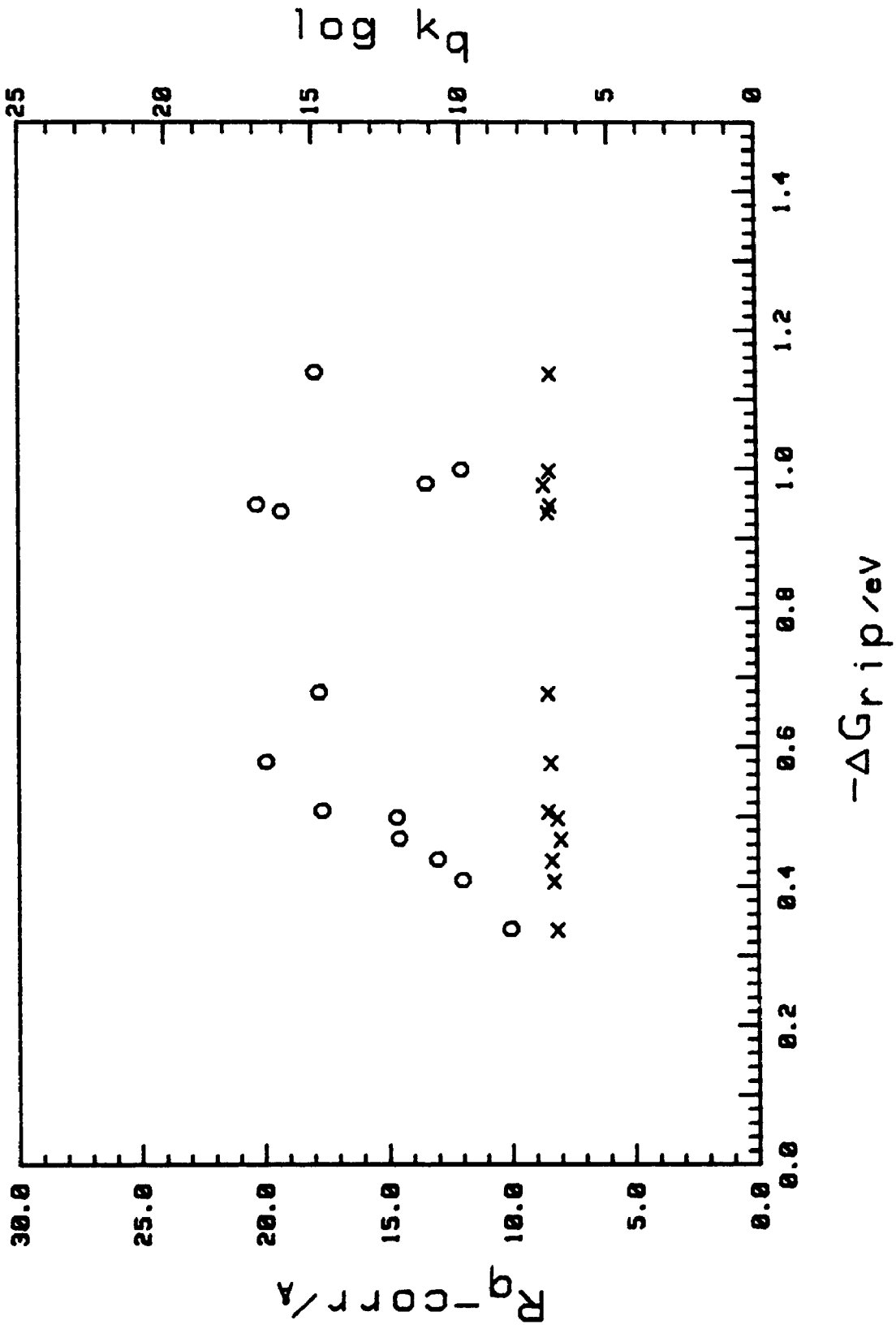
log k_q
25
20
15
10
5
0
30.0
25.0
20.0
15.0
10.0
5.0
0.0
0.0
0.2
0.4
0.6
0.8
1.0
1.2
1.4
R_q-corr/Å
$-\Delta G_{rip}$/eV

and R_q is striking and results only from the method of measurement. The same sample cells were used to obtain k_q from transient emission decay experiments (with eq. 5.1) and to obtain R_q from emission quenching experiments (with eq. 2.58).

These results provide clear evidence that the Marcus inverted region is seen in bimolecular charge-separation ET in the absence of diffusion.

8.2 Comparison of EPR and Emission Quenching Results

Figure 8.4 presents values of R_q-corr calculated from both EPR and emission quenching experiments. The general trend of the EPR and emission quenching results is quite similar but one difference is evident. Although the pattern of relative R_q values is almost identical, R_q values calculated from EPR data are larger.

The principal differences between the two experiments are that the EPR experiments measured the increase in acceptor radical concentration and the emission quenching experiments measured the decrease in unquenched donor concentration, samples were subjected to magnetic fields ($\approx$0.32 T) in the EPR experiments, and the EPR samples contained EDTA.

Equating an increase in product with a decrease in reactant is valid when only one reaction occurs or when the proportion of reactants contributing to the product under observation remains constant through time and through experimental conditions. When electron trar fer reactions are investigated via emission quenching as a funct: on of acceptor concentration, it is necessary to assume that the presence of quenchers does not affect the proportions of excited state donors that decay by emission to those that decay by some other mechanism (e.g. nonradiative decay). This assumption cannot be tested but, if it were

Figure 8.4: Comparison of R_q-corr obtained from emission quenching results (o) and EPR results (x).

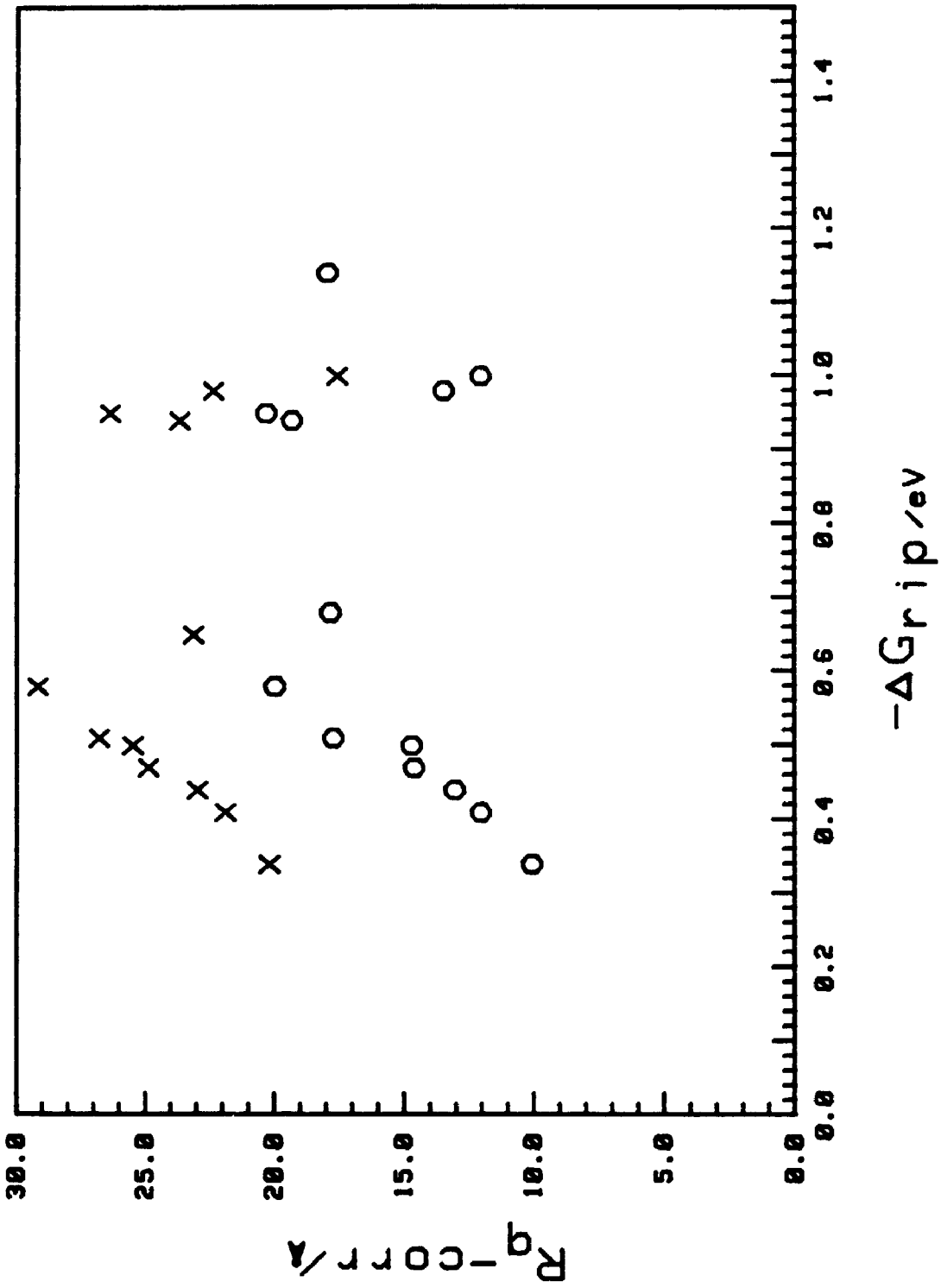
30.0
25.0
20.0
15.0
10.0
5.0
0.0
0.0
0.2
0.4
0.6
0.8
1.0
1.2
1.4
R_q-corr/Å
$-\Delta G_{rip}$/eV

not correct, the greatest error would occur in samples containing the largest amount of quencher and the largest discrepancies would appear in samples which used larger quencher concentrations. These samples were used in the experiments which found the smaller values of R_q since smaller values of R_q resulted from more shallow acceptor concentration dependence curves. Larger acceptor concentrations were required to reach the concentration independent range necessary to obtain a measure of A_{max}. However, as can be seen in Fig. 8.4, the differences are approximately constant regardless of the magnitude of R_q.

The effect of magnetic fields on processes involving triplet states is well established.[129,130] However, the design of the experiments described here results in cancellation (in the ratio A/A_{max}) of any effect which increases the product signals by proportional amounts. This feature of the design would eliminate artifacts resulting from extending the lifetime of the excited state. An extended lifetime would result in slight errors where lifetimes are included in the calculation, e.g. in normalizing all values of R_q to lifetimes of 1 μs, but these errors are small and would not account for the systematic difference seen in Fig 8.4.

Some preliminary experiments, using optical absorption spectroscopy to detect the presence of acceptor radical products, found greatly inflated values of R_q (e.g. 24 Å for $Ru[bpy]_3^{2+}$). These samples were not subjected to magnetic fields but they did contain EDTA, suggesting that EDTA, rather than magnetic field effects, is the cause of the observed differences.

The effect of EDTA was investigated at all stages of these experiments. Lifetimes and bimolecular quenching constants are reported

in Table 5.1 for five donors with and without EDTA. Although small differences are evident, the values are within the range of one standard deviation of the values found in the absence of EDTA and are therefore not significant. It was concluded that EDTA did not disturb the systems significantly.

Values of R_q found by emission quenching from samples containing EDTA are rather large also (see Table 6.1). This was attributed to interference by light absorption of the methyl viologen radical. It exhibits a broad absorption maximum around 608 nm (see Fig. 4.4) and after sample irradiation the light path through the sample was visibly blue.

This provides the most likely explanation of the difference seen in Figure 8.4. The presence of EDTA does not disrupt the forward ET reaction kinetics but blocks the back reaction, trapping methyl viologen radicals which absorb light. Samples containing higher concentrations of MV^{2+} experience more interference and less light impinges on the photosensitizers during the irradiation time. Consequently, the value of A_{max} (or I from emission quenching experiments in the presence of EDTA) is underestimated resulting in larger calculated values of R_q.

This phenomenon is impossible to avoid with these experimental systems. One solution would be to use a different acceptor whose radical product absorbed light less strongly or not at all through the range of wavelengths in which the donors absorb.

Another explanation of the observed phenomenon involves the salt effect. The effect of ionic strength on electron transfer rates in aqueous media has been widely investigated.[131] As ionic strength increases, ET rates increase. This effect is believed to result from the effect that increasing the concentration of charged particles has on

decreasing the efficiency of reactant escape from the solvent cage. As escape is impeded, the observed rate constant increases. Thus, this process is not expected to alter R_q, but could affect k_q which would interfere with the calculation of R_q. This effect is most pronounced at low salt concentations and at high concentrations the effect diminishes. A study to determine the specific effect of EDTA on the $Ru[bpy]_3^{2+}$ - MV^{2+} ET reaction reported somewhat complex behavior related to absolute and relative EDTA and MV^{2+} concentrations.[112] At high concentrations of EDTA (≈0.10 M) and MV^{2+} (≈0.02 M), an interaction between EDTA and MV^{2+} was found which appeared to enhance reverse ET or retard solvent cage escape. In the context of the present experiment, this phenomenon would result in larger signal amplitudes and the net effect would depend on exactly what constituted a high enough ionic strength to decrease the effect.

If this process were occurring, one might predict difficulty in obtaining a concentration-independent plateau related to the value of A_{max}. Such difficulty was noted occasionally, as signal amplitudes began to decrease slightly with increasing $[MV^{2+}]$ where a flat plateau was expected, although in other cases such difficulty did not occur (see Figure 7.1b).

The salt effect is clearly complex and has only recently become the focus of systematic investigation. Since the phenomenon was expected to be less pronounced in a viscous, organic liquid such as glycerol, the present experiments excluded control of ionic strength in a first approximation to a study of the hypothesis (concerning the relationship between R_q and $\Delta G^{\bullet}$).

Further work with the EPR experiments is recommended in which

ionic strength is controlled by the addition of $Na_2C_2O_4$ which is reported to extinguish the salt effect on reactant cage escape in aqueous solutions.[112] However, since $Na_2C_2O_4$ is insoluble in glycerol, another solvent such as ethylene glycol might be useful to approximate the desired conditions for solubility, viscosity, and the presence of hydroxyl groups.

8.3 Conclusion

Forward bimolecular electron transfer has been observed in the presence and absence of diffusion, as a function of reactant decay and of product formation. Observation of both reactant decay and product formation validates emission quenching as a measure of electron transfer in the systems studied and shows identical rate-energy relationships (with the difference discussed above). It is concluded that the reactions illustrate slightly non-adiabatic electron transfer in systems distorted by solvent hydrogen bonding. The inverted region rate decreases predicted by Marcus theory are observed when rate measurements are independent of diffusion.

The use of R_q as a parameter to investigate very fast reactions by steady state measurements provides interesting opportunities for further work. The range of time resolution that is available is limited by technology; probability theory permits us to transcend this limitation.

APPENDIX 1

Calculation of pH Required to Maximize Trianionic EDTA

Let E be the total concentration of EDTA.

$$E = [H_4Y] + [H_3Y^-] + [H_2Y^{2-}] + [HY^{3-}] + [Y^{4-}] \quad (1)$$

Each ion is in equilibrium with its deprotonated form and the equilibrium is controlled by an equilibrium constant. For example:

$$H_4Y \rightleftharpoons H_3Y^- + H^+ \quad (2)$$

$$K_1 = \frac{[H_3Y^-][H^+]}{[H_4Y]} \quad (3)$$

Similarly:

$$K_2 = \frac{[H_2Y^{2-}][H^+]}{[H_3Y^-]} \quad (4)$$

$$K_3 = \frac{[HY^{3-}][H^+]}{[H_2Y^{2-}]} \quad (5)$$

$$K_4 = \frac{[Y^{4-}][H^+]}{[HY^{3-}]} \quad (6)$$

Rearranging and substituting equations (3), (4), (5), and (6), one obtains expressions for each ion in terms of equilibrium constants, $[H^+]$, and $[HY^{3-}]$:

$$[H_4Y] = \frac{[H^+]^3[HY^{3-}]}{K_1K_2K_3} \tag{7}$$

$$[H_3Y^-] = \frac{[H^+]^2[HY^{3-}]}{K_2K_3} \tag{8}$$

$$[H_2Y^{2-}] = \frac{[H^+][HY^{3-}]}{K_3} \tag{9}$$

$$[Y^{4-}] = \frac{K_4[HY^{3-}]}{[H^+]} \tag{10}$$

From (7), (8), (9), and (10) into (1):

$$E = \frac{[HY^{3-}]}{[H^+]} \left\{ \frac{[H^+]^4}{K_1K_2K_3} + \frac{[H^+]^3}{K_2K_3} + \frac{[H^+]^2}{K_3} + [H^+] + K_4 \right\} \tag{11}$$

Let α_3 be the fraction of EDTA in 3^- ions.

$$\alpha_3 = \frac{[HY^{3-}]}{E} \tag{12}$$

and from (11) into (12):

$$\alpha_3 = \frac{K_1K_2K_3[H^+]}{[H^+]^4 + K_1[H^+]^3 + K_1K_2[H^+]^2 + K_1K_2K_3[H^+] + K_1K_2K_3K_4} \tag{13}$$

α_3 is maximized at

$$\frac{\partial \alpha_3}{\partial [H^+]} = 0 \qquad (14)$$

and from (13) into (14):

$$[H^+]^4 + \frac{2K_1[H^+]^3}{3} + \frac{K_1K_2[H^+]^2}{3} - \frac{K_1K_2K_3K_4}{3} = 0 \qquad (15)$$

Equation (15) was solved by the Basic program "QUARTIC", which follows, (using the solution equations for a quartic equation[132]) on a Hewlett Packard 9816 computer using pK_a values of 2.00, 2.69, 6.16, and 10.26.[133] The acceptable root was $[H^+]$ = 6.10E-9 M. Therefore $[EDTA^{3-}]$ is maximized at a pH of 8.21.

```
10    REM "QUARTIC "
20    REM This program solves a quartic equation for the specific case where
          the coefficients have been found to maximize [EDTA^3-]:
30    REM [H]^4 + (2*K1/3)[H]^3 + (K1*K2/3)[H]^2 - (K1*K2*K3*K4/3) = 0
40    Pk1=2.00
50    Pk2=2.69
60    Pk3=6.16
70    Pk4=10.26
80    K1=10^(-Pk1)
90    K2=10^(-Pk2)
100   K3=10^(-Pk3)
110   K4=10^(-Pk4)
120   A1=((2*K1)/3)
130   A2=((K1*K2)/3)
140   A3=0
150   A4=(0-(((K1*K2)*K3)*K4))/3
160   PRINTER IS 701
170   PRINT
180   PRINT "QUARTIC"
190   PRINT "This program solves the quartic equation found to maximize the
            concentration of trianionic EDTA:"
200   PRINT
210   PRINT "[H]^4 + A1*[H]^3 + A2*[H]^2 + A3*[H] + A4  =  0."
220   PRINT
230   PRINT "A1 = 2*K1/3, A2 = K1*K2/3, A3 = 0, A4 = -(K1*K2*K3*K4/3)"
240   PRINT
250   REM The following is a general program to solve the quartic equation:
          X^4 + A1*X^3 + A2*X^2 + A3*X + A4  =  0.
260   REM The solution equations are given in Spiegel, "Mathematical Handbook".
270   PRINT "The coefficients of the quartic equation are:"
280   PRINT "A1 =",A1
290   PRINT "A2 =",A2
300   PRINT "A3 =",A3
310   PRINT "A4 =",A4
320   REM Let Y be the real root of the cubic equation
340   REM Y^3  + B1Y^2  + B2Y + B3  =  0
350   B1=0-A2
360   B2=(A1*A3)-(4*A4)
370   B3=(((4*A2)*A4)-(A3*A3)-((A1*A1)*A4))
380   Q=((3*B2)-(B1*B1))/9
390   R=(((9*B1*B1)-(27*B3))-(2*B1*B1*B1))/54
400   U=((Q*Q*Q)+(R*R))
410   IF U<0 THEN GOTO 620
420   V=SQR(U)
430   Z1=R+V
440   Z2=R-V
450   S1=LOG(Z1)
460   S2=S1/3
470   S=EXP(S2)
480   IF Z2>0 THEN GOTO 550
490   Z2=-Z2
500   T1=LOG(Z2)
510   T2=T1/3
520   T=EXP(T2)
530   T=-T
540   GOTO 580
550   T1=LOG(Z2)
560   T2=T1/3
570   T=EXP(T2)
580   Y=(S+T)-(B1/3)
```

```
590   PRINT
600   PRINT "When the discriminant of the relevant cubic equation is greater
            than zero, there is one real root (Y)."
610   GOTO 830
620   Q3=(Q^3)
630   Q3=-Q3
640   Qs=SQR(Q3)
650   Cth=R/Qs
660   Th=1.570796-ATN(Cth/SQR(1-(Cth^2)))
670   Sq=2*(SQR(-Q))
680   Y1=(Sq*(COS(Th/3)))-(B1/3)
690   Y2=(Sq*(COS((Th/3)+(120*PI/180))))-(B1/3)
700   Y3=(Sq*(COS((Th/3)+(240*PI/180))))-(B1/3)
710   REM The solutions are the four roots of the quadratic equation
          Z^2 + C1*Z + C2  =  0.
720   PRINT
730   PRINT "When the discriminant of the relevant cubic equation is less than
            zero, the three roots (Y) are real and unequal."
740   PRINT
750   PRINT "Y = Y1"
760   Y=Y1
770   GOTO 830
780   PRINT "Y = Y2"
790   Y=Y2
800   GOTO 830
810   PRINT "Y = Y3"
820   Y=Y3
830   C11=((A1+SQR(((A1*A1)-(4*A2))+(4*Y)))/2)
840   C12=((A1-SQR(((A1*A1)-(4*A2))+(4*Y)))/2)
850   C21=((Y-SQR((Y*Y)-(4*A4)))/2)
860   C22=((Y+SQR((Y*Y)-(4*A4)))/2)
870   C112=C11*C11
880   C214=C21*4
890   IF C214>C112 THEN GOTO 920
900   H1=((0-C11)+SQR(C112-C214))/2
910   H2=((0-C11)-SQR(C112-C214))/2
920   C122=C12*C12
930   C224=C22*4
940   IF C224>C122 THEN GOTO 970
950   H3=((0-C12)+SQR(C122-C224))/2
960   H4=((0-C12)-SQR(C122-C224))/2
970   PRINT "The roots of the quartic equation are:"
980   PRINT "H1 =",H1
990   PRINT "H2 =",H2
1000  PRINT "H3 =",H3
1010  PRINT "H4 =",H4
1020  PRINT
1030  REM CHECK THAT H1*H2*H3*H4 = A4
1040  Ca4=H1*H2*H3*H4
1050  PRINT "CHECK: does H1*H2*H3*H4 = A4?  If yes, then accept roots."
1060  PRINT "H1*H2*H3*H4 =",Ca4
1070  PRINT "A4 =",A4
1080  PRINT
1090  IF Y=Y1 THEN GOTO 780
1100  IF Y=Y2 THEN GOTO 810
1110  PRINT "END"
1120  END
```

APPENDIX 2

Computer Program SVCALC to Calculate k_q from Eq. 5.1

SVCALC obtains the coefficients of a linear equation required to minimize χ^2.[134] Data and the calculated line of best fit may be printed or plotted.

```
10    REM "SVCALC"
20    REM This program calculates k(q) and t(0) from the Stern-Volmer eq. 2.43:
          1/t = 1/t(0) + k(q)[Q].
30    REM The input consists of an array of quencher concentrations, [Q],
          and corresponding emitter lifetimes, t.
40    REM The optimum fit is found from the coefficients required to minimize
          X-sqr.
50    OPTION BASE 1
60    DIM R$[50]
70    INPUT "The donor is ",R$
80    INPUT "Lab book.page # ",Lb
90    INPUT "N =",N
100   ALLOCATE T(N),Q(N),A(N),B(N),C(N),D(N),E(N),F(N),G(N),Y(N)
110   INPUT "Q/M DATA =",Q(*)
120   INPUT "t/us DATA =",T(*)
130   MAT Y= (1)/T
140   Sq=SUM(Q)
150   Ssq=Sq*Sq
160   MAT B= Q*Q
170   Sb=SUM(B)
180   Z=(N*Sb)-(Ssq)
190   R=1/Z
200   Sy=SUM(Y)
210   MAT A= Q*Y
220   Sa=SUM(A)
230   I=(R*((Sb*Sy)-(Sq*Sa)))
240   Sl=(R*((N*Sa)-(Sq*Sy)))
250   L=1/I
260   Kq=Sl*1.0E+6
270   Kql=Kq*L*1.0E-6
280   MAT F= Y-(I)
290   MAT G= (Sl)*Q
300   MAT C= F-G
310   MAT D= C*C
320   Xsqr=SUM(D)
330   PRINT "SVCALC calculates k(q) and t(o) from eq. 2.43."
340   PRINT "-------------------------------------------------------------"
350   PRINT
360   PRINT "The donor is ",R$
370   PRINT
380   PRINT "Lab book.page #",Lb
390   PRINT
400   PRINT "N =",N
410   PRINT "[Q]/M data ="
420   PRINT USING "DD.DDDDD";Q(*)
430   PRINT "t/us data ="
440   PRINT USING "DD.DDDDD";T(*)
450   PRINT "- - - - - - - - - - - - - - - - - - - - - - - - - - - - - - - - "
460   PRINT "k(q)/1/(Ms) =",Kq
470   PRINT
480   PRINT "t(0)/us =",L
490   PRINT "- - - - - - - - - - - - - - - - - - - - - - - - - - - - - - - - "
500   PRINT "X-sqr =",Xsqr
510   PRINT
520   PRINT "The residuals are "
530   PRINT USING "DD.DDDDD";C(*)
540   PRINT
550   PRINT "The product kq*to is expected to be small.  kq*to = "
560   PRINT USING "DDDD.DDDD";Kql
570   PRINT "-------------------------------------------------------------"
```

```
580    PRINT "**********************************************************************"
590    PRINT "----------------------------------------------------------------------"
600    END
```

APPENDIX 3

Computer Program PER_EM to Calculate R_q and R_q-corr From Emission Quenching Data

PER_EM Calculates R_q from eq 2.58 by interating with increasingly smaller increments of the critical volume v until χ^2 is minimized. The smallest increments are approximately equal to v/1000. v_{min} is then found by parabolic interpolation.[134] R_q-corr is calculated from eqs. 2.69 and 2.70. Data and the calculated function may be printed or plotted to show the $[MV^{2+}]$ dependence of $1 - I/I_o$.

```
EM "PER_EM"
20    REM This program uses (Yi - Yc)^2 in Xsq.
30    REM This program determines the Perrin critical quenching volume, V, and
      hence Rq from EM data for a bimolecular reaction under the condition of
40    REM static quenching.  k(q) and t(o) are obtained from SVCALC, and data
      values for [Q], Ii, and Io are input.
50    REM V is found by minimizing X-sqr with respect to V by iteration.
60    REM (1-Ii/Io) = 1-{1/(1 + k(q)t(o)Qi)exp[VNQi]}
70    OPTION BASE 1
80    DIM Do$[50]
90    INPUT "Do you want to plot or print the results?  Answer N, Y, or YPLOT.",
Gr$
100   INPUT "The donor is ",Do$
110   INPUT "Lab book,page # =",Lbp
120   INPUT "t(o)/us =",To
130   Tu=To*1.0E-6
140   INPUT "k(q)/1/(Ms) =",Kq
150   INPUT "N =",N
160   Kt=Tu*Kq
170   ALLOCATE I(N),B(N),C(N),D(N),F(N),F2(N),G(N),H(N),J(N),L(N),M(N),O(N),P(N)
,Q(N),Q2(N),R(N),S(N),Y(N),Y2(N),R1(N),R2(N),R3(N),R4(N)
180   ALLOCATE R5(N),R6(N),Vm(N)
190   !INPUT "Io =",Io
200   INPUT "I DATA =",I(*)
210   INPUT "MV vol. DATA =",Vm(*)
220   INPUT "Total Sample Vol. =",Tv
230   INPUT "MV conc. =",Mvc
240   Mv=Mvc/Tv
250   MAT Q= Vm*(Mv)
260   MAT B= (I(1))/I
270   MAT C= (1)/B
280   PRINTER IS 701
290   PRINT "PER_EM calculates Rq from EMISSION data."
300   PRINT "Xsq is NOT weighted."
310   PRINT "kq is FIXED."
320   PRINT "-------------------------------------------------------------------"
330   PRINT
340   PRINT "The donor is",Do$
350   PRINT
360   PRINT "Lab book,page # =",Lbp
370   PRINT
380   PRINT "t(o)/us =",To
390   PRINT "k(q)/1/(Ms) =",Kq
400   PRINT
410   PRINT "N =",N
420   PRINT "I data ="
430   PRINT USING "DDDD.DDD":I(*)
440   PRINT "Io =",Io
450   PRINT "Q data ="
460   PRINT USING "DDDD.DDD";Q(*)
470   PRINT
480   PRINT "RESULTS"
490   PRINT "-------"
500   GOTO 680
510 Cc:             !Minimization of Xsq w.r.t. V.
520   MAT D= Q*(E)
530   FOR Z=1 TO N
540   F(Z)=EXP(D(Z))                          !F = exp[VNQ]
550   NEXT Z
560   REM Calculation of Xsq.
```

```
570   REM Xsq = SUM{[C - [1-1/((1 + k(q)t(o)Q)exp(VNQ))]]2}
580   MAT M= (Kt)*Q
590   MAT O= (1)+M
600   MAT P= O . F
610   MAT R1= B-P
620   MAT R2= R1 . R1
630   !S1=SUM(R4)
640   !IF S1=0 THEN GOTO 630
650   Xsq=SUM(R2)
660   RETURN
670   REM END OF CALC----------------------------------------------------------
680   E=.200
690   GOSUB Cc
700   Xsq1=Xsq
710   E=E+.5
720   GOSUB Cc
730   Xsq2=Xsq
740   IF Xsq2<Xsq1 THEN GOTO 690
750   E=E-1.0
760   IF E>0 THEN GOTO 790
770   Rq=0
780   GOTO 1230
790   REM E incremented by 0.01
800   GOSUB Cc
810   Xsq1=Xsq
820   E1=E
830   E=E+.01
840   GOSUB Cc
850   Xsq2=Xsq
860   E2=E
870   IF Xsq2<Xsq1 THEN GOTO 800
880   E=E-.02
890   E0=E
900   GOSUB Cc
910   Xsq0=Xsq
920   Emin=E2-(.01*(((Xsq2-Xsq1)/(Xsq2-(2*Xsq1)+Xsq0))+1/2))
930   E=Emin
940   GOSUB Cc
950   Xsqm=Xsq
960   E=E0
970   GOSUB Cc
980   Xsq1=Xsq
990   E1=E
1000  E=E+.001
1010  GOSUB Cc
1020  Xsq2=Xsq
1030  E2=E
1040  IF Xsq2<Xsq1 THEN GOTO 970
1050  E=E2-.002
1060  GOSUB Cc
1070  E0=E
1080  Xsq0=Xsq
1090  Emin=E2-(.001*(((Xsq2-Xsq1)/(Xsq2-(2*Xsq1)+Xsq0))+1/2))
1100  E=Emin
1110  GOSUB Cc
1120  Xsqm=Xsq
1130  Rq3=((3*E)/((4*PI)*6.02204531))*10000
1140  Lrq=(LOG(Rq3))/3
1150  Rq=EXP(Lrq)
1160  REM Calculation of Rq normalized to a lifetime of 1 us and corrected for
```

```
        finite molecular volume (assuming Ro = 10 angs).
1170  REM It is also assumed that the range parameter "a" = 0.75 angs.
1180  C1=(Rq-10)/.75
1190  C2=EXP(C1)
1200  C3=C2/To
1210  C4=LOG(C3)
1220  Rqc=(.75*C4)+10
1230  C5=((Rqc*Rqc)*Rqc)+1000
1240  C6=LOG(C5)
1250  C7=C6/3
1260  Rqcc=EXP(C7)
1270  REM Calc of resids
1280  MAT R3= (I(1))/P
1290  MAT R4= (1)/P
1300  MAT R5= C-R4
1310  MAT R6= (1)-C
1320  PRINT "XSQmin =",Xsqm
1330  PRINT "Vmin*L =",Emin
1340  !PRINT USING "DDD.DDD":Emin
1350  PRINT
1360  PRINT "Rq/angs =",Rq
1370  !PRINT USING "DDD.DDDDD":Rq
1380  PRINT
1390  PRINT "Rq, corrected for molecular volume and normalized to t(o) = 1 us."
1400  PRINT "Rq-corr/angs =",Rqcc
1410  !PRINT USING "DDD.DDDDD":Rqcc
1420  PRINT "-----------------------------------------------------------------"
1430  PRINT
1440  PRINT "Calculated dependent variables."
1450  PRINT "-------------------------------"
1460  PRINT "I(calc) ="
1470  PRINT USING "DDDD.DDD":R3(*)
1480  PRINT
1490  PRINT "Residuals"
1500  PRINT "---------"
1510  PRINT "(Ic - Ii)/Io ="
1520  PRINT USING "DDDD.DDD":R5(*)
1530  REM Program Name:  PERRIN
1540  REM This program prints or plots 1 - I/Io versus [Q] and the residuals
        found by "PER_EPR".
1550  GINIT
1560  IF Gr$="Y" THEN GOTO 1590
1570  IF Gr$="N" THEN GOTO 2560
1580  IF Gr$="YPLOT" THEN GOTO 2440
1590  VIEWPORT 20,110,20,80
1600 Plot1:GRAPHICS ON
1610  WINDOW 0,.3,0,1.20
1620  AXES .01,.04,0,0.5,5,3
1630  FRAME
1640  CLIP OFF
1650  CSIZE 2.5,.6
1660  LORG 4
1670  FOR K=0 TO .34 STEP .1
1680  MOVE K,-.07
1690  LABEL USING "Z.DD":K
1700  NEXT K
1710  LORG 5
1720  FOR K=.2 TO 1.24 STEP .2
1730  MOVE -.0160,K
1740  LABEL USING "Z.DD":K
```

```
1750  NEXT K
1760  CSIZE 4,.6
1770  MOVE .15,-.13
1780  LABEL "[MV    "
1790  MOVE .155,-.13
1800  LABEL "    ]/M"
1810  CSIZE 2.5,.6
1820  MOVE .152,-.11
1830  LABEL "2+"
1840  DEG
1850  LDIR 90
1860  MOVE -.041,.61
1870  CSIZE 4,.6
1880  LABEL "1-I/Io"
1890  DEG
1900  LDIR 0
1910  CSIZE 3,.6
1920  MOVE .15,1.3
1930  LABEL "(c)"
1940  CSIZE 2.5,.7
1950  FOR K=1 TO N
1960    MOVE Q(K),R6(K)
1970    LABEL "X"
1980  NEXT K
1990  MOVE 0,0
2000  FOR K1=0 TO .3 STEP .0005
2010  S0=Emin*K1
2020  S1=EXP(S0)
2030  S2=(1+(Kt*K1))*S1
2040  S11=1/S2
2050  S3=1-S11
2060  DRAW K1,S3
2070  NEXT K1
2080  IF Gr$="Y" THEN
2090    PRINTER IS 701
2100    DUMP GRAPHICS
2110  END IF
2120  GCLEAR
2130  IF Gr$="Y" THEN GOTO 2160
2140  REM Return to main program.
2150  RETURN
2160  VIEWPORT 20,110.45,75
2170 Plot2:  REM START OF RESIDUALS PLOT
2180  WINDOW 0,.3,-.1,.1
2190  AXES .01,.01,0.0,5,5,3
2200  CLIP OFF
2210  CSIZE 2.5,.6
2220  LORG 5
2230  FOR K=-.1 TO .11 STEP .1
2240  MOVE -.026,K
2250  LABEL USING "SZ.DD":K
2260  NEXT K
2270  CSIZE 4,.6
2280  LORG 5
2290  MOVE .15,.15
2300  LABEL "Residuals"
2310  MOVE 0,0
2320  FOR K=1 TO N
2330  MOVE Q(K),R5(K)
2340  CSIZE 2.5,.7
```

```
2350  LABEL "X"
2360  NEXT K
2370  IF Gr$="Y" THEN
2380    PRINTER IS 701
2390    DUMP GRAPHICS
2400  END IF
2410  GCLEAR
2420  IF Gr$="Y" THEN GOTO 2560
2430  RETURN
2440  REM This is the start of the plotter command.
2450  PRINTER IS 1
2460  PRINT "SET PAPER AND PEN READY ON PLOTTER & PRESS ""CONT""."
2470  PAUSE
2480  PLOTTER IS 702,"HPGL"
2490  OUTPUT 702;"VS10"
2500  Xmax=100*MAX(1,RATIO)
2510  Ymax=100*MAX(1,1/RATIO)
2520  VIEWPORT .2*Xmax,.85*Xmax,.35*Ymax,.8*Ymax
2530  GOSUB Plot1
2540  VIEWPORT .2*Xmax,.85*Xmax,.1*Ymax,.2*Ymax
2550  GOSUB Plot2
2560  REM This is the end of this program segment.
2570  GRAPHICS OFF
2580  BEEP
2590  PRINT "THE END"
2600  END
```

APPENDIX 4

Computer Program PER_EPR to Calculate R_q and R_q-corr From EPR Data

PER_EPR is similar to PER_EM only it is modified for EPR data input. Data and the calculated function may be printed or plotted to show the $[MV^{2+}]$ dependence of A/A_{max}.

```
10    REM "PER_EPR"
20    REM This program uses (Ai - Ac)^2 in Xsq, i.e. Xsq is NOT weighted.
30    REM This program determines the Perrin critical quenching volume, V, and
      hence Rq from EPR data for a bimolecular reaction under the condition of
40    REM static quenching.  k(q) and t(o) are obtained from SVCALC, and data
      values for [Q], Ai, and Amax are input.
50    REM V is found by minimizing X-sqr with respect to V by iteration.
60    REM Amax is constant through the iteration.
70    REM 1/(1-Ai/Amax) = (1 + k(q)t(o)Qi)exp[VNQi]
80    OPTION BASE 1
90    DIM Do$[50]
100   INPUT "Do you want to plot or print the results?  Answer N, Y, or YPLOT.",
Gr$
110   INPUT "The donor is ",Do$
120   INPUT "Lab book.page # =",Lbp
130   INPUT "t(o)/us =",To
140   Tu=To*1.0E-6
150   INPUT "k(q)/1/(Ms) =",Kq
160   INPUT "Amax =",Amax
170   INPUT "N =",N
180   ALLOCATE A(N),B(N),C(N),D(N),F(N),F2(N),G(N),H(N),J(N),L(N),M(N),O(N),P(N)
,Q(N),Q2(N),R(N),S(N),Y(N),Y2(N),R1(N),R2(N),R3(N),R4(N)
190   ALLOCATE R5(N),R6(N),Vm(N),R8(N)
200   INPUT "A DATA =",A(*)
210   INPUT "MV vol. DATA =",Vm(*)
220   INPUT "MV conc. =",Mvc
230   MAT Q= Vm*(Mvc)
240   MAT B= A/(Amax)
250   !MAT C= (1)-B
260   !MAT Y= (1)/C                                !Y
270   PRINTER IS 701
280   PRINT "PER_EPR calculates Rq from EPR data.  Amax is constant."
290   PRINT "Xsq is NOT weighted."
300   PRINT "-------------------------------------------------------------------"
310   PRINT
320   PRINT "The donor is",Do$
330   PRINT
340   PRINT "Lab book.page # =",Lbp
350   PRINT
360   PRINT "t(o)/us =",To
370   !PRINT USING "DD.DDDD";To
380   PRINT "k(q)/1/(Ms) =",Kq
390   !PRINT USING "D.DDDDESZZ";Kq
400   PRINT
410   PRINT "N =",N
420   PRINT "Amax (input) =",Amax
430   PRINT "A data ="
440   PRINT USING "DDDD.DDD";A(*)
450   PRINT "Q data ="
460   PRINT USING "DDDD.DDD";Q(*)
470   PRINT
480   PRINT "RESULTS"
490   PRINT "-------"
500   GOTO 740
510 Cc:             !Minimization of Xsq w.r.t. V.
520   MAT D= Q*(E)
530   FOR Z=1 TO N
540   F(Z)=EXP(D(Z))                               !F = exp[VNQ]
550   NEXT Z
560   Kt=Kq*Tu
```

```
570   REM Calculation of Xsq.
580   REM Xsq = SUM{[Y - (1 + k(q)t(o)Q)exp(VNQ)]2}
590   MAT M= (Kt)*Q
600   MAT O= (1)+M
610   MAT P= O . F
620   MAT R1= (1)/P
630   MAT R2= (1)-R1
640   MAT R3= R2*(Amax)
650   MAT R4= R3-A
660   MAT R8= R4/(Amax)
670   S1=SUM(R4)
680   IF S1=0 THEN GOTO 710
690   MAT R5= R4 . R4
700   MAT R6= R5/A
710   Xsq=SUM(R5)
720   RETURN
730   REM END OF CALC-------------------------------------------------------
740   E=.200
750   GOSUB Cc
760   Xsq1=Xsq
770   E=E+.5
780   GOSUB Cc
790   Xsq2=Xsq
800   IF Xsq2<Xsq1 THEN GOTO 750
810   E=E-1.0
820   IF E>0 THEN GOTO 850
830   Rq=0
840   GOTO 1290
850   REM E incremented by 0.01
860   GOSUB Cc
870   Xsq1=Xsq
880   E1=E
890   E=E+.01
900   GOSUB Cc
910   Xsq2=Xsq
920   E2=E
930   IF Xsq2<Xsq1 THEN GOTO 860
940   E=E-.02
950   E0=E
960   GOSUB Cc
970   Xsq0=Xsq
980   Emin=E2-(.01*(((Xsq2-Xsq1)/(Xsq2-(2*Xsq1)+Xsq0))+1/2))
990   E=Emin
1000  GOSUB Cc
1010  Xsqm=Xsq
1020  E=E0
1030  GOSUB Cc
1040  Xsq1=Xsq
1050  E1=E
1060  E=E+.001
1070  GOSUB Cc
1080  Xsq2=Xsq
1090  E2=E
1100  IF Xsq2<Xsq1 THEN GOTO 1030
1110  E=E2-.002
1120  GOSUB Cc
1130  E0=E
1140  Xsq0=Xsq
1150  Emin=E2-(.001*(((Xsq2-Xsq1)/(Xsq2-(2*Xsq1)+Xsq0))+1/2))
1160  E=Emin
```

```
1170  GOSUB Cc
1180  Xsqm=Xsq
1190  Rq3=((3*E)/((4*PI)*6.02204531))*10000
1200  Lrq=(LOG(Rq3))/3
1210  Rq=EXP(Lrq)
1220  REM Calculation of Rq normalized to a lifetime of 1 us and corrected for
          finite molecular volume (assuming Ro = 10 angs).
1230  REM It is also assumed that the range parameter "a" = 0.75 angs.
1240  C1=(Rq-10)/.75
1250  C2=EXP(C1)
1260  C3=C2/To
1270  C4=LOG(C3)
1280  Rqc=(.75*C4)+10
1290  C5=((Rqc*Rqc)*Rqc)+1000
1300  C6=LOG(C5)
1310  C7=C6/3
1320  Rqcc=EXP(C7)
1330  REM CONSISTENCY TEST
1340  REM IF Q=0.05, WHAT IS A/Amax?
1350  T1=Emin*.05
1360  T2=EXP(T1)
1370  T3=1+(Kt*.05)
1380  T4=T3*T2
1390  T5=1-(1/T4)
1400  PRINT "CONSISTENCY TEST"
1410  PRINT "A/Amax AT Q = 0.05 M =",T5
1420  PRINT
1430  PRINT "XSQmin =",Xsqm
1440  PRINT "Vmin*L =",Emin
1450  !PRINT USING "DDD.DDD";Emin
1460  PRINT
1470  PRINT "Rq/angs =",Rq
1480  !PRINT USING "DDD.DDDDD";Rq
1490  PRINT
1500  PRINT "Rq, corrected for molecular volume and normalized to t(o) = 1 us."
1510  PRINT "Rq-corr/angs =",Rqcc
1520  !PRINT USING "DDD.DDDDD":Rqcc
1530  PRINT "-------------------------------------------------------------------"
1540  PRINT
1550  PRINT "Calculated dependent variables."
1560  PRINT "------------------------------"
1570  PRINT "A(calc) ="
1580  PRINT USING "DDDD.DDD";R3(*)
1590  PRINT
1600  PRINT "Residuals"
1610  PRINT "---------"
1620  PRINT "Ac - Ai ="
1630  PRINT USING "DDDD.DDD":R4(*)
1640  REM Program Name:  PERRIN
1650  REM This program prints or plots A/Amax versus [Q] and the residuals found
          by "PER_EPR".
1660  GINIT
1670  IF Gr$="Y" THEN GOTO 1700
1680  IF Gr$="N" THEN GOTO 2670
1690  IF Gr$="YPLOT" THEN GOTO 2550
1700  VIEWPORT 20,110,20,80
1710 Plot1:GRAPHICS ON
1720  WINDOW 0,.3,0,1.20
1730  AXES .01,.04,0,0,5,5,3
1740  FRAME
```

```
1750  CLIP OFF
1760  CSIZE 2.5,.6
1770  LORG 4
1780  FOR K=0 TO .34 STEP .1
1790  MOVE K,-.07
1800  LABEL USING "Z.DD";K
1810  NEXT K
1820  LORG 5
1830  FOR K=.2 TO 1.24 STEP .2
1840  MOVE -.016,K
1850  LABEL USING "Z.DD";K
1860  NEXT K
1870  CSIZE 4,.6
1880  MOVE .15,-.13
1890  LABEL "[MV    "
1900  MOVE .155,-.13
1910  LABEL "    ]/M"
1920  CSIZE 2.5,.6
1930  MOVE .152,-.11
1940  LABEL "2+"
1950  DEG
1960  LDIR 90
1970  MOVE -.045,.61
1980  CSIZE 4,.6
1990  LABEL "A/Amax"
2000  DEG
2010  LDIR 0
2020  CSIZE 3,.6
2030  MOVE .15,1.3
2040  LABEL "(c)"
2050  CSIZE 2.5,.7
2060  FOR K=1 TO N
2070    MOVE Q(K),B(K)
2080    LABEL "X"
2090  NEXT K
2100  MOVE 0,0
2110  FOR K1=0 TO .3 STEP .0005
2120  S0=Emin*K1
2130  S1=EXP(S0)
2140  S2=(1+(Kt*K1))*S1
2150  S11=1/S2
2160  S3=1-S11
2170  DRAW K1,S3
2180  NEXT K1
2190  IF Gr$="Y" THEN
2200    PRINTER IS 701
2210    DUMP GRAPHICS
2220  END IF
2230  GCLEAR
2240  IF Gr$="Y" THEN GOTO 2270
2250  REM Return to main program.
2260  RETURN
2270  VIEWPORT 20,110,45,75
2280 Plot2:  REM START OF RESIDUALS PLOT
2290  WINDOW 0,.3,-.1,.1
2300  AXES .01,.01,0,0,5,5,3
2310  CLIP OFF
2320  CSIZE 2.5,.6
2330  LORG 5
2340  FOR K=-.1 TO .11 STEP .10
```

```
2350  MOVE -.02,K
2360  LABEL USING "SZ.DD";K
2370  NEXT K
2380  CSIZE 4,.6
2390  LORG 5
2400  MOVE .15,.15
2410  LABEL "Residuals"
2420  MOVE 0,0
2430  FOR K=1 TO N
2440  MOVE Q(K),R8(K)
2450  CSIZE 2.5,.7
2460  LABEL "X"
2470  NEXT K
2480  IF Gr$="Y" THEN
2490    PRINTER IS 701
2500    DUMP GRAPHICS
2510  END IF
2520  GCLEAR
2530  IF Gr$="Y" THEN GOTO 2670
2540  RETURN
2550  REM This is the start of the plotter command.
2560  PRINTER IS 1
2570  PRINT "SET PAPER AND PEN READY ON PLOTTER & PRESS ""CONT""."
2580  PAUSE
2590  PLOTTER IS 702,"HPGL"
2600  OUTPUT 702;"VS10"
2610  Xmax=100*MAX(1,RATIO)
2620  Ymax=100*MAX(1,1/RATIO)
2630  VIEWPORT .2*Xmax,.85*Xmax,.35*Ymax,.8*Ymax
2640  GOSUB Plot1
2650  VIEWPORT .2*Xmax,.85*Xmax,.1*Ymax,.2*Ymax
2660  GOSUB Plot2
2670  REM This is the end of this program segment.
2680  GRAPHICS OFF
5470  BEEP
5480  PRINT "THE END"
5490  END
```

APPENDIX 5

Computer Program SCDATAFIT to Fit R_q Values Using Eqs. 2.26 and 2.67

SCDATAFIT fits eqs. 2.26 and 2.67 to experimentally determined values of R_q. The fitting parameters H_{ps}, λ_s, and λ_v are varied by increasingly smaller increments to minimize χ^2. The smallest increments are 1/100 of the value obtained in the preceding iteration level. Values of the high frequency $\hbar\omega$ are input from an external iteration loop that increments $\hbar\omega$ by 10 cm^{-1}.

```
10    REM "SCDATAFIT"
20    REM This program fits experimental values of Rq to the semi-classical
        rate-energy equation 2.26.
30    REM k(r) = (pi/(hLskBT))^1/2(V(Ro))^2 F
40    REM F  =  SUM(w)(e^-S*S^w/w! exp-[(dG + Ls + whv)^2/4LskBT]
50    REM Rq = Ro + a ln(v(o)Ft
60    OPTION BASE 1
70    INPUT "low freq/1/cm =",Oml
80    INPUT "high freq/1/cm =",Omh
90    INPUT "a =",A
100   INPUT "number of data sets =",N
110   ALLOCATE B(N),C(N),E(N),J(N),M(N),P(N),R(N),F(0:50),Dg(N),Rq(N),Rc(N),Ro(N
),X(N),Xs(N),Lo(N),X8(N),Y4(N),X2(N),T0(N)
120   INPUT "Rq/angs exptl. =",Rq(*)
130   INPUT "-DG/eV =",Dg(*)
140   MAT Dg= (0)-Dg
150   INPUT "to/us =",Lo(*)
160   MAT Lo= T0
170   INPUT "Ro/angs =",Ro(*)
180   MAT Lo= Lo*(1.E-6)
190   GOTO 1740
200 Calck:          !Calculation of v(o)F
210   Lt=Ls*(298*1.38065812E-23)/1.6021773349E-19          !units = eV^2
220   Pr=SQR((PI/(((1.0545726663E-34/1.6021773349E-19)^2)*Lt)))! =1/[eV^2*s]
230   Ho=(Omh/8065.479)
240   S=Lv/Ho
250   FOR Z=1 TO N
260   FOR W=0 TO 50
270       Ft=1
280    IF W=0 THEN GOTO 320
290       FOR I=W TO 1 STEP -1
300       Ft=I*Ft
310       NEXT I
320   X0=(W*Ho)
330   Y=EXP(-S)
340   X6=(S^W)
350   X1=(Dg(Z)+Ls+X0)
360   X20=(X1^2)
370   X3=(X20/(4*Lt))
380   X4=-X3
390   IF X3>1.E+2 THEN GOTO 420
400   X5=EXP(X4)
410   GOTO 430
420   X5=0
430   F(W)=((Y*X6)/Ft)*X5
440   NEXT W
450   Fc=SUM(F)
460   K=((Pr*Fc)*(V*V))
470   X7=K*Lo(Z)
480   X8(Z)=LOG(X7)
490   NEXT Z
500   MAT B= (A)*X8
510   MAT Rc= Ro+B
520   MAT X= Rc-Rq
530   MAT Xs= X . X
540   Xsq=SUM(Xs)
550   RETURN
560   REM Eq 2.26 is fit to the data by minimizing X-sqr with respect to lambda
        s, lambda v, and the electronic matrix element V.
570   !ls and lv are held constant, and V is varied.
```

```
580 Cmin:                                   ! X-sqr is minimized by iteration
590   REM V is incremented by powers of 10
600   GOSUB Calck
610   Xsq1=Xsq
620   V=V*10
630   GOSUB Calck
640   Xsq2=Xsq
650   IF Xsq2<Xsq1 THEN GOTO 580
660   V=V/10
670   Va=V
680   REM V is incremented by 1.0*V
690   GOSUB Calck
700   Xsq1=Xsq
710   V=V+Va
720   GOSUB Calck
730   Xsq2=Xsq
740   IF Xsq2<Xsq1 THEN GOTO 680
750   V=V-Va
760   Va=.1*V
770   REM V is incremented by 0.1*V.
780   GOSUB Calck
790   Xsq1=Xsq
800   V=V+Va
810   GOSUB Calck
820   Xsq2=Xsq
830   IF Xsq2<Xsq1 THEN GOTO 770
840   V=V-Va
850   Va=.01*V
860   REM V is incremented by 0.01*V.
870   GOSUB Calck
880   Xsq1=Xsq
890   V=V+Va
900   V1=V
910   GOSUB Calck
920   Xsq2=Xsq
930   V2=V
940   IF Xsq2<Xsq1 THEN GOTO 860
950   V=V-(2*Va)
960   GOSUB Calck
970   Xsq0=Xsq
980   Vmin=V2-(Va*(((Xsq2-Xsq1)/(Xsq2-(2*Xsq1)+Xsq0))+(1/2)))
990   V=V1
1000  REM With V and Ls constant, Lv is varied to minimize X-sqr.
1010  Lv=.2
1020  REM Lv is incremented by 0.1.
1030  GOSUB Calck
1040  Xsq1=Xsq
1050  Lv=Lv+.1
1060  GOSUB Calck
1070  Xsq2=Xsq
1080  IF Xsq2<Xsq1 THEN GOTO 1020
1090  Lv=Lv-.1
1100  REM Lv is incremented by .01.
1110  GOSUB Calck
1120  Xsq1=Xsq
1130  Lv=Lv+.01
1140  GOSUB Calck
1150  Xsq2=Xsq
1160  Lv2=Lv
1170  IF Xsq2<Xsq1 THEN GOTO 1100
```

```
1180  Lv=Lv-.02
1190  GOSUB Calck
1200  Xsq0=Xsq
1210  Lvmin=Lv2-(.01*(((Xsq2-Xsq1)/(Xsq2-(2*Xsq1)+Xsq0))+(1/2)))
1220  Lv=Lvmin
1230  REM With V and Lv constant, Ls is varied to minimize X-sqr.
1240  Ls=.1
1250  REM Ls is incremented by .1.
1260  GOSUB Calck
1270  Xsq1=Xsq
1280  Ls=Ls+.1
1290  GOSUB Calck
1300  Xsq2=Xsq
1310  IF Xsq2<Xsq1 THEN GOTO 1250
1320  Ls=Ls-.1
1330  REM Ls is incremented by 0.01.
1340  GOSUB Calck
1350  Xsq1=Xsq
1360  Ls=Ls+.01
1370  GOSUB Calck
1380  Xsq2=Xsq
1390  Ls2=Ls
1400  IF Xsq2<Xsq1 THEN GOTO 1330
1410  Ls=Ls-.02
1420  GOSUB Calck
1430  Xsq0=Xsq
1440  Lsmin=Ls2-(.01*(((Xsq2-Xsq1)/(Xsq2-(2*Xsq1)+Xsq0))+(1/2)))
1450  Ls=Lsmin
1460  GOSUB Calck
1470  RETURN
1480  REM Begin iteration.
1490  V=1.E-10
1500  Lv=.6
1510  Ls=.2
1520  GOSUB Cmin
1530  Xsq10=Xsq
1540  V=V/10
1550  GOSUB Cmin
1560  Xsq20=Xsq
1570  Z1=Xsq10-Xsq20
1580  Z2=(SQR(Z1*Z1))/Xsq20
1590  PRINT "% DIF IN XSQ =",Z2
1600  IF Z2<.01 THEN GOTO 1670
1610  V=V-(.1*V)
1620  GOSUB Cmin
1630  Xsq30=Xsq
1640  Z3=Xsq20-Xsq30
1650  Z4=(SQR(Z3*Z3))/Xsq30
1660  PRINT "Z4 =",Z4
1670  REM End of calc.
1680  PRINT "X-sqr is ",Xsq
1690  PRINT "V =",V
1700  PRINT "Lambda v =",Lv
1710  PRINT "Lambda s =",Ls
1720  PRINT "THE END."
1730  RETURN
1740  REM VARY W
1750  FOR Hf=100 TO 1500 STEP 10
1760  Omh=Hf
1770  PRINT
```

```
1780  PRINT "HHHHHHHHHHHHHHHHHHHHHHHHHHHHHHHHHHHHHHHHHHHHHHHHHHHHHHHHHHHHHHHHHHHHHHHHHHHHHHHH"
1790  PRINT "HIGH FREQ -",Hf
1800  GOSUB 1480
1810  NEXT Hf
1820  PRINT "THE VERY VERY END"
1830  END
```

APPENDIX 6

Preliminary Experiments at Low Temperature

Preliminary experiments attempted to obtain R_c with measurements of photo-induced EPR signals in a test system comprising $Ru[bpy]^{2+}$, MV^{2+}, and $EDTA^{3-}$ dispersed in rigid glycerol matrices. Both the saturation method and the probability method, described in sections 3.3.1 and 3.3.2 , were used.

Initial work used the saturation method exclusively and controlled the sample temperature with a Varian Variable Temperature Controller. Gaseous nitrogen passed through a copper coil immersed in a liquid nitrogen bath and through an insert dewar placed in the EPR cavity. A small heater warmed the nitrogen gas to the required temperature. The temperature was measured with a copper-constantan thermocouple approximately 4 cm above the detection window. The temperature at this location, which was cool enough to prevent diffusion during the time of measurement and warm enough to allow signal (radical) formation, was $-65.0^{\circ}C$.

An $EDTA^{3-}$ concentration dependence curve showed a concentration-independent range between approximately 0.04 and 0.12 M; experimental samples used constant concentrations of 0.1 M.

Each sample was irradiated constantly with light from a 200 W mercury-xenon lamp (Oriel, Model 8500) passed through the series of filters described in section 7.2. The EPR signal amplitude was measured every hour until it had increased by less than 0.25 cm ($\simeq$ 1 %) in the preceding hour. In practice, this took between 12 to 48 hours. During longer experiments, the time between measurements was increased to 2½ hours, which was the effective lifetime of the liquid nitrogen.

When signal saturation had been achieved, it was assumed that all

acceptors within R_c of any donor had been reduced. The concentration of reduced acceptors was determined by comparing the signal amplitude to a standard curve previously prepared by irradiating dilute solutions of MV^{2+} (and $EDTA^{3-}$) without Corning filters until signal saturation occurred. The volume occupied by the reduced acceptors was calculated from the solution acceptor concentration. The volume per donor was then found from the solution donor concentration.

Preliminary experiments determined that the signal amplitude at saturation was a linear function of acceptor concentration up to $[MV^{2+}]$ = 0.06 M and a linear function of donor concentration up to $[Ru(bpy)_3^{2+}]$ = 1.25×10^{-4} M. Samples containing reactant concentrations less than these values were used to calculate R_c = 17.2 ±1.0 Å. The error was reasonably random and probably due in part to the rigorous demand of the experimental design that the irradiation volume be identical from sample to sample. (Since the lamp had to be moved between experiments, an "optical bench" was approximated with labelled masking tape.)

The difference between this and the published value (10.9 Å[75]) is presumably due to the very different method of measurement.

Since these experiments consumed great quantities of expensive nitrogen gas, a temperature control system was built which did not use commercially available gas. Cold nitrogen gas was produced by passing small currents (≃ 0.55 A) from Hewlett Packard Model 6205B DC power sources through three 50-ohm Nichrome resistors (Tandy Corp.) immersed in liquid nitrogen in a dewar sealed with silicone rubber glue and Armaflex. The cold gas passed through a copper coil immersed in a circulating methanol bath contained in an optical pyrex dewar. Since the temperature in the bath fluctuated with the room temperature, three

attempts were made to install a feedback-controlled heating system. One circuit was built by me, one by the Chemistry Department Electronics Shop, and one was adapted from a commercially built temperature control system. All three failed. To reduce temperature fluctuations, the pyrex dewar was immersed in a constant low-temperature water bath controlled by a Thermolyne heater-stirrer and cooled by a thermoelectric heat pump. The water bath was maintained at 3.00°C and the methanol bath at -76°C. The temperature in the methanol bath was monitored by a copper-constantan thermocouple connected to a Cole-Parmer Model 8373-10 chart recorder and the temperature was found to vary approximately ±1°C over 12 hours.

A merry-go-round was designed for insertion into the methanol bath. It was built by the University of Western Ontario Machine Shop. It was made from solid aluminum and designed to rotate eight samples past two windows. Insurmountable difficulties were experienced in trying to obtain two suitable light sources and the apparatus was finally abandoned in favour of a fixed single sample holder which exposed one sample at a time to irradiation from the 200 W Oriel lamp mentioned previously.

Preliminary experiments established that saturation time in this apparatus was approximately 48 hours.

Several experiments were performed to investigate the probability method using eq. 3.12 and the test system containing $Ru[bpy]_3^{2+}$. Irradiation times were 11 hours per sample, and reactant concentrations were chosen to provide measures of both A and A_{max} (see section 7.3). From 14 experiments the value found for R_c was 24.9 ±3.3 Å. The large error range was attributed to temperature fluctuations.

In view of the long times required to obtain one datum, the high

percentage of data that was invalidated by temperature fluctuation, and the large error ranges found, it was decided to postpone the low-temperature experiments until a more effective temperature control system could be purchased.

REFERENCES

(1) D.A McQuarrie; **Statistical Mechanics**, (1976), Harper and Row, New York.

(2) I.N. Levine; **Quantum Chemistry**, 2nd ed. (1974), Allyn and Bacon, Inc., Boston.

(3) P.W. Atkins; **Molecular Quantum Mechanics**, vol I, (1970), Clarendon Press, Oxford.

(4) E. Grunwald; **Chemtech.**, (1984), 698-705.

(5) O. Exner; The Hammett Equation -- the Present Position. p.1-69, in N. B. Chapman, J. Shorter, Eds.; **Advances in Linear Free Energy Relationships**, (1972), Plenum Press, London.

(6) J. E. Leffler, E. Grunwald; **Rates and Equilibria of Organic Reactions**, (1963), Wiley, New York.

(7) E. R. Thornton; **J. Am. Chem. Soc.**, (1967), 89, 2915-2927.

(8) J. N. Brønsted, K. Pedersen; **Z. Physik. Chem.**, (1924), 108, 185-234.

(9) M. Eigen; **Angew. Chem. Int. Ed.**, (1964), 3, 1-19.

(10) D. Rehm, A. Weller; **Ber. Bunsenges. Phys. Chem.**, (1969), 73, 834-839.

(11) D. Rehm, A. Weller; **Isr. J. Chem.**, (1970), 8, 259-271.

(12) R. A. Marcus; **J. Chem. Phys.**, (1956), 24, 966-978.

(13) R. A. Marcus; **Disc. Faraday Soc.**, (1960), 29, 21-31.

(14) R. A. Marcus; **J. Chem. Phys.**, (1965), 43, 679-701.

(15) J. R. Bolton, M. D. Archer; **Photoconversion of Solar Energy**. to be published.

(16) V. Balzani, F. Boletta, M. T. Gandolfi, M. Maestri; **Topics in Current Chemistry**, (1978), 75. 1-64.

(17) A. Haim, N. Sutin; **Inorg. Chem.**, (1976), 15, 476-478.

(18) A. Weller; Z. Phys. Chem. Neue Folge, (1982), 133, 93-98.

(19) R. A. Marcus, N. Sutin; Biochim. Biophys. Act., (1985), 811, 265-322.

(20) T. M. Meyer; Prog. Inorg. Chem., (1983), 30, 389-440.

(21) N. Sutin; Prog Inorg. Chem., (1983), 30, 441-498.

(22) R. D. Cannon; Electron Transfer Reactions, (1980), Butterworths, London.

(23) W. F. Libby; J. Phys. Chem., (1952), 56, 863-868.

(24) K. J. Laidler, K. E. Shuler; Chem. Revs., (1951), 48, 153-224.

(25) N. Sutin, C. Creutz; J. Chem. Educ., (1983), 60, 809-814.

(26) A. A. Lamola; in Technique of Organic Chemistry, P. A. Leermakers, A. Weissberger, Eds.; Wiley: New York, 1969, vol. XIV.

(27) J. R. Murdoch; J. Am. Chem. Soc., (1983), 105, 2667-2672.

(28) C. P. Smith; Dielectric Behaviour and Structure, McGraw-Hill: New York, 1955.

(29) R. D. Cannon; Chem. Phys. Lett., (1977), 49, 299-304.

(30) M. D. Newton, N, Sutin; Ann. Rev. Phys. Chem., (1984), 35, 437-480.

(31) W. Siebrand; in The Triplet State, A. B. Zahlan, Ed., Cambridge University Press: London, 1967.

(32) W. Robinson, R. P. Frosch; J. Chem. Phys., (1963), 38, 1187-1203.

(33) R. A. Marcus; Int. J. Chem. Kin., (1981), 13, 865-872.

(34) P. Siders, R. A. Marcus; J. Am. Chem. Soc., (1981), 103, 748-752.

(35) R. A. Marcus, P. Siders; J. Phys. Chem., (1982), 86, 622-630.

(36) J. R. Miller, J. V. Beitz, R. K. Huddleston; J. Am. Chem. Soc., (1984), 106, 5057-5068.

(37) N. R. Kestner, J. Logan, J. Jortner; J. Phys. Chem., (1974), 78, 2148-2166.

(38) J. Ulstrup, J. Jortner; J. Phys. Chem., (1975), 63, 4358-4368.

(39) O. Stern, M. Volmer; Physik. Z., (1919), 20, 183-188.

(40) J. A. Barltrop, J. D. Coyle; Excited States in Organic Chemistry, Wiley: London, 1975.

(41) J. K. Baird, J. S. McCaskill, N. H. March; J. Chem. Phys., (1983), 78, 6598-6601.

(42) W. R. Ware; in Creation and Detection of the Excited State, A. A. Lamola, Ed.; Marcel Dekker: New York, 1971, vol. I, part A, 213-302.

(43) L. Bruninghaus; Compt. Rend. Acad. Sci., (1909), 149, 1375-1376.

(44) F. Perrin; Compt. Rend. Acad. Sci., (1924), 178, 1978-1980; ibid., (1924), 178, 2252-2254.

(45) S. I. Wawilow; Z. Phys., (1925), 31, 750-764.

(46) J. Perrin; Ann. Phys., (1919), 11, 5-108.

(47) J. Perrin; Compt. Rend. Acad. Sci., (1927), 184, 1097-1100.

(48) E. Merrit; J. Opt. Soc. Am., (1926), 12, 613-622.

(49) B. Y. Sveshnikoff; Compt. Rend. Acad. Sci. URSS, (1937), 15, 177-182.

(50) M. Smoluchowski; Z. Phys. Chem., (1917), 92, 129-168.

(51) N. J. Turro; Modern Molecular Photochemistry, The Benjamin/Cummings Pub. Co., Inc.: Menlo Park, 1978, p. 317.

(52) T. Forster; Ann. Phys., (1948), 2, 55-75.

(53) I. M. Frank, S. I. Vavilov; Z. Phys., (1931), 69, 100-110.

(54) J. B. Birks; Photophysics of Aromatic Molecules, Wiley: London, 1970.

(55) J. R. Miller; J. Chem. Phys., (1972), 56, 5173-5183.

(56) J. V. Beitz, J. R. Miller; J. Chem. Phys., (1979), 71, 4579-4595.

(57) R. K. Huddleston, J. R. Miller; J. Phys. Chem., (1982), 86, 200-203.

(58) B. Brocklehurst; Chem. Phys., (1973), 2, 6-18.

(59) M. Inokuti, F. Hirayama; J. Chem. Phys., (1965), 43, 1978-1989.

(60) D. L. Dexter; J. Chem. Phys., (1953), 21, 836-850.

(61) N. J. Turro, I. E. Kochevar, Y. Noguchi, M. F. Chow; J. Am. Chem. Soc., (1978), 100, 3170-3177.

(62) J. R. Miller, J. A. Peeples, M. J. Schmitt, G. L. Closs; J. Am. Chem. Soc., (1982), 104, 6488-6493.

(63) R. Ballardini, G. Varani, M. T. Indelli, F. Scandola, V. Balzani; J. Am. Chem. Soc., 1978), 100, 7219-7223.

(64) M. T. Indelli, R. Ballardini, F, Scandola; J. Phys. Chem., (1984), 88, 2547-2551.

(65) R. J. Klingler, J. K. Kochi; J. Am. Chem. Soc., (1982), 104, 4186-4196.

(66) J. K. Nagle, M. Dressick, T. J. Meyer; J. Am. Chem. Soc., (1979), 101, 3993-3995.

(67) A. Weller, K. Zachariasse; Chem. Phys. Lett., (1971), 10, 590-594.

(68) R. P. Van Duyne, S. F. Fischer; Chem. Phys., (1974), 5, 183-197.

(69) C. Creutz, N. Sutin; J. Am. Chem. Soc., (1977), 99, 241-243.

(70) A. Frank, M. Gratzel, A. Henglein, E. Janata; Ber. Bunsenges. Phys. Chem., (1976), 80, 547-551.

(71) A. Henglein; Can. J. Chem., (1977), 55, 2112-2123.

(72) C. D. Jonah, M. S. Matheson, D. Meisel; J. Am. Chem. Soc., (1978), 100, 1449-1456.

(73) W. L. Wallace, A. J. Bard; J. Phys. Chem., (1979), 83, 1350-1357.

(74) A. Kira; J. Phys. Chem., (1981), 85, 3047-3049.

(75) T. Guarr, M. McGuire, S. Strauch, G. McLendon; J. Am. Chem. Soc., (1983), 105, 616-618.

(76) G. McLendon, J. R. Miller; J. Am. Chem. Soc., (1985), 107, 7811-7816.

(77) J. R. Miller, L. T. Calcaterra, G. L. Closs; J. Am. Chem. Soc., (1984), 106, 3047-3049.

(78) M. R. Wasielewski, M. P. Niemczyk, W. A. Svec, E. B. Pewitt; J. Am. Chem. Soc., (1985), 107, 1080-1082.

(79) M. P. Irvine, R. J. Harrison, G. S. Beddard, P. Leighton, J. K. M. Sanders; Chem. Phys., (1986), 104, 315-324.

(80) T. Onno, A. Yoshimura, N. Mataga; J. Phys. Chem., (1986), 90, 3295-3297.

(81) I. R. Gould, J. E. Moser, D. Ege, S. Farid; J. Am. Chem. Soc., (1988), 110, 1991-1993.

(82) E. Vauthey, P. Suppan, E. Haselbach; Helv. Chim. Act., (1988), 71, 93-99.

(83) D. S. Miller; Ph. D. Dissertation, University of Rochester, 1981.

(84) C. Bock, T. J. Meyer, D. G. Whitten; J. Am. Chem. Soc., (1974), 96, 4710-4712.

(85) P. Keller, A. Moradpour, E. Amouyal, H. B. Kagan; Nouv. J. Chim., (1980), 4, 377-384.

(86) D. Miller, G. McLendon; Inorg. Chem., (1981), 20, 950-953.

(87) A. Nakahara, J. H. Wang; J. Am. Chem. Soc., (1963), 85, 496-498.

(88) D. A. Skoog, D. M. West; Fundamentals of Analytical Chemistry, 3rd ed., Holt, Rinehart and Winston: New York, 1976, p. 274.

(89) H. A. Benesi, J. H. Hildebrand; J. Am. Chem. Soc., (1949), 71, 2703-2707.

(90) M. Z. Hoffman, D. R. Prasad, G. Jones, II, V. Malba; J. Am. Chem. Soc., (1983), 105, 6360-6362.

(91) E. E. Mercer, R. R. Buckley; Inorg. Chem. (1965), 4, 1692-1695.

(92) C. T. Lin, W. Bottcher, M. Chou, C. Creutz, N. J. Sutin; J.Am. Chem. Soc., (1976), 98, 6536-6544..

(93) C. F. Liu, N. C. Liu, J. C. Bailar; Inorg. Chem. (1964), 3, 1197-1198.

(94) J. N. Demas, T. F. Turner, G. A. Crosby; Inorg. Chem. (1969), 8, 674-675.

(95) J. N. Demas, J. W. Addington, S. H. Peterson, E. W. Harris; J. Phys. Chem. (1977), 81, 1039-1043.

(96) B. P. Sullivan, D. T. Salmon, T. J. Meyer; Inorg. Chem. (1978), 17, 3334-3341.

(97) J. V. Caspar, T. J. Meyer; Inorg. Chem. (1983), 22, 2444-2453.

(98) D. Pinnick, B. Durham; Inorg. Chem. (1984), 23, 1440-1445.

(99) P. A. Adcock, F. R. Keene, R. S. Smythe, M. R. Snow; Inorg. Chem. (1984), 23, 2336-2343.

(100) K. J. Takeuchi, M. S. Thompson, D. W. Pipes, T. J. Meyer; Inorg Chem., (1984), 23, 1845-1851.

(101) M. J. Ridd, F. R. Keene; J. Am. Chem. Soc., (1981), 103, 5733-5740.

(102) S. Anderson, E. C. Constable, K. R. Sedden, J. E. Turp, J. E. Baggott, M. J. Pilling; J. Chem. Soc. Dalton Trans. (1985), 2247-2261.

(103) G. Maerker, F. H. Case; J. Am. Chem. Soc., (1958), 80, 2745-2748.

(104) M. J. Cook, A. P. Lewis, G. S. G. McAuliffe, V. Skarda, A. J. Thomson, J. L. Glasper, D. J. Robbins; J. Chem. Soc. Perkin Trans. II, (1984), 1293-1301.

(105) A. I. Krasna; Photochem. Photobiol., (1979), 29, 267-276.

(106) M. E. Rose, R. A. W. Johnstone; Mass Spectrometry for Chemists

and Biochemists, Cambridge University Press: Cambridge, 1982.

(107) C. Fenselau, R. J. Cotter; Chem. Rev., (1987), 87, 501-512.

(108) G. Chevreau, B.Sc.$_{hon}$ Thesis, University of Western Ontario, 1987.

(109) T. Osa, T. Kuwana; J. Electroanal. Interfac. Chem., (1969), 22, 380-406.

(110) S. Hünig, J. Groβ, W. Schenk; Liebigs Anns. Chem., (1973), 324-338.

(111) H. Taube; Adv. Chem. Ser., (1977), 162, 127-144.

(112) C. Chiorboli, M. T. Indelli, M. A. R. Scandola, F. Scandola; J. Phys. Chem., (1988), 92, 156-163.

(113) V. Skarda, M. J. Cook, A. P. Lewis, G. S. G. McAuliffe, A. J. Thomson; J. Chem. Soc. Perkin Trans. II, (1984), 1309-1311.

(114) D. V. O'Connor; D. Phillips, Time-Correlated Single Photon Counting, Academic Press: London, 1984.

(115) W. R. Ware, M. Pratinidhi, R. K. Bauer; Rev. Sci. Instrum., (1983), 54, 1148-1156.

(116) D. J. James, W. R. Ware; J. Phys. Chem., (1985), 89, 5450-5458.

(117) J. E. Wertz, J. R. Bolton; Electron Spin Resonance: Elementary Theory and Practical Applications, McGraw-Hill: New York, 1972.

(118) I. Mills, T. Cvitas, K. Homann, N. Kallay, K. Kuchitsu; Quantities, Units and Symbols in Physical Chemistry, Blackwell Scientific Publications: Oxford, 1988.

(119) C. S. Johnson, H. S. Gutowsky; J. Chem. Phys., (1963), 39, 58-62.

(120) J. F. Stargardt, F. M. Hawkridge; Anal. Chim. Acta, (1983), 146, 1-8.

(121) A. L. Reiger, P H. Reiger; J. Phys. Chem., (1984), 88, 5845-5851.

(122) K. W. Frese; J. Phys. Chem., (1981), 85, 3911-3916.

(123) H. C. Stynes, J. A. Ibers; Inorg. Chem., (1971), 10, 2304-2308.

(124) A. Zalkin, D. H. Templeton, T. Ueki; Inorg. Chem., (1973), 12, 1641-1646.

(125) J. T. Hupp, T. J, Meyer; J. Phys. Chem., (1987), 91, 1001-1003.

(126) J. V. Caspar, B. P. Sullivan, E. M. Kober, T. J. Meyer; Chem. Phys. Lett., (1982), 91, 91-95.

(127) T. Guarr, E. Buhks, G. McLendon; J. Am. Chem. Soc., (1983), 105, 3763-3767.

(128) E. Buhks, M. Bixon, J. Jortner; J. Phys. Chem., (1981), 85, 3763-3766.

(129) M. R. Wasielewski, J. R. Norris, M. K. Bowman; Faraday Discuss. Chem. Soc. , (1984), 78, 279-288.

(130) A. Weller, H. Staerk, R. Treichel; Faraday Discuss. Chem. Soc., (1984), 78, 271-278.

(131) M. Hoffman; J. Phys. Chem., (1988), 3458-3464.

(132) M. R. Spiegel; Mathematical Handbook, McGraw-Hill: New York, 1968.

(133) R. Bonneau, J. Joussot-Dubien, J. Faure; Photochem. Photobiol., (1973), 17, 313-319.

(134) P. R. Bevington; Data Reduction and Error Analysis for the Physical Sciences, McGraw-Hill: New York, 1969.